Model Predictive Control of Switched Reluctance

Machine Drives

MODEL PREDICTIVE CONTROL OF SWITCHED

RELUCTANCE

MACHINE DRIVES

BY

DIEGO FERNANDO VALENCIA GARCIA, M.Sc.

A THESIS

SUBMITTED TO THE DEPARTMENT OF ELECTRICAL & COMPUTER ENGINEERING

AND THE SCHOOL OF GRADUATE STUDIES

OF MCMASTER UNIVERSITY

IN PARTIAL FULFILMENT OF THE REQUIREMENTS

FOR THE DEGREE OF

DOCTOR OF PHILOSOPHY

Doctor of Philosophy (2020)   McMaster University

(Electrical & Computer Engineering)   Hamilton, Ontario, Canada

TITLE: Model Predictive Control of Switched Reluctance
                        Machine Drives

AUTHOR: Diego Fernando Valencia Garcia

                        M.Sc. (Sustainable Transportation and Electrical Power
                        Systems)

                        University of Oviedo (Spain),

                        University of Nottingham (United Kingdom),

                        University of Rome (Italy).

                        M.Eng., (Engineering)

                        Universidad Autonoma de Occidente (Colombia)

SUPERVISOR: Dr. Ali Emadi

                        Ph.D. (Texas A&M University)

                        IEEE Fellow

                        Canada Excellence Research Chair in Hybrid Powertrain

NUMBER OF PAGES: xxi, 190

To my parents, Nilza & Gilberto

Abstract

Model predictive control (MPC) for switched reluctance machine (SRM) drives is studied in this thesis. The objective is to highlight the benefits of implementing MPC to overcome the main drawbacks of SRMs and position them as an attractive alternative among electrical drives. A comprehensive literature review of MPC for SRM is presented, detailing its current trends as an application still at an early stage. The different features of MPC are highlighted and paired with the most challenging and promising control objectives of SRMs. A vision of future research trends and applications of MPC-driven SRMs is proposed, thus drawing a road-map of future projects, barriers to overcome and potential developments. Several important applications can take advantage of the improved features that SRM can get with MPC, especially from the possibility of defining a unified control technique with the flexibility to adapt to different system requirements. The most important cluster for SRM drives is the high- and ultrahigh-speed operative regions where conventional machines cannot work efficiently. SRMs with MPC can complement then the existing demand for electrical drives with high performance under challenging conditions.

Three techniques based on the finite control set model predictive control (FCS-MPC) approach are developed out of the proposed road-map. The first one defines a virtual-flux current tracking technique that improves the existing ones in operating

at different speeds and more than one quadrant operation. The method is validated for low- and high- power SRMs in simulations and diverse types of current waveform, making it easy to adapt to existing current shaping techniques. It is also validated experimentally for different operating conditions and robustness against parameter variation. The second technique proposed a predictive torque control that bases its model on static-maps, thus avoiding complex analytical expressions. It improves its estimation through a Kalman filter. The third technique uses a virtual-flux predictive torque control, similar to the first technique for current tracking. The techniques are validated at a wide speed range, thus evidencing superiority in performance without modification on the control structure.

Acknowledgements

First and foremost, I would like to express my sincerest gratitude to my supervisor, Dr. Ali Emadi, for offering me the opportunity to work alongside the most successful researchers on electrified transportation in the world. Thank you for your patience, guidance, motivation, and for your sincere advises through this process. Thank you for being such a great inspiration.

I would also like to thank Dr. Sandra Castaño, who first suggested my name as a PhD candidate, and who convinced me about this amazing adventure both at McMaster and in Canada. Thank you for always being so warm and helping me out during my transition to PhD life.

This thesis would not have been possible without the initial help and guidance of Dr. Berker Bilgin, through his comprehensive course about switched reluctance machines. Dr. Bilgin is one of the most admirable professionals not only because of his expertise but also his extreme hard work. He also guided me through different projects and showed me the path towards excellence.

My gratitude also goes to Dr. José Rodriguez and Dr. Cristián Garcia, from Chile, who guided me through the most innovative applications of model predictive control as well as the top quality research in this topic. Thank you for the countless hours you spent with me writing papers and simulating controllers. Thank you for

Notation

Abbreviations

DITC Direct instantaneous torque control

DTC Direct torque control

EV Electric vehicle

FCS-MPC Finite Control Set - MPC

FEA Finite element analysis

GPC Generalized Predictive Control

IGBT Insulated-Gate Bipolar Transistor

ITC Indirect torque control

MPC Model Predictive Control

NVH Noise Vibrations and Harshness

PCC Predictive Current Control

PI Proportional-integral

PMSM Permanent magnet synchronous machine

PTC Predictive Torque Control

PWM Pulse Width Modulation

SRM Switched Reluctance Machine

Contents

List of Tables

List of Figures

Chapter 1

Introduction

1.1 Background and Motivation

Electric machines industry constitutes a worldwide electricity consumption of around 60% , with an expected growth in demand up to 30% of the total growth estimated to 2040 [4]. Induction motors ruled the market for several years, given their capability to offer high torque with direct three-phase grid connection. However, recent applications involve the use of high-performance variable speed drives, which pushed the inclusion of power electronics, microprocessors and advanced control techniques [5]. One of the most recent clusters for innovation is electrified vehicles, leading the international efforts to develop a sustainable transportation paradigms [6].

Although, to date, induction machines have been used in counted cases for automotive applications [7], PMSMs are currently in the center of electric drives for EVs. High efficiency and high power density are the main attributes of these motors, which became required features in electrified powertrains given the space and weight restrictions [5, 8]. In particular, interior PMSMs provide additional torque thanks to

1

the interaction of their saliency in the reluctance torque and the magnetic torque due to the permanent magnets. However, the use of permanent magnets is a drawback for these machines; the magnets are relatively fragile for high-speed and high temperature operations, thus compromising the reliability and robustness of the drive. Furthermore, economical and political constraints are tied to the use of permanent magnets, which are fundamentally made from rare-earth materials given the high dependence of a single government for mass-production [6].

Switched reluctance machines (SRM) have recently got more attention with the efforts of moving towards a magnet-free motor technology. Their structure has a simple, low-cost and robust design allowing a more reliable high-speed and high-temperature operation [9]. However, it is still not common to find them in practical scenarios due to their inherent torque ripple, vibrations and acoustic noise. These issues are particularly problematic in automotive applications such as the traction in passenger vehicles, as very strict NVH regulations must be accomplished [2].

Numerous approaches to improve the SRM performance targeting torque ripple and acoustic noise reduction have been considered. The combination of comprehensive electromechanical studies, finite element analysis (FEA) and advanced optimization techniques such as genetic algorithms has evidenced significant improvements in the design characteristics of SRM drives [9]. To guarantee the design performance a proper control must be implemented, but conventional strategies cannot be applied in SRMs. In fact, the use of the well-known proportional-integral (PI) controller becomes challenging for these machines due to their highly-nonlinear behaviour [10].

The control passes then to be in the spotlight for research by putting together the optimal design and the recent development of high-performance power electronics and

better microprocessing capabilities. The simplest control technique is the ITC with optimum commutation angles, which defines a reference current integrated with a hysteresis current controller [11]. The torque ripple can be minimized by shaping the phase currents with methods including the torque sharing functions (TSF) [12] and current profiling [13], while other techniques like direct instantaneous torque control (DITC) attack directly the torque variation by controlling the converter switching states [14]. Acoustic noise is reduced by controlling the radial force produced in the machine. Here, current shaping reduces the harmonics in specific spatial orders [3]. With a proper controller, SRM drives have shown an incredible potential for propulsion, with the possibility to replace PMSMs in terms of developed torque and outer diameter characteristics [15].

Whether torque or force are controlled, these techniques follow either the indirect torque control (ITC) structure, defining a reference current to be tracked by an inner loop, or they directly regulate the phase torque by direct torque control (DTC). In any case, the classic control approach tends to use a pulse width modulation (PWM) or a hysteresis stage; however, these strategies offer either a limited dynamic response or a variable switching frequency with small bandwidth and range of operation [16]. Besides, as the phases in SRMs are independently controlled and the total torque is obtained from the algebraic sum of individual phase torque contributions, another challenge appears in deciding the torque sharing between the active phases during the phase commutation [17]. These issues are added to the SRMs' doubly salient pole configuration and nonlinear flux distribution, thus making the control a more complex task to fulfil.

Predictive control is a control family that has been applied in industry for several

years in processes with relatively slow time constant [18]. Recently, there has been an increasing interest for its application in other areas such as power electronics and motor drives, given the improvement in computational capability and memory storage of microprocessors [19]. Predictive control constitutes an alternative for conventional controllers as it can handle nonlinearities. It is recognized as *digital controller friendly*, as it can consider the discrete nature of power converters in the calculation of control actions [20]. The most appealing features of predictive control are the simplicity of implementation, flexibility to consider constraints and effectiveness in dynamic response [21]. Predictive control has been successfully applied to power converters and AC drives, which include induction [22], permanent magnet (PM) [23] and synchronous reluctance motors [24]. It becomes even more interesting when applied to higher-complexity systems like multilevel inverters [25] and multi-phase drives [26].

These characteristics are promising strategies to regulate the SRMs steady state behaviour as well as their transient response. Therefore, SRM drives have recently become a target application for predictive control, opening a gap with vast potential for related uses from current and torque control, to acoustic noise and heating. The vision of future applications places SRMs as a high-performance drive technology with adaptation to several requirements of the electrified automotive sector.

1.2   Contributions

The author has contributed a number of original developments in the areas of control for switched reluctance machines with model predictive control, which are listed as follows:

1. A comprehensive literature review and analysis of predictive control techniques implemented for switched reluctance machine control.

2. A detailed analysis of the challenges and potential improvements that the predictive control techniques has on SRM drives.

3. A road-map of future research opportunities using MPC for SRM drives control to enhance its attractive for commercial applications.

4. The virtual-flux FCS-MPC method for a simple and effective current regulation in low- and high-power SRM designed for automotive traction applications. The technique has been validated to work in four-quadrant operation.

5. An improved PTC technique with an *online* torque sharing algorithm for SRM. Unlike several solutions in the literature, the algorithm has been proven to work on a wide range of speeds without modification of the control structure.

1.3   Thesis Outline

This thesis is aimed to investigate potential of using MPC to control SRM drives, thus improving their overall performance. Two study-cases are presented to demonstrate the enhanced performance of SRMs with these techniques.

Chapter 2 introduces the general background of switched reluctance machines starting from its construction characteristics, pole configuration and modelling. A brief review of the power electronic converters used to drive SRMs is also presented. Besides, the basic concepts behind predictive control, classification and general formulation are discussed.

Chapter 3 presents the literature review of predictive control for SRMs. It includes the classification of the different control techniques according to the control objective mainly as PCC and PTC, but also including a few works on predictive speed control and overload control. A comprehensive analysis of the different modeling techniques, voltage vector calculation, phase torque distribution algorithms and switching behaviour is also discussed, and suggestion for further improvement of the existent techniques is concluded.

In Chapter 4, a vision of future research trends and applications of predictive control for SRM drives is presented. The different control objectives that can be achieved or improved in SRMs with the use of MPC are described. Also, the challenges that the use of MPC presents of each of them, as acoustic noise and vibrations, fault-tolerance, and control at high and ultrahigh-speed are discussed. Some potential commercial applications for the SRM are also presented, and the approaches to make MPC and SRM to achieve the demanded targets from the next generation applications.

In Chapter 5, an experimental setup implementation is described. The setup is intended to test predictive control techniques in SRM drives coupled to a loading machine. The dyno is selected as a permanent magnet machine, and the correspondent mechanical settings are designed. Moreover, the characteristics of a 5 kW 12/8 SRM are obtained experimentally, which allows using the machine to validate the techniques proposed in the next chapters.

An example of the possible applications of MPC on SRM is presented in Chapter 6 to regulate phase current. A PCC algorithm based on FCS-MPC and the concept of *virtual-flux* is proposed. The concept of virtual-flux is discussed along with the advantages of mapping machine variables in the virtual-flux domain. The technique

offers a simplified and more robust current tracking, which relies on the use of static maps with the machine characteristics. The technique is also simulated for a 60 kW traction SRMs for automotive applications, finding out the advantage of such a technique for machines of higher power.

Chapter 7 presents a second application of MPC with a PTC technique. The latest is also based on the principle of FCS-MPC, but it implements recent developments of the predictive control theory such as using filtering techniques and a static-map-based model to regulate the torque with the use of virtual-flux mapping.

Chapter 8 provides the conclusion of the thesis and suggestions for future work. It also presents a summary of publications and contributions made from this work.

Chapter 2

Fundamentals of Switched Reluctance Machines (SRMs) and Model Predictive Control (MPC)

2.1 Switched Reluctance Machines and Drives

2.1.1 Operating principle and electrical angle

The switched reluctance machine (SRM) is a doubly salient machine with an uneven distribution of stator/rotor poles. By sequentially energizing the different windings, flux paths are generated throughout the stator and rotor poles and the air gap. As a consequence, a magneto-motive force is produced, which makes the poles moving towards an aligned position. As all the poles cannot be aligned simultaneously, it is always possible to push an unaligned rotor pole towards the next stator pole. Fig. 2.1 shows the pole configuration of a four-phase 8/6 SRM, where 8 corresponds to
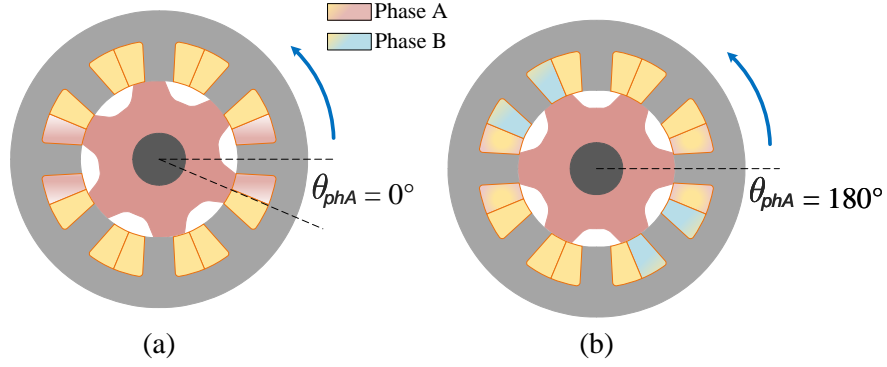
Figure 2.1: Example of the structural construction of the SRM. A 8/6 SRM with 8 stator poles and 6 rotor poles (a) Rotor unaligned with respect to stator poles of phase A (b) Rotor poles aligned with respect stator poles of phase A

the number of stator poles and 6 the number of rotor poles. In the figure, phase A is energized, and a reference rotor pole, initially unaligned in Fig. 2.1(a) comes in alignment with the reference stator pole in Fig. 2.1(b).

In SRMs, the electric angle can be represented by θ_{phj}, where $j = 1, 2, ..., m$, and m is the number of phases. The unaligned position in Fig. 2.1(a) is considered the initial condition, thus the electric angle of phase A is $\theta_{phA} = 0°$. If the shaft is required to move in a counterclockwise direction, phase A must be energized, making the reference rotor pole move towards an aligned position, as in Fig. 2.1(b) where $\theta_{phA} = 180°$. Then, phase A must be de-energized, and the next phase should be energized to guarantee continuous movement. The electrical angle can be represented mathematically by [9],

$$\theta_{phj} = mod\left[(N_r \cdot \theta_r + 180°) + \frac{360}{m} k_{ph}, 360° \right],$$

(2.1)

where N_r is the number of rotor poles, θ_r is the rotor position or mechanical angle, m is the number of phases and k_{ph} represents the phase excitation sequence, which

determines the direction of rotation of the shaft.

2.1.2   Electromagnetic model

The phase voltage equation of the SRM, neglecting mutual coupling between phases, can be expressed by (2.2),

$$v_{ph} = i_{ph}R_{ph} + \frac{d\lambda_{ph}}{dt} \tag{2.2a}$$

$$\lambda_{phj} = \mathscr{L} \circ i_{phj} \approx L(i_{phj}, \theta_{phj})i_{phj}, \tag{2.2b}$$

where v_{ph}, i_{ph}, R_{ph} and λ_{ph} are the phase voltage, current, resistance and flux linkage, respectively. The term $\mathscr{L}$ is a static map relating the phase current and the produced flux linkage, which can be represented as the nonlinear inductance L. A common flux linkage map is shown in Fig.2.2(b) for a 8/6 machine. Fig.2.2(a) illustrates how the variable reluctance paths allow higher flux linkage at the aligned position, and minimum linkage at unaligned rotor position. From the same figure, it is possible to analyze how further increase in the current does not represent significant increase in the flux linkage around rated values, which is given by the saturation phenomenon of the material.

Combining (2.2a) and (2.2b) results in a current-based representation of the voltage equation for SRM shown in (2.3), where the sub-index phj has been omitted for the sake of compactness.

$$v = iR + L(i,\theta)\frac{di}{dt} + \epsilon \tag{2.3a}$$

$$\epsilon = i \cdot \omega \cdot \frac{\partial L(i,\theta)}{\partial \theta}, \tag{2.3b}$$

10
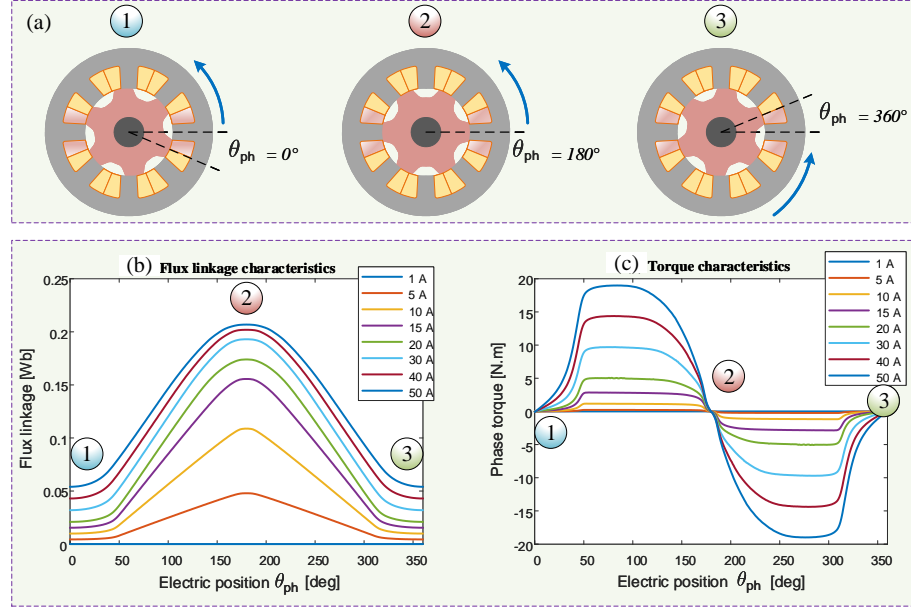
Figure 2.2: Static characteristics of an 8/6 SRM (a) Relative rotor alignments (b) Flux linkage (c) Electromagnetic torque

where $\omega = d\theta/dt$ is the electrical angular velocity of the rotor, and the term ϵ is the generated back-EMF, which opposes the current injection.

The use of current-based models helps to analyze the back-EMF and phase inductance. Some approaches take advantage of it for a straightforward state-space representation of the machine model.

The electromagnetic torque is defined as the rate of change of the energy stored in the magnetic circuit with respect to the rotor position for a given phase flux linkage [9]. A common approximation considers the use of the magnetic co-energy as,

$$T = \left.\frac{dW_c(i,\theta)}{d\theta}\right|_{i=const} = \left.\frac{dW_e(i,\theta)}{d\theta}\right|_{\lambda=const}, \tag{2.4}$$

where $W_s = \int_0^\lambda i\,d\lambda$ is the stored energy in the airgap and $W_c = \int_0^i \lambda\,di$ is the co-energy.

Whether energy or co-energy are used to compute the torque, as the flux linkage depends on the rotor position, the final torque expression depends on both the phase current and the electrical angle. This nonlinear behaviour is commonly represented by a static map, which can be obtained either experimentally or by FEA. It is worth mentioning that the saturation phenomenon evidenced in the flux linkage map in Fig. 2.2(b) plays a decisive role in terms of torque production. The core saturation reduces the capability of the magnetic circuit to store energy as a magnetic field and therefore allows a greater energy transfer as electromagnetic torque. Therefore, *SRMs find the optimal operating point in the saturation region.* Typical torque waveforms are shown in Fig. 2.2(c). It is worth noticing that the operation between 180° and 360° produces a negative torque, thus making the machine operate as a switched reluctance generator (SRG). This occurs if the shaft keeps its rotation (by a prime mover) passed the 180° and the correspondent phase is not deactivated.

Besides, the maximum torque decreases at high speed as the back-EMF from (2.3) limits the current injection at a given terminal voltage. As a consequence, the torque vs speed characteristics of SRM presents a natural field weakening area. A common drawback of torque control is the lack of consideration of the limits of each phase in producing torque, based on the dc link voltage and the actual back-EMF [27].

2.1.3   Power converter

Fig. 2.3(a) shows the topology of a m-phase asymmetric half-bridge converter, regularly used for SRM drives. Each phase has three possible switching states: the one in Fig. 2.3(b), where the phase voltage is positive and equal to v_{dc}, with s_{j1} and s_{j2} (j = active phase). In this state, the injection of phase current is limited by the
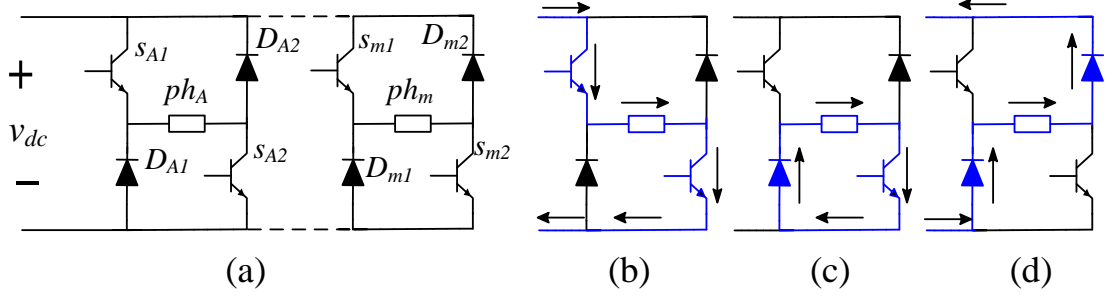
Figure 2.3: (a) m-phase asymmetric converter (b) positive terminal voltage (c) zero terminal voltage (freewheel) (d) negative terminal voltage

inductance and back-EMF terms from (2.3). The freewheeling mode makes $v = 0V$ while the existing phase current circulates through the diode and the switch s_{j2}, as shown in Fig. 2.3(c). Finally, Fig. 2.3(d) shows the state in which negative voltage $v = -v_{dc}$ is applied to machine terminals, and the phase current is sent back to the source through the diodes.

The strategy with this converter topology uses the state 1 to increase the current. Depending on the electric angle, the freewheeling mode can be used to slowly decrease the current, while the -1 if the current must be quickly reduced. If the three states are considered, it is said that the converter works in soft-switching (SS) mode, while the omission of the freewheeling mode is denominated as hard-switching (HS) operation.

Other converter topologies for the SRM drive include $(N + 1)$-switch, C-dump, N-switch, split AC and split DC converters, each of them with a trade-off between performance, control complexity and the number of switching components. A comparison of these converters in presented in [28, 29]. Besides, multilevel topologies have also been proposed, which potentially improves the performance of the drive at high-speeds and in machines with low inductance [30, 31].

13

2.1.4   Generalities of control in SRM

Control in SRM drives adopts similar strategies as AC drives. A speed loop can be easily regulated by a PI controller given the slow dynamics of mechanical systems. Besides, to track the consequent torque reference, generally two control topologies are implemented: ITC or DTC. However, these torque tracking controllers are more elaborated than the conventional ones as in SRM there are m independently controlled phases contributing to the total torque in a highly nonlinear manner. Beyond the speed control, in automotive applications, the torque reference is given by the vehicle operating conditions, and the electric drive must respond to its dynamics in a quick and reliable way. In addition, the torque regulation must be be guaranteed with several restrictions such as high efficiency, low NVH levels and proper power factor.

ITC uses a cascaded control loops, similar to the field-oriented control (FOC) in conventional AC drives. The external loop tracks a reference torque, usually as a speed regulator, and the inner loop regulates the reference current obtained from the torque loop. Fig. 2.4(a) represents this control scheme. In DTC instead, the inner current loop is omitted, and the developed torque is compared directly to the reference to produce the control action either by hysteresis torque control or by a PWM stage. Fig. 2.4(b) shows the block diagram of the most common type of DTC technique in SRM, the direct instantaneous torque control DITC.

Although DITC is the most popular technique for torque control in SRM, ITC-based techniques have gained relevance given the possibility to pre-define current shapes that can provide a smooth torque while minimizing secondary objectives such as losses or acoustic noise. A more detail analysis of these control techniques is discussed in Chapter 3 of this thesis along with the literature review.
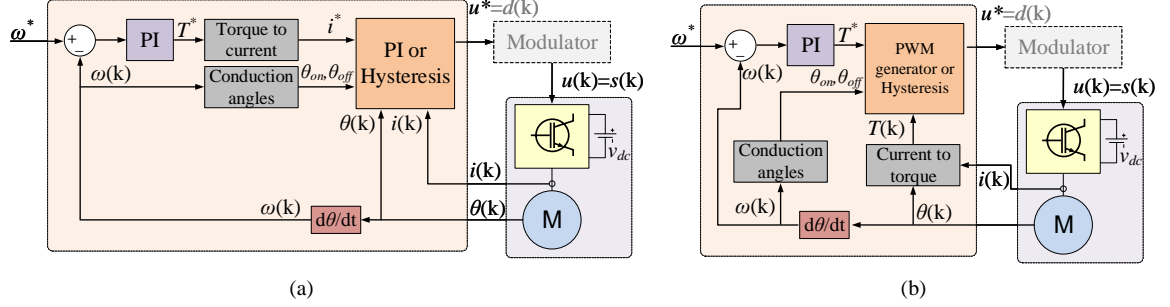
Figure 2.4: Conventional control schemes for SRM (a) indirect torque control (b) direct instantaneous torque control

2.2 Predictive Control

Far from being a simple control strategy, predictive control is a whole family of techniques sharing the same operating principle: the control decisions are totally based on the knowledge of future events, which are predicted using only the information of the present states. Predictive control has been applied in industry for several years in processes with a relatively slow time constant [18]. Recently, there has been an increasing interest in its application in other areas such as power electronics and motor drives, given the improvement in the computational capability of microprocessors [21].

Unlike the conventional regulators where the control action is based on a predefined feedback law, in predictive control, it is decided *online* and based on a prediction of the future states. As shown in Fig. 2.5, predictive control uses the prediction of the future system state to determine, online, the optimal control action $u(k) \in \mathbb{U} \subseteq \mathbb{R}^m$ of the next sampling period. The prediction is computed based on the states of the plant and its parameters, which improves the response capability of the controller but increases the computation complexity; therefore, predictive control calculates the optimal input by solving a constrained finite-horizon optimization control (CFHOC)
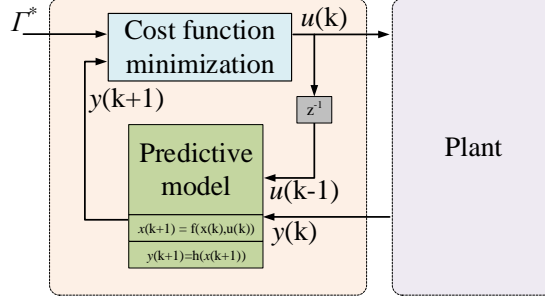
Figure 2.5: General control diagram of MPC for electric drives

problem at each sampling period [32]. The system model can be usually adopted as a discrete-time and time-invariant representation,

$$x\left(k+1\right) = f\left(x\left(k\right), u\left(k\right)\right) \tag{2.5a}$$

$$y\left(k\right) = h\left(x\left(k\right)\right), \tag{2.5b}$$

where $x\left(k\right) \in \mathbb{X} \subseteq \mathbb{R}^n$ are the system states at the instant $k \in \mathbb{N}$ and $f\left(\cdot\right)$ is obtained from the plant differential equation. $y\left(k\right)$ is the actual output, which is a function $h\left(\cdot\right)$ of the state $x\left(k\right)$. Given the discrete nature of drive systems, the derivative term is usually represented using discretization strategies, with the forward-Euler approximation as the most popular. Other approaches consider second-order discretization to improve the prediction accuracy [33].

Given a constant reference Γ^*, the objective is to obtain the optimal reference $u\left(k+1\right)$ that drives the system to an equilibrium point x_{Γ^*} in which $y_{\Gamma^*} = h(x_{\Gamma^*}) = \Gamma^*$. The solution of the CFHOC problem results in a sequence $\mathbf{U}(k) = \{u(k), u(k+1), ..., u(k+N_p-1)\} \in \mathbb{U}$ with N_p defined as the finite horizon [34]. This sequence is calculated either by the explicit solution that eliminates the error $|\Gamma^* - \hat{y}(k+N_p-1)|$,

or by minimizing the cost function,

$$\min_{\mathbf{U(k)}} g\left(x(k), \mathbf{U}(k)\right) = g_1\left(x(k), \mathbf{U}(k)\right) + g_2\left(\mathbf{U}(k)\right) \tag{2.6a}$$

$$g_1\left(x(k), \mathbf{U}(k)\right) = \sum_{j=1}^{N_p} |\hat{y}(k+j|k) - \Gamma^*(k+j)| \tag{2.6b}$$

$$g_2\left(\mathbf{U}(k)\right) = \sum_{j=1}^{N_u} |\delta(\Delta\mathbf{U}(k+j-1))|, \tag{2.6c}$$

where g_1 represents the tracking error, and g_2 is a term that penalizes the control action with a factor of δ, and N_u is the control horizon [35]. g_1 in (2.6b) is commonly adopted in electric drives to track either current or torque reference, while (2.6c) minimizes the switching frequency.

The selection of control and predictive horizons drastically affects the performance of the predictive algorithm. The use of a control horizon $N_u < N_p$ has demonstrated benefits for closed-loop stability [32, 36]. Similarly, as the time constants in electric drives are in the order of ms, the prediction horizons tend to be one or two. The use of high horizon becomes a compromise between control performance and complexity, as higher N_p values increase the computational requirements exponentially [37]. Recent developments have evaluated calculation alternatives to predict horizons up to $N_p = 4$ [38], with promising results in medium-voltage and high-efficiency electric drives [35, 39].

2.2.1 Classification of predictive control of SRMs

Predictive control is known for its better dynamic response [40], simple control structure and straightforward implementation [21]. Besides, it is capable of effectively
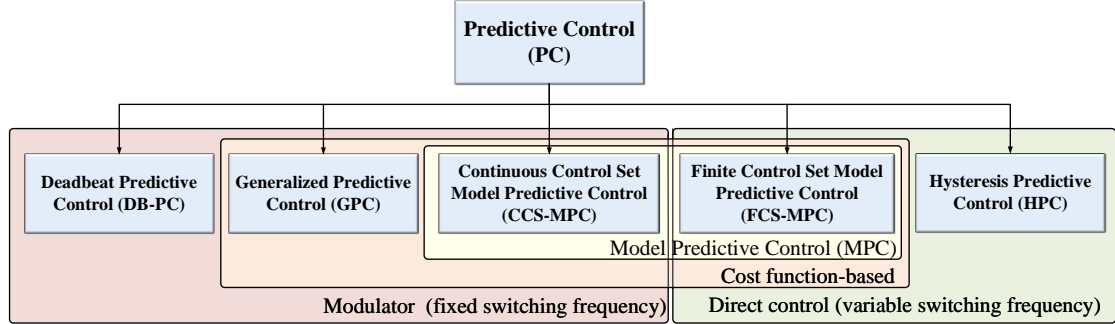
Figure 2.6: Predictive control techniques applied to switched reluctance machines. Classification and main characteristics

handle the constraints and nonlinearities of the system. It all comes at the expense of higher computational burden, which can be managed by the recent advancements in microprocessor technology.

Predictive control determines the optimal inputs to the system (switching signals in case of a motor drive) to achieve the desired performance target by predicting the future state of the plant using a predictive model. Different approaches have been considered for control in SRM drives. The optimal solution is obtained by solving the CFHOC problem either by a cost function or calculation from the defined predictive model. The selected $u(k)$ is then applied during the next sampling period $k + 1$. According to the strategy, the selected input $u(k)$ can be applied, whether using a modulator or not, which affects the performance and switching frequency characteristics of the closed-loop controller. If the predictive strategy uses both a predictive model and a cost function, the technique is known as *model predictive control (MPC)*. In this thesis, predictive control is classified with the criteria shown in Fig. 2.6 for the techniques concerning to switched reluctance machines [41].

Sensitivity to parameter mismatch and measurement noise is considered as one of

the main drawbacks of predictive methods. In practice, parameter variations are un-avoidable, which can happen due to the nonlinear nature of physical systems, ageing, temperature effects or other external factors. The effect of parameter variations on the performance of predictive methods is even worsened, if no integration elements are implemented to mitigate the steady-state error of MPC [42]. This can be usually tackled by considering longer receding horizons in the prediction, implementing active disturbance rejection schemes [43], or applying filtering techniques, like the Kalman filter [44]. Integrating online parameter estimation methods with predictive approach is another method to alleviate the effect of disturbances resulting from the parameter variations increasing the robustness of the predictive controller [45].

Generalized Predictive Control

A classic approach of predictive control deals with the CFHOC problem by linearizing the plant model. The generalized predictive control (GPC) uses this model to compute the optimal control action using a transfer function-based predictive model and a cost function [46]. Fig.2.7(a) shows the block diagram of this technique. The main advantage of GPC is the consideration of the effect of the disturbances, thus obtaining a more realistic representation of the steady-state error [47]. This, along with the linearized model, allows obtaining an optimal response for longer prediction horizons without loss of accuracy. However, this technique cannot consider the nonlinear nature of the power converter and other inherent nonlinearities [48].

The predictive model is commonly represented by the Controlled Auto-Regressive and Integrated Moving Average (CARIMA) model, which represents the model in state space and includes the disturbances effect. This approach allows obtaining an

19
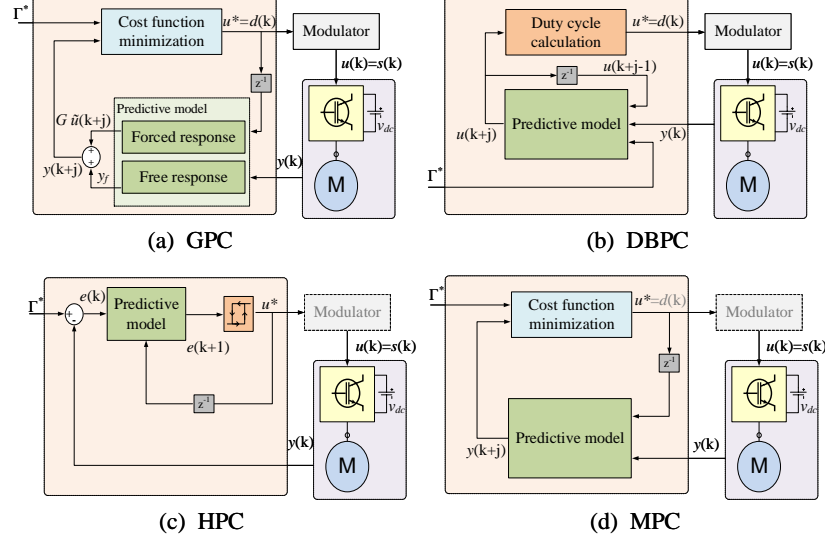
Figure 2.7: Predictive control techniques applied to switched reluctance machines (a) Generalized predictive control strategy (b) Deadbeat predictive control (c) Hysteresis-based predictive control (d) Model predictive control

unbiased representation of the steady-state error [47]. The adopted model is shown in (2.7),

$$A(z^{-1})y(t) = B(z^{-1})u(t) + C(z^{-1})\frac{\xi(t)}{\Delta}, \tag{2.7}$$

where $A(z^{-1})$, $B(z^{-1})$ and $C(z^{-1})$ are the known parameters of the system, z^{-1} is the backward shift operator and Δ is an integrator $\Delta = 1 - z^{-1}$. The disturbances are included in $\xi(t)$, which is an uncorrelated zero-mean variable. In this way, the term $C(z^{-1})\xi(t)$ is an incremental component that does not affect the steady-state value and can be neglected to simplify the calculations under this condition. The prediction stage can be executed either by techniques such as Kalman filter or by standard prediction models such as the Diophantine equations in (2.8a) [47]. The latest is usually the choice for implementation in GPC, which is combined with the model in (2.7) to obtain, based on the definition in (2.8b), the prediction model in

(2.8c) [46]:

$$1 = E_j(z^{-1})\Delta A(z^{-1}) + z^{-j}F_j(z^{-1}) \tag{2.8a}$$

$$G_j(z^{-1}) = E_j(z^{-1})B(z^{-1}) \tag{2.8b}$$

$$\hat{y}(k+j) = G_j(z^{-1})\Delta u(k+j-1) + F_j(z^{-1})y_f(t), \tag{2.8c}$$

where $E_j(z^{-1})$ and $F_j(z^{-1})$ are polynomials of the order $j-1$ and Na, respectively. $\Delta u(k+j-1)$ represents the variation of the actuating signal with respect to the previous sampling period. It is worth noticing that (2.8c) allows estimating the response for an N-horizon period computing for each step j [46]. The equations take advantage of the linearity of the model to decompose the response into the sum of the two responses, the one affected by the previous actuation variable, also called a natural response, and the one with an output depending on the future actuating variable called a forced response [49]. These variables are represented in Fig. 2.7(a) like y_f and $G\tilde{u}(k+j)$, as the free and forced response, respectively. The prediction for the sampling period j is then compared with the reference value Γ^* through a cost function. A minimization stage is added to solve the cost function and calculate the optimal input sequence $\hat{u}(k+j)$.

$$g = \sum_{j=N_1}^{N_2} \mu_j(\hat{y}(k+j) - \Gamma^*)^2 + \sum_{j=1}^{N_u} \lambda_j(\Delta u(k+j-1))^2, \tag{2.9}$$

where N_1 is the lower cost horizon, N_2 is the upper cost horizon and N_u is the control horizon. μ_j and λ_j are the weight factors. The first component in (2.9) tracks the reference, and it is called the *main objective*. In contrast, the second term or *secondary objective* minimizes the variations in the actuating variable, which is especially used

21

in electric drives to reduce the commutation in the switching devices.

The main feature of GPC is the long prediction horizon with a relatively low computational burden with respect to other predictive-based techniques [48]. With the solution of heavy computations obtained offline, GPC provides an exact solution of the CFHOC problem and the possibility to include a modulation stage, thus providing a fixed switching frequency; however, when applied to motor control, the method considers neither the PWM nor the semiconductors or inverter [19].

In comparison with other techniques, GPC has more complex formulation and implementation, and the application into highly nonlinear plants such as SRM drives limits the potential of this technique. In fact, GPC had not been a popular technique in recent years. Recently, it has started to be considered using technology able to support higher computational burden and complex calculations. It has been implemented for control in grid-connected inverters [50, 51], opening the possibility for its enhancement in electric machines.

Deadbeat Predictive Control

In deadbeat predictive control (DBPC), the predictive model directly calculates the optimal input sequence to solve the CFHOC problem [21]. The predictive model uses the information of the machine parameters, the actual state $x(k)$ and the previously computed optimal input sequence $u(k)$ to estimate a continuous value of future input sequence $u(k + j)$ that makes the error zero. The general block diagram of this technique is shown in Fig. 2.7(b). By accomplishing an error equal to zero in the next sampling period, it is expected that $y(k + 1) = \Gamma^*$; therefore, the model can be

represented as,

$$\hat{u}(k+j) = u(k) + \frac{\Gamma^* - y(k)}{Ts}. \tag{2.10}$$

In (2.10), the optimal input sequence $\hat{u}(k+j)$ makes the output $y(k+j) = y(\hat{u}(k+j)) = \Gamma^*$. In electric machines, the reference sequence is then normalized with respect to the dc-link voltage v_{dc} to obtain a duty cycle. Then, the duty cycle feeds a modulation stage, which sends the PWM signal to the drive, thus guaranteeing a fixed switching frequency operation.

Hysteresis-based Predictive Control

The hysteresis-based predictive control (HPC) follows the same guidelines as the conventional hysteresis controller. However, it obtains the optimal input sequence $u(k)$ based on a predicted representation of the error signal, thus improving the already high dynamic response of the technique. Fig. 2.7(c) illustrates the working diagram of HPC. This strategy does not regulate the output variable itself, but the instantaneous error between the reference and the predicted state, which keeps the output $y(k)$ within a defined boundary. Besides, it can be combined with strategies such as space vector modulation to provide a nearly fixed switching frequency [52]. However, HPC is not popular in literature since the use of predictive models requires the knowledge of the plant parameters. This issue eliminates the main advantage of the hysteresis controller, which is to be an effective regulator of average reference without prior knowledge of the system characteristics.

Model Predictive Control

Model predictive control (MPC) is currently the most popular predictive control strategy in literature. In this work, the concept of MPC is based on the use of both a predictive model to estimate the output $\hat{y}(k+j)$ and a cost function to determine the optimal input sequence in the next sampling period $\hat{u}(k+1)$.

There exist, in general, two types of MPC, the one with a continuous control set (CCS-MPC) and with a finite control set (FCS-MPC). Although, in strict terms, the GPC in Fig. 2.7(a) can be categorized as a CCS-MPC technique, the particular modelling and prediction of natural and forced variables make it a different technique, as explained in Section 2.2.1. The block diagram of the MPC strategy is depicted in Fig. 2.7(d), but there are differences whether CCS- or FCS-MPC are used.

Both MPC strategies use a predictive model to estimate the future behaviour of the output variable $y(k+j)$ as a function of the input $u(k)$. However, CCS-MPC presents the prediction as a continuous state. This prediction feeds a cost function along with the desired reference Γ^*, and a minimization strategy is applied, usually relying on techniques such as the Newton method. This allows obtaining a duty cycle that feeds a modulator, thus guaranteeing a constant switching frequency.

Contrarily, the FCS-MPC implements a cost function based on discrete states. The states depend on the possible switching states as inputs to the power converters. In a two-level voltage source inverter (2L-VSI) there are seven possible states. These states allow obtaining seven possible outcomes, the one with the smallest error is chosen, and the corresponding switching state is applied. This selection avoids the modulator but causes variable switching frequency, limited only by the sampling frequency [20]. The sacrifice of variable switching frequency is compensated with a

faster dynamic response [37].

Different authors have shown the advantages and flexibility that the use of weighted cost function brings to control primary and secondary objectives [20]. Recent trends in MPC include nested cost functions [53], model-free MPC [54] and MPC with virtual vectors [55].

2.2.2 Delay compensation

As predictive control determines the control law online and based on measurements of system states and model parameters, the response relies on the accuracy of these variables with respect to the real system. If model mismatches and noise are not an issue, the controller must still deal with the delay in the control action. In practical scenarios, a non-negligible time period passes between the state measurement and the application of the optimal switching period, thus producing inaccuracies in the predicted system behaviour and control action. Therefore, the concept of delay compensation gains high relevance, being nowadays a fundamental component of such algorithms. Depending on the predictive strategy, the delay compensation method can be classified as direct or indirect compensation [56]. In the former, it is assumed that the delay takes around one sampling period, and the next optimal control action is updated as the one to be applied two steps ahead [57]. The direct compensation is mostly implemented for FCS-MPC, which estimates the change of the measured state once the optimal switching pattern has been applied, and then it evaluates its further change according to all possible switching states. On the other hand, indirect compensation is considered for continuous-based techniques such as DCPC [58, 59] and GPC [60]. It consists of including the delay within the problem formulation, so

the predictive strategy solves the compensation problem itself.

2.3   Summary

This Chapter defines the operating principles and modelling of switched reluctance machine drives. The model is proposed in terms of the machine voltage equation and based on the concept of electrical angle. Flux linkage and torque static characteristics are discussed, and the relevance of saturation conditions for SRM operation is concluded. A brief description of the most popular power converter is also presented, along with a mention to diverse topologies in the literature. The fundamental concepts behind predictive control are also presented. A general classification of predictive control techniques implemented for SRM drives is proposed, and each technique is defined and formulated as a control block diagram. These concepts will help understanding the literature review and the previous works on predictive control for SRM in the next Chapters.

Chapter 3

Predictive Control of SRM Drives

As previously described in Section 2.1.4, the torque control of an SRM can be either defined as a DTC- or an ITC-based strategy. The latest emulates the FOC in AC drives defining a current reference that must be tracked by an inner current loop. Different control objectives can be translated into current shapes, thus simplifying the problem into a current control task.

Predictive control adopts the same structure, defining either predictive torque control (PTC), which is analog to DTC, or an outer torque control with inner predictive current control (PCC) loops, just like ITC. In SRM drives, the predictive-based techniques implemented to date have mostly followed one of these trends. Therefore, this chapter reviews these predictive control techniques for SRMs, comparing the characteristics, advantages and challenges still present. Besides, an analysis is presented regarding the opportunities and potential research elements that the existing publications leave to make this work complementary to the already existing surveys about predictive control.

The chapter presents the adopted classification and a literature review of PCC

Table 3.1: Current control in SRM drives

Control type	Control technique	Modelling approach	Calculation of reference voltage or switching state	Modulator	High-speed	Four-quadrants	References
Classic Current Control	HCC	Model-free	Hysteresis band	☐	☑	☐	[61]
	PI + PWM	Various	PI regulator	☑	☑	☑	[62]
	Delta modulation	Model-free	Hysteresis band	☑	☐	☐	[63]
	Back-EMF compensation	Various	PI regulator	☑	☑	☑	[64]
Predictive Current Control	DBPC	Analytical model / Static maps	Direct calculation	☑	☑	☐	[16, 65–77]
	GPC	Linearized transfer function	Continuous cost function	☑	☐	☐	[78]
	CCS-MPC	Analytical model / Static maps	Continuous cost function	☑	☑	☐	[45, 79–81]
	HPC	Analytical model / Model-free	Hysteresis band	☑	☑	☑	[82, 83]
	FCS-MPC	Discrete function / Static maps	Discrete Cost function	☐	☐	☑	[84–89]

and PTC strategies. The control techniques are analyzed according to their modelling approach, phase torque distribution, switching behaviour and calculation of optimal actuation variable. A performance comparison is also presented, and the current challenges and improvement opportunities are discussed. Furthermore, potential applications of predictive control are also described, and a general conclusion on potential research based on the literature review is directed, thus opening the discussion for future applications beyond the current works.

3.1 Current Control

Fig. 3.1 represents the ITC scheme on SRMs. In this figure, a current reference is obtained from an outer speed control loop, which defines the required torque. The relationship torque-current in SRM is defined as part of torque control techniques, in Section 3.2.

Current control in SRM is challenging due to the nonlinear phase inductance profile. As described in Section 2, the variable reluctance paths and the saturation produce a flux linkage that is a function of the electrical angle and the phase current. Failing in smoothly tracking the reference current might increase the torque ripple
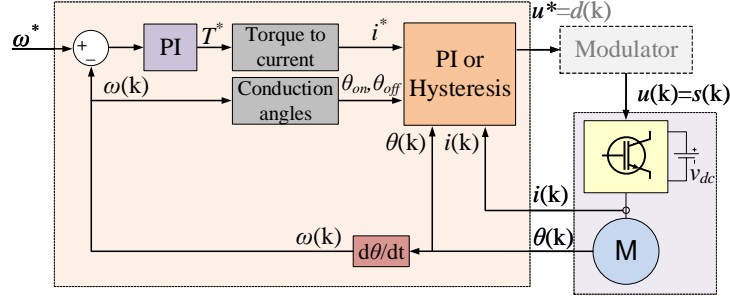
Figure 3.1: Conventional control loop for SRM

and even acoustic noise as a consequence of the high current ripples [9]. In addition, different current waveforms have been proposed, shaped to attack particular problems such as torque ripple during to phase commutation [12] or acoustic noise [3]. This section synthesizes the current tracking techniques commonly used in SRM, briefly reviews the conventional methods and describes the works using predictive control. Table 3.1 shows the classification of these control techniques and corresponding references.

3.1.1   Conventional techniques

In the conventional current control of SRM in Fig. 3.1, the gray blocks represent static maps, external to the control loop and calculated offline. In addition to the torque-to-current static map, the algorithm also requires the conduction angles θ_{on} and θ_{off}. These angles define the span of conduction per phase. The reference voltage is calculated and then applied to the inverter either by a modulation stage in the form of PWM or by choosing the switching states (direct actuation).

Traditionally, the use of hysteresis current control (HCC) is the choice for current

regulation in SRM. Its tuning is not complex, and it does not require to know machine parameters. This technique defines upper and lower boundaries and modifies the switching state to keep the instantaneous current within the error band. This direct-actuation controller provides proper reference tracking and dynamic response at the expense of variable switching frequency and high current ripples [9]. The HCC performance can be improved by adjusting the tolerance band [61] or including additional levels in the hysteresis logic [90]. Delta modulation also appeared as an effort to overcome the variable switching frequency of HCC, maintaining its dynamic response [63]. It uses a hysteresis response around the reference value to obtain a duty cycle, limited by a triggered system to set a maximum switching frequency. However, this frequency limitation comes with an inherent increase in the current ripples.

Proportional-integral (PI) regulators compensate for the error in the current tracking. The reference voltage is applied using a modulation stage as a PWM [90], providing a constant switching frequency and zero steady-state error [62–64,91]. The drawback is the limited transient response and the requirement of knowing the machine parameters to tune the gains properly. Although there exist methods to improve the dynamics such as the back-EMF compensation [64,92], the gains still might change at different operating points, and dynamic gains should be proposed [93,94].

3.1.2 Predictive current control

The algorithm of a general predictive current control (PCC) starts at the instant k, with the measurement of phase current $i(k)$ and rotor position $\theta(k)$, as shown in the Fig. 3.2. Then, the predictive model estimates the phase current in the next sampling period using the previous states and machine parameters. The predicted
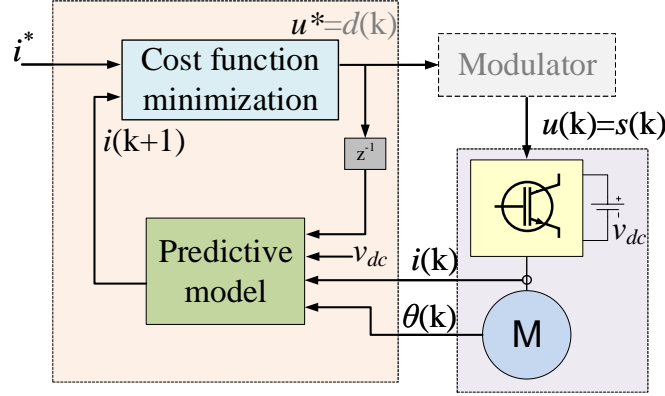
Figure 3.2: Conventional PCC

state in this case is the current $x(k + 1) = i(k + 1)$, which is used to determine the optimal input sequence $u(k + 1)$, representing the voltage reference. It is worth noticing that the use of $i(k+1)$ considers that the prediction has been compensated for measurement and computational delays [57]. The use of a cost function to minimize the control problem is optional, as, for instance, DBPC directly computes a duty cycle. The reference voltage can be applied either with a modulator or directly selecting the switching pattern. From Table 3.1, PCC modelling strategy, calculation of the actuation variable and switching behaviour adopted for SRM in the literature are analyzed.

Predictive model

Fig. 3.3 classifies the different modelling approaches adopted in literature for PCC in SRMs. An accurate model guarantees a proper tracking response for both transient and steady-state operation. Intuitively, it should use a current-based approach to represent the system as a state-space model; however, given its nonlinear inductance, a direct estimation of the current would require the solution of a nonlinear problem.
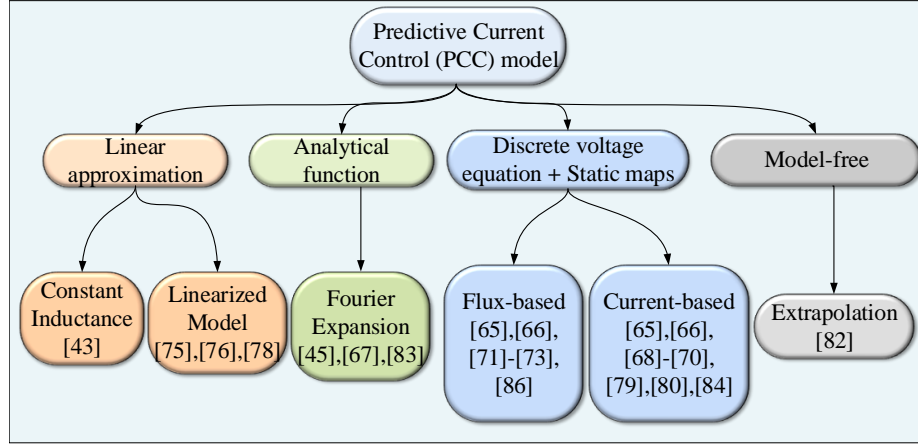
Figure 3.3: Modelling techniques adopted in literature for PCC in SRM

In the simplest case, the model neglects nonlinearities and considers a constant inductance value L in (2.3), which results in a first-order transfer function [16]. Despite the simplicity of this approach, in practice the dependence of the electrical angle is significant and, in consequence, non-negligible. An alternative has been the consideration of at least two inductance values at the aligned and unaligned positions, which gives the maximum and minimum inductance values, respectively. This sketches the flux and inductance like a triangular waveform as a function of the angle [77]. However, SRMs find their optimal energy conversion rate working on saturation [9], which requires the consideration of this condition. If saturation and fringing effects are also considered, then the static map in Fig. 2.2(a) is obtained.

Alternatively, linearization can be done on the nonlinear static map. This option has been brought by GPC, as in Fig. 3.1(b), presenting it as a transfer function [78]. The small-signal model can relate the phase current and the duty cycle D as a function dependent on the machine parameters [95], the speed and a constant to represent the

nonlinear inductance like,

$$G(s) = \frac{I}{D} = \left(\frac{2V_{dc}}{L(\theta)\omega_r\kappa(\theta) + R} \right), \tag{3.1}$$

where ω_r is the rotor speed, and κ represents the nonlinear variation of the phase inductance L with respect to the electrical angle. The expression in (3.1) is used as a plant in a closed-loop analysis in which parameter uncertainties are considered.

The discrete-time transfer function can be tuned based on the relay feedback method [95], which has been implemented for low power SRMs [78]. This model simplifies the use of GPC by defining the controller behaviour offline. Another option consists of assuming linear inductance values during a few sampling periods, which reduces the calculations but still allows nonlinear effects in longer control horizons [75, 76].

The problem with the linearization is that it compromises the accuracy of the flux behaviour, especially in the areas where the fringing effect is prominent. From Fig. 3.3, the next option is the use of analytical models. The representation using analytical equations has been a popular solution as it allows reconstruction of the static maps without compromising the memory usage of the processor with LUTs. It can also simplify the online calculations, depending on the obtained expression. The use of Fourier series expansion has been a suitable adaptation of SRM profile for analytical equations, expressed as [45],

$$L(k) = l_0 + l_1 cos(8 \cdot \theta(k)) + l_2 cos(16 \cdot \theta(k)), \tag{3.2}$$

where the coefficients l_0, l_1 and l_2 are tuned based on selected points of the static map
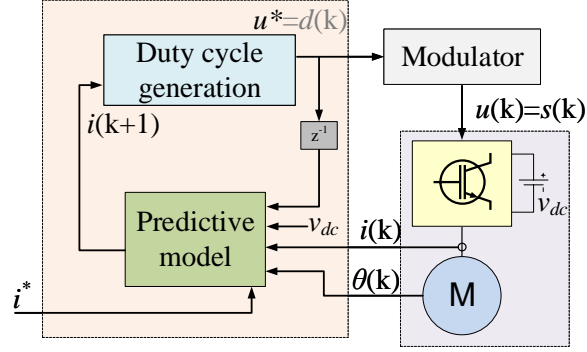
Figure 3.4: Deadbeat PCC

in Fig. 2.2(a). These points are usually chosen considering the rotor at unaligned (0° elect.), aligned, (180° electrical) and midpoint (90° electrical) [45, 67], but there could also be a third point aligned with the maximum back-EMF occurrence [83]. Besides, the obtained equation facilitates applying filtering techniques to produce a smoother prediction, even in four-quadrant operation [83]. The main drawback in this approximation is the assumption of invariable Fourier coefficients to map the nonlinearities for every operating point [79].

Next in Fig. 3.3 is the use of discrete-time models fed by static maps. For instance, current-based models have been parameterized with the inductance and back-EMF. These values come from static maps, which are usually obtained by FEA or self-commissioning, and updated online according to the operating behaviour of the machine [68, 69]. The discrete model can be easily implemented in deadbeat predictive control with discretization techniques such as the forward Euler approximation for the derivative terms. The block diagram of this technique is presented in Fig. 3.4. The variables at the times $(k+1)$ and (k) are obtained from look-up tables to estimate $v(k+1)$ as [65, 66, 70],

$$v(k + 1) = Ri(k + 1) + \omega \left(\frac{L(k+1)-L(k)}{\theta(k+1)-\theta(k)} \right) i(k + 1) + \epsilon(k), \tag{3.3}$$

where $L(k + 1) = \mathcal{L}(i(k + 1), \theta(k + 1))$ and the reference $\Gamma^* = i(k + 1)$ is used since a zero error is required.

MPC techniques, defined in Section 2.2.1, have been mostly based on discrete-time modelling. FCS-MPC can also use the discrete-time representation, in which the model is evaluated with all possible switching states to predict all possible phase currents and decide on the optimal one [84, 87]. Finally, CCS-MPC takes advantage of the model to define a convex space within a continuous cost function, which can be optimized to find a minimum point and solve the CFHOC problem [79–81, 89].

Although the use of inductance and back-EMF static maps requires additional memory, it is compromised by enhancing the accuracy of the prediction. Filtering techniques can improve the robustness against noise in the measurements and the prediction, while online adjustment of inductance values reduces the parameter sensitivity issues [69, 79]. However, the derivative term of the inductance and the additional difficulties it brings for four-quadrant operation make the use of flux-model more suitable for particular applications [67].

Flux-based models also address static maps, as shown in Fig. 3.3, but the flux linkage value is obtained instead of inductance. This allows using Forward-Euler discretization in (2.2a) to obtain a simple predictive model with a sampling period T_s,

$$\lambda (k + 1) = \lambda (k) + T_s [v(k) - Ri(k)]. \tag{3.4}$$

The use of (3.4) simplifies the prediction with the use of tables to obtain the flux using only measured variables [65, 66, 71–73]. In a more simplified way, it is possible to use a flux-based model and define the entire controller as a *virtual-flux* (VF) MPC control. The concept of VF was initially addressed in control of grid-connected
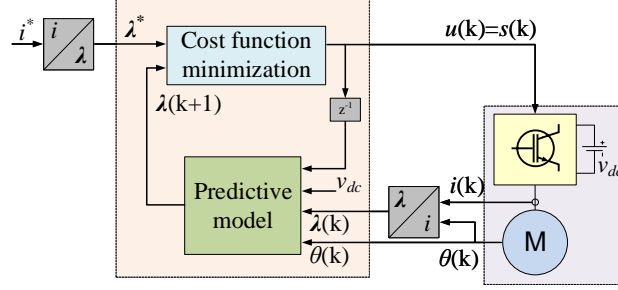
Figure 3.5: Virtual-flux FCS-PCC

interfaces [96] and permanent magnet machines [97]. This method performs the control in a virtual flux domain bringing several advantages such as simplification of the model and inherent linearization of the current-tracking problem. The algorithm tracks VF instead of current, being able to predict $\lambda(k + 1)$ using (2.2a). Fig. 3.5 shows a representation of the VF-PCC approach, in which both the sampled current and the reference current are mapped in the VF-domain, thus cancelling out the flux tracking and behaving like a current controller [86]. As the static map is external to the controller, it allows simplifying the closed-loop analysis and the evaluation of robustness or stability [98].

Another technique uses model-free predictive control, which has been successfully applied to AC drives [54]. This approach obtains the predictive variable based on regressions and extrapolations from the previous measurements. It has been applied to SRM drives by taking into consideration the error tracking instead of the current, and feeding it into a hysteresis regulator, as shown in Fig. 3.6 [82].

Calculation of the reference voltage

The reference voltage is computed in predictive control either by direct calculation using the predictive model in DBPC or using a cost function. In the first case, the
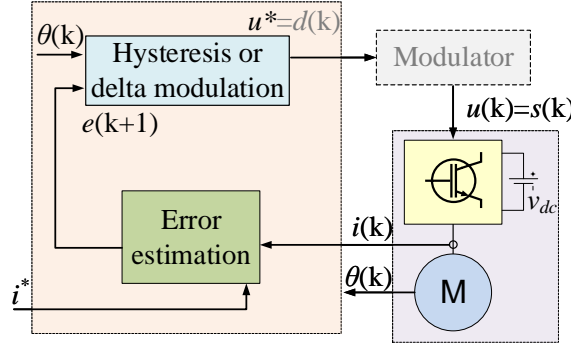
Figure 3.6: Hysteresis-based PCC

calculation has been implemented considering the sampling and switching behaviour to choose whether to use a current- or flux-based model, depending on the computational time [66]. Pre-computed duty cycles can also be implemented in the form of a decision table within the control loop, reducing computational burden [75, 76]. Although this method is known for its noise sensitivity and parameter dependence, it can be combined with static maps, which are updated every sample period, thus offering self-tuning characteristics [68, 69].

The use of a cost function offers flexibility with the possibility of including restrictions from different nature thanks to the incorporation of multiple objectives [20]. Fig. 3.7 shows the different cost functions proposed in PCC for SRM in the literature. As current tracking is a non-cascaded control, the cost function tends to be simple, considering only a primary objective [78, 84, 88]. Although in power converters it is also desired to reduce switching frequency by costing the input [45, 72, 79, 89], this limitation is not recommended as it worsens their behaviour.

The flexibility of the cost function allows to transcend the operational limits of the original system and, for instance, defining operating limits like the maximum current when VF tracking is the main objective [86], or controlling the machine as a battery
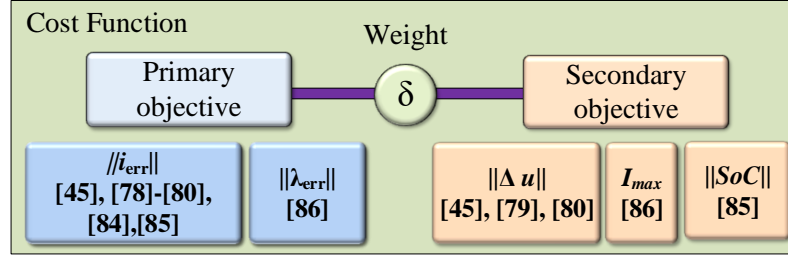
Figure 3.7: Objectives considered within the cost function on PCC for SRM

charger regulating current and state of charge (SoC) at the same time [85].

Switching behaviour

Table 3.1 includes a comparison of the switching behaviour of each PCC technique. The switching frequency depends on whether or not a modulator is used. On the one hand, the use of a modulator fixes the switching frequency but jeopardizes the dynamic response [37]. DBPC, CCS-MPC and GPC are the techniques conventionally using a modulator, but this can also be extended to HPC by including a delta-modulation strategy [82]. FCS-MPC, on the other hand, produces a variable switching frequency, which is inconvenient for high-power and high-voltage SRMs. The direct application of the switching pattern in SRM might cause an exaggerated ripple in the areas with the lowest inductance, that is, near the rotor unaligned position [9]. Research in MPC-based techniques has shown the possibility to overcome this limitation by modulated MPC strategies, primarily implemented for multi-phase machines [55].

3.1.3   Performance comparison and future trends of predictive current control

A four-phase, 8/6, 5.5 kW SRM with an asymmetric converter is simulated to evaluate the performance of these techniques. The flux linkage characteristic of the machine is depicted in Fig. 2.2(b). Two different reference currents are applied to the machine to compare the complete behaviour of the controllers: one produced by a torque sharing function (TSF) algorithm and the second from a radial force shaping (RFS) technique. A maximum switching frequency of 20 kHz is set for all simulations with an SRM running at constant 2000 rpm and 6 Nm.

TSF aims to reduce the torque ripple caused by the transition from one phase to the next one by distributing the total reference torque and current, among the individual phases. The transition between the phases is usually represented as a linear, quadratic, cubic or even sine function [99]. In this work, the cubic transition is considered, which affects its dynamics unlike the steady-state operation, which defines a constant current. Fig. 3.8a(a) shows the behaviour of the PI+PWM combination. Although this presents a proper steady-state response, it suffers delays, thus evidencing the limited dynamic response capability. HCC in Fig. 3.8a(b) has the best transient response, but it cannot track the decrements in current at the right rate of change, given the higher inductance around the aligned position. Moreover, the HCC is reported to be unable to operate in the four-quadrants due to the back-EMF [86]. VF-FCS-MPC in Fig. 3.8a(c) offers a good trade-off between dynamic response and phase turning-off tracking. It can also track the current in generating mode without modification in the control algorithm even though its steady-state tracking is inferior compared to PI+PWM. A more comprehensive analysis on the design and

(a) TSF-based   (b) RFS-based
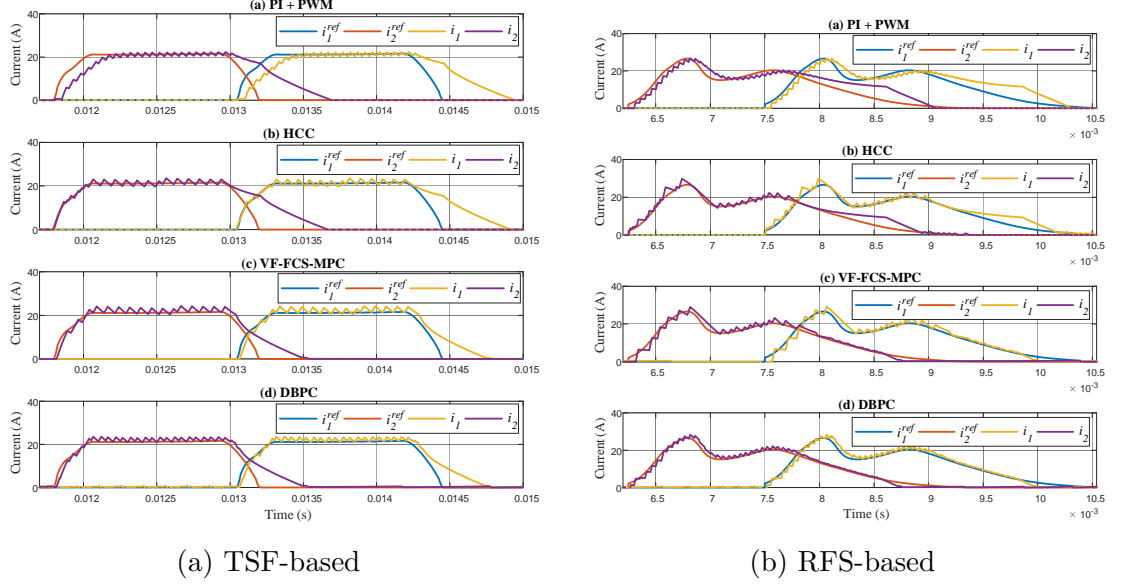
Figure 3.8: TSF and RFS reference currents and phase currents of 8/6 SRM (only phases 1 and 2 are shown) using (a) PI+PWM (b) HCC (c) VF-FCS-MPC (d) DBPC

performance of VF-MPC algorithm are presented in Chapter 6. Finally, DBPC in Fig. 3.8a(d) is comparable to FCS-MPC in dynamic response with a slightly better steady-state error.

On the other hand, Fig. 3.8b shows the reference and phase currents obtained by the RFS technique, which is aimed to reduce both torque ripple and acoustic noise in SRMs [3]. Unlike TSF, the waveform in RFS presents a dynamic behaviour, like a Gaussian curve which does not reach a constant value. As before, PI+PWM is limited in its dynamic response in Fig. 3.8a(a), while HCC in Fig. 3.8a(b) properly tracks the curves; however, HCC produces a higher error around the unaligned position and fails to regulate during turning-off. At the same time, both VF-FCS-MPC in Fig. 3.8a(c) and DBPC in Fig. 3.8a(d) accurately track the current reference, the latest technique providing a better current ripple.

Predictive control presents an improved dynamic operation with respect to the conventional PI. However, it still suffers from inaccuracies in current tracking for SRM when it operates near the unaligned position as previously reported [66]. The low inductance region makes the phase current sensitive to voltage transients and complicates the regulation task. A potential approach could be the use of higher switching frequencies in this region, or the implementation of multilevel inverters to reduce the machine terminal voltage. The latest has been implemented for torque control considering virtual voltages [55]; however, this technique inherently increases the switching frequency.

The previous techniques should also be considered to regulate the current in a wider operating range, i.e., at high-speed and generating mode. In fact, from Table 3.1, most of the presented work is focused at low-speed (below base speed) and in the first-quadrant operation, which limits the possibilities of evaluation of PC techniques in the regenerative braking region. This table considers that the method works for high-speed or four-quadrant operation if at least one of the references has considered these operating points. For instance, although DBPC should be suitable for regenerative operation, none of the presented works has evidenced its performance is such an operating point. However, other techniques have explored higher-speeds [73, 79, 80, 82] and four-quadrant operation [83, 86].

The review also shows that most of the publications consider only the conventional asymmetric converter. There exist different variations of the power converter to drive the SRM, as addressed in Section 2.1.3. The topology of the converter can be combined with the current control technique to propose other functions such as drive self-commissioning [68, 69] or battery charging in electrified vehicles [85]. Recent

works have also shown the applicability of predictive control in high-power SRMs, with an assessment focused on a 60 kW automotive traction SRM [100]. Results highlighted the importance of a more accurate model in machines with such rating and the simplicity to adapt techniques such as DBPC and MPC to improve current tracking.

Finally, the pole configuration and the number of phases in SRM is also an advantage of these machines, which can be selected according to the power rating and requirements. The most popular configuration is 12/8, which is suitable for low power $(0.5 - 10$ kW$)$ machines. There is still room for evaluation of the behaviour of predictive control techniques in high-power and high-pole configuration SRM, which are mainly suitable for traction in hybrid vehicles, e.g., the 35 kW presented in [75, 76] or the 60 kW one in [84].

3.2   Torque Control

In conventional AC drives such as permanent magnet machines, the electromagnetic torque production can be approximated to a relationship between the direct and quadrature axis currents, after a proper rotation of the phase currents has been applied into a rotating reference frame, usually at the synchronous speed. However, from Fig. 2.2(c), it is clear that such a mathematical approximation is not possible in SRM drives. If a similar structure as FOC wants to be adopted, a proper relationship between torque and current must be defined. This relation is illustrated in Fig. 2.7 as the torque-to-current static map, which is usually obtained from the inversion of the torque-current-angle LUT [9]. From these tables, current control tracks the obtained references, as discussed in the previous section. Alternatives include the

approximation to analytical expressions or the use of direct torque control (DTC). The use of predictive control can handle these issues either by deciding the optimal reference current online, or by selecting directly the switching states to emulate the DTC approach.

In this section, the main characteristics of the predictive torque control techniques applied to SRMs are discussed. A comprehensive literature review is presented and the different works are analyzed and classified. The general trend of PTC in SRM is identified as well as the current challenges and potential improvements based on the finding in literature. Finally, an assessment between conventional and predictive techniques is presented in simulation for a 5 kW SRM.

3.2.1 Conventional techniques

Torque control in SRM drives not only cares about maintaining an average tracking on a torque reference but also considers its ripple. Smooth torque control has been addressed by indirect regulation, which defines the current reference and relies on a current tracking technique, as shown in Fig. 3.1. The simplest approach uses the optimal activation angles θ_{on} and θ_{off} to guarantee taking maximum advantage from the torque generation capability of each phase [101, 102]. However, in order to obtain these optimal angles, offline optimization routines must be executed, thus increasing the algorithm development time and effort. In addition, the transition between one phase and the next one produces dips in the total torque, as the equivalent flux linkage is different at each phase, being the electrical angles different. Torque sharing function (TSF) appears as a response to the last issue. It considers a smoother transition between the outgoing and upcoming phases to minimize the torque dips

during phase commutation [17]. This transition has been proposed in a variety of algebraic functions of the electrical angle, being the most popular quadratic and cubic, due to the simplicity and smoothness [99]. Moreover, the resultant reference currents can be shaped offline in the so-called current profiling technique, thus saving computational burden [13].

Alternatively, the use of DTC bypasses the need of current loop and directly decides the control action based on predefined switching rules stored as LUTs [43,103]. DTC offers then a faster transient response with a robust structure, but it lacks on simplicity due to the extra effort on calculating the complex switching tables offline. For this reason, the direct instantaneous torque control (DITC) is currently the most popular technique for torque ripple minimization, as it uses a closed-loop structure to directly regulate the torque error with a simple hysteresis law [104,105]. It provides satisfactory results but fails to regulate it at a wide speed range. Furthermore, both DTC and DITC lack of current regulation, thus loosing control on transients on the phase current and potentially decreasing efficiency. Recent works have addressed this issue, but it requires additional features such as adaptive controllers and multi-stage control laws [106].

Table 3.2 presents some of the conventional techniques for torque ripple minimization in SRM as well as some of their main features and references.

3.2.2 Recent torque control strategies

Recent trends in torque control of SRMs have followed a similar approach as conventional techniques, being these classified into the ITC and DTC categories. DTC strategies have adopted secondary objectives to enhance the machine operation, being

Table 3.2: Torque control in SRM drives

Control type	Control technique		Need for offline calculations	Calculation of reference voltage or switching state	Modulator	Current regulation	High-speed	Four-quadrant	References
Classic Torque Control	DTC		☑	Switching table	☐	☐	☐	☑	[43]
	DITC		☑	Switching table	☐	☐	☐	☐	[104]
	ITC with optimum conduction angles		☑	Inner current loop	n/a	☑	☑	☑	[101, 102]
	TSF		☑	Inner current loop	n/a	☑	☑	☑	[17, 99]
	Current profiling		☑	Inner current loop	n/a	☑	☑	☑	[13, 107]
Predictive Torque Control	DBPC		☐	Direct calculation	☑	☐	☐	☐	[27, 108–112]
	GPC		☑	Continuous cost function	☑	☐	☐	☐	[113]
	FCS-MPC	Conventional	☐	Discrete cost function	☐	☑	☑	☐	[114–121]
		VF-FCS-MPC	☐	Discrete cost function	☐	☑	☑	☐	[122, 123]
		VV-FCS-MPC	☐	Discrete cost function	☑	☑	☐	☐	[124]

the most relevant for electric drives the torque-per-ampere ratio [125, 126]. The controller designs have also included the use of online torque sharing optimization, even adapting genetic algorithms into the closed-loop control [127]. More complex alternatives have included neural networks to capture the nonlinear relation between torque and flux, thus obtaining a flux linkage sharing and an inner virtual-flux tracking [128]. The use of DITC has also been improved with respect to early works. In [129], for instance, the hysteresis torque stage is replaced by a PWM-based component with online compensation, thus improving the resultant torque ripple.

The ITC-based techniques have recently adopted formulations with higher complexity in order to guarantee a more accurate torque tracking. For instance, in [130], the proposed technique generates a reference current and flux to achieve the desired average torque based on the flux-current characteristics and the estimated torque production from the stored magnetic energy. Hybrid control using both current and virtual-flux ensures the proper tracking of the electromagnetic torque from the flux linkage characteristics.

Finally, as SRM finds its most promising operation at high-speed, a unified control

for a wide speed range is of interest. This control has been proposed by a combination of both DITC and ITC as a function of both the speed and the rotor position, taking advantage of DITC during magnetization and ITC for constant current and demagnetization of each phase [131]. However, the transition between different techniques might compromise the stability, and the implementation of previously mentioned techniques result in complex development or tedious implementation. Predictive control instead has the potential to perform a unified control with development simplicity and good dynamic response.

3.2.3   Predictive torque control

Predictive torque control (PTC) can be considered as an extension of DTC, where a predictive model is used to estimate the future behaviour of the drive, and a cost function minimizes the output error. The control diagram for a FCS-PTC is depicted in the Fig. 3.9. The output variable $y(k) = T(k)$ as the total electromagnetic torque, product of the algebraic sum of the phase torque ($\sum T_{ph}$). However, total torque is not usually measured directly from the shaft, or the ones used do not provide sufficient resolution to identify ripples; therefore, the torque is obtained through the static map in Fig. 2.2(c) fed by the phase currents $i(k)$ and electrical position $\theta(k)$. After a delay compensation, the predictive model estimates the future torque $T(k+1)$ and current $i(k+1)$ and uses a cost function to track the reference torque T^* while imposing a current limitation with a weight factor δ_i [114]. It is worth to highlight that $T(k+1)$ is an n-size array, where n is the number of possible switching states, being $3^4 = 81$ in the four-phase SRM. Although the evaluation of 81 possible outcomes is certainly a drawback of this technique, there are several methods and proposals to reduce
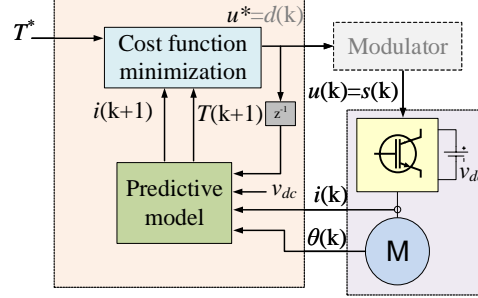
Figure 3.9: FCS-Predictive torque control in SRM

(a) Deadbeat predictive torque control

(b) Virtual-flux deadbeat predictive torque control
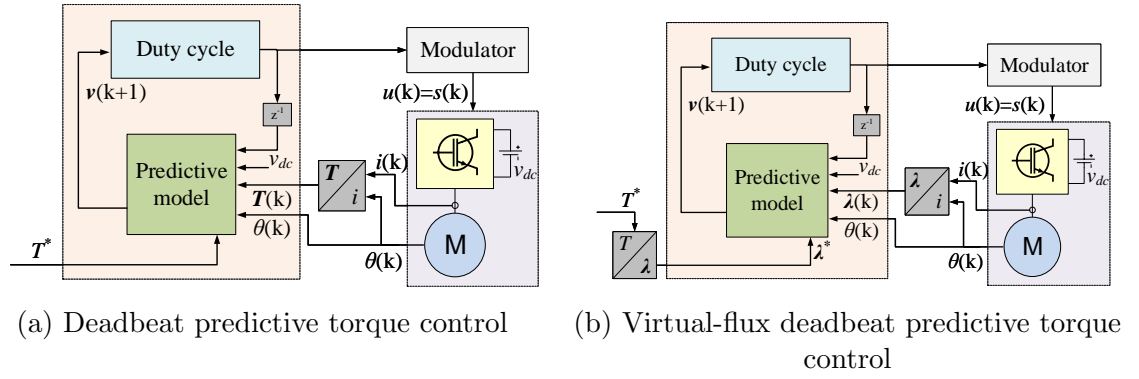
Figure 3.10: Deadbeat predictive torque control techniques for SRM drives

the number of computations. The simplest alternative evaluates only the phases that should be active according to the rotor position, thus the size n is reduced to maximum $3^2 = 9$ during phase commutation, and only 3 during single phase operation [116].

Another option uses the deadbeat predictive control (DBPC) just like in current control. In this case, the deadbeat predictive torque control excludes the cost function and calculates the control action $v(k+1)$ that makes $|T^* - T(k+1)| = 0$. The optimal voltage is then applied through the modulator which fixes the switching frequency. In addition, the torque can also be mapped into the virtual-flux domain, as illustrated in Fig. 3.10a where a virtual-flux deadbeat predictive torque control is proposed.

Fig. 3.10b uses a current-to-flux and a torque-to-flux static maps to represent the
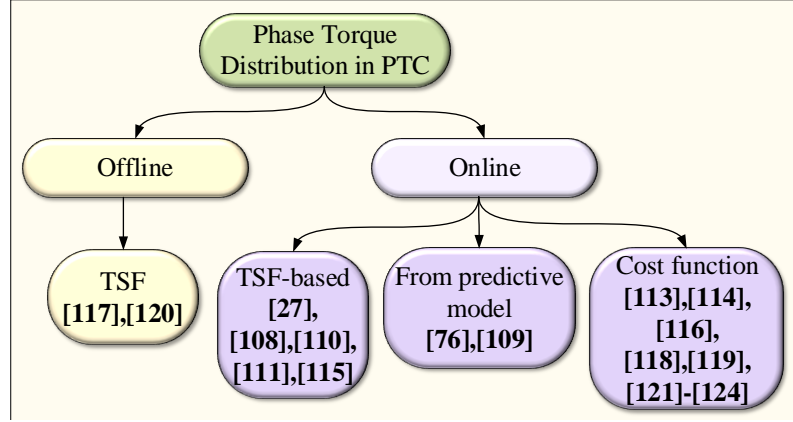
Figure 3.11: Phase torque distribution used for PTC for SRM drives

control task into the *vf* domain. Although it requires higher memory allocation for two LUTs, this technique simplifies the prediction allowing using (3.4).

As seen in Figs. 3.9-3.10b, PTC is analyzed according to its predictive model, the technique to determine the control action (cost function or direct calculation) and the switching behaviour. In addition, as the SRM torque comes from the individual phase torque contribution, there are differences in the method used to determine the torque sharing as a function of the shaft position. These characteristics are discussed next.

Phase torque sharing

Fig. 3.11 summarizes the different strategies to split the torque reference among the phase torque contributions. Predictive torque control in SRM can be designed to distribute the phase torque references either *offline* or *online.* In the offline approach, techniques such as TSF can define the optimal reference phase torque as a function of the electrical angle; therefore, the input to the predictive algorithm is a vector of m references, with m being the number of phases. The predictive control technique

then identifies the optimal switching pattern to track the individual references. As the torque sharing is defined offline, these techniques can be easily implemented in machines with multiple phases [117, 120]. It also allows spending more computational power into the current regulation at higher speeds [12]. The main drawback is the consideration of static maps for the torque sharing, as the distribution might change with the parameter variation or at high speeds.

The TSF principle can be easily implemented online by considering the maximum torque that each phase can produce, according to its electrical position. In this way, priority is given to the phase with the highest torque contribution, while the difference between the reference torque and the produced torque is assigned to the upcoming phase [27, 108, 115]. These torque assignments can be dynamically modified by adding weight factors that penalize for low efficiency or potential faults [110, 111].

The problem with the use of TSFs is the consideration of the torque as a simple algebraic distribution between the phases, neglecting the further interaction between them. Alternatives using predictive control have included an implicit phase distribution [109], or even the mapping of the whole system into a rotating frame, where it can use conventional DTC for AC drives [122]. This is further simplified by representing the torque variables into a virtual-flux domain.

Another option is just to let the cost function decide. As the cost function evaluates the optimal switching, it can be extended to evaluate which combination of all phase contributions tracks better the torque reference [114, 116, 118, 119, 124]. This brings also the advantages of including restrictions of different nature into the torque sharing, thus improving the algorithm flexibility. Of course, this has been simplified as a virtual-flux tracking too [122, 123]. These techniques, although promising,
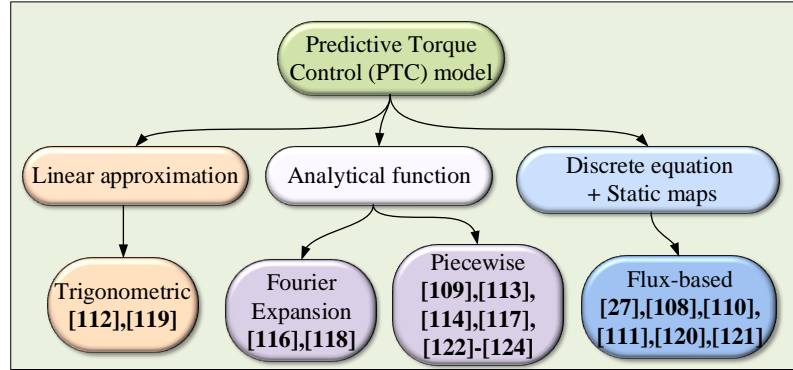
Figure 3.12: Modelling techniques of predictive torque control in SRM

have not been tested in generating mode or in a full-speed range. The high speed operation is especially interesting in SRM as the cost function must allow certain negative phase torque for angle advanced, required to build-up currents at such speed and back-EMF. As a response, adaptive commutation angles are proposed to enhance these conditions [121].

Predictive model

Fig. 3.12 summarizes the models used in PTC for SRM and the references. Predictive models for current control were discussed in section 3.1.2, but they require additional considerations for torque estimation. From definition, the torque depends on the energy stored in the machine magnetic circuit; therefore, a proper knowledge of the flux linkage is expected. Just as the techniques for phase current prediction, the simplest approach represents an inductance L as a function of electrical angle based on aligned and unaligned conditions, and then extended to calculate the torque based on [112, 119],

$$T = 0.5i^2 \frac{\partial L}{\partial \theta}. \tag{3.5}$$

However, a dependence of inductance on the electrical angle is expected, given the saliency of the machine. A common alternative to represent flux in current control relies on Fourier coefficients, which can be extended to compute the torque based on the expression (3.6) [116, 118],

$$\lambda = \lambda_s(1 - e^{-p(\theta)i}) \tag{3.6a}$$

$$p(\theta) = \alpha + \beta \cos(q) + \gamma \sin(q) \tag{3.6b}$$

$$q = N_r\theta - (j-1)2\pi/3, \tag{3.6c}$$

where N_r is the number of rotor poles, j is the active phase, and α and β are empirically found. The uncertainty of heuristically tune the constants above is the main drawback of this technique. A variation of an angle-dependent function considers the use of a piece-wise function denoted in (3.7) [132]. The use of $p(\theta)$ simplifies the flux as it is a function of the current independent from rotor position. It has been successfully adapted to PTC in [109, 114, 117, 122–124].

$$p(\theta) = \begin{cases} 128\frac{\theta^3}{\pi^3} - 48\frac{\theta^2}{\pi^2} + 1 & \theta \in [0, \pi/4] \\ f(\frac{\pi}{2}) - \theta & \theta \in [\pi/4, \pi/2]. \end{cases} \tag{3.7}$$

Finally, the direct use of static maps like in Fig. 2.2(b)-(c) allows getting a simpler and straightforward control development, at the expenses of higher memory allocation and even computational burden required for the interpolation within the LUTs. Nevertheless, they seem to be the most popular for PTC applications, as they provide accurate parameter information with a simple predictive stage [27, 108, 110, 111, 120, 121], allowing to improve the predictive algorithm in other aspects such
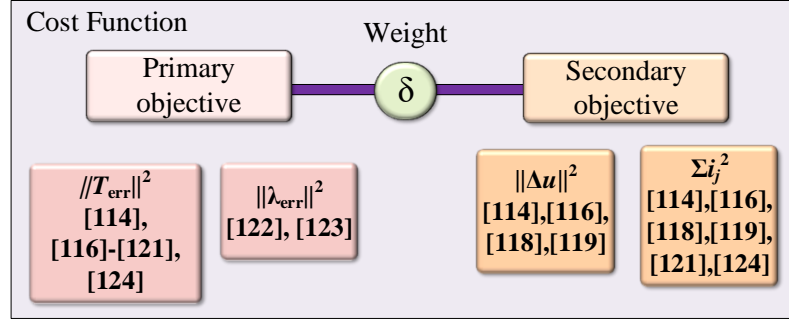
Figure 3.13: Cost function objectives in FCS-MPC for torque control in SRM

as the cost function. This can potentially lead to the optimization of the required memory space and a good performance [133].

Calculation of actuation variable

Once the torque sharing and prediction stages are defined, the use of the predicted variable can lead to the control action either through a calculation process or a cost function. The first alternative has been implemented in deadbeat control through different approaches.

Both the phase currents and the reference have been mapped into an equivalent rotating frame, where the virtual-flux λ_{dq} allows operating an algorithm similar to AC drives, even with the space vector modulation stage [76]. The virtual-flux have been also implemented in the natural frame, as it can be represented by the simple discretized voltage equation in (3.4), and the optimal reference voltage can be calculated and applied through a modulator [27, 108–111].

However, unlike PCC, table 3.2 evidences preferences for using a cost function, as torque control requires the regulation of variables of different nature, being these currents, flux and torque. Fig. 3.13 summarizes the different designs of cost function

considered in the literature to determine the actuating variable. As expected, the primary objective tends to be either the minimization of torque error [114, 116–121, 124] or its equivalent in the virtual-flux domain [122, 123]. Secondary objectives include the phase current limitation as a safety measure and to reduce conduction losses [114, 116, 118, 119, 121, 124]. The reduction on switching losses is also considered by limiting the number of switching transitions Δu [114, 116, 118, 119]. However, the dynamics of a cost function is heavily impacted by the selection of secondary objectives. Therefore, the inclusion of a δ factors as a weight is common in MPC applications. To simplify the tuning process of these factors, an adaptive time-varying cost function has been proposed [134], which guarantees robustness and high performance, but increases the computational load.

Another common practice in MPC is to add safety penalization. On top of the reduction of the phase currents, another term is usually added to the cost function. This term only has an associated weight if $i(k) > I_{max}$, and the assigned weight makes the cost function tend to infinity, thus avoiding that particular solution [119].

A novel approach have considered the use of virtual states. The idea is to evaluate the cost function with virtual switching states that provide terminal voltages in between V_{dc} and zero. These states can be synthetized later by a modulation state and the volts-second approach, just like in conventional space vector modulation [124]. This not only allows obtaining a better dynamic response having more voltage states but also fixes the switching frequency. The drawback of this technique is the inherent increase in the switching frequency.

Switching behaviour

The use of deadbeat of generalized predictive control use a modulator with a fixed switching frequency, which results in a better loss distribution among the switches. This has been considered for SRM drives using both duty cycle calculations [27, 108–111] and conventional space vector modulation [112, 124].

On the other hand, FCS-MPC eliminates the modulation stage raises some problems related to loss distribution and thermal management of the semiconductor devices as a trade-off for simplifying the control development and improving the dynamic response [114–123]. Other applications have pointed solutions for this problem such as the use of modulated model predictive control (MMPC) [135, 136] or MPC-PWM [137]. A control with a variable switching frequency results in a non-uniform switching loss distribution among the switches, thus making the thermal management of the switches more challenging. The objective becomes then the reduction of the maximum and average switching frequency. There have been several approaches to alleviate this issue. The simplest solution is the increase of the sampling period, which reduces the switching frequency, and therefore the related losses [138]; however, this requires a more accurate predictive model if the same performance is expected. An alternative solution includes a term in the objective function to limit the changes in the state of power switches in a prediction horizon [114, 116, 119]. Although the latest has been widely adopted in MPC, other alternatives include the restriction of the next switching states based on the previous ones [139], the prediction of the switching losses to be included in the optimization problem [140], and the inclusion of advanced variables like the frequency domain representation of the output waveform [141]. Most of these techniques compromise the memory usage, computational

time or dynamics of the control strategy. The use of virtual filters with low computational burden into the cost function has also been evaluated [142]. More recently, the attempt of getting the dynamics of FCS with a fixed switching frequency appeared with the use of virtual voltages, in which an optimum voltage $v_{vv} < v_{dc}$ is applied to the converter by shopping the terminal voltage during the same sampling period, just like the volts-second strategy in SVM [124, 143].

3.2.4   Performance comparison and challenges of PTC

Fig. 3.14 presents an estimated comparison between the different predictive control techniques based on the results presented in the literature and the references in Table 3.2. In terms of dynamic response, DBPC is the fastest one, with the minimum steady-state error even though it does not have an integration stage as MPC, but the method itself provides a one-step elimination of tracking error. However, this feature compromises its robustness, making it more sensitive to noise measurements and parameter mismatches. Although all predictive-based techniques are sensitive to such variations, DBPC has been reported to have major effects from it, being equivalent to an FCS-MPC with one-step predictive horizon ($N_p = 1$) or a multi-step prediction without penalization on the control effort [144]. GPC has lower computational time as most of the optimization is performed offline [56, 113]. On the other hand, FCS-MPC has demonstrated a better disturbance rejection capability [116] and improved robustness against parameter uncertainties. With the proper penalization on the control effort, ripples and harmonics can be also minimized using this technique [144]. In terms of computational burden, MPC offers a trade-off increasing its complexity exponentially when the predictive horizon (and so robustness and closed-loop stability)
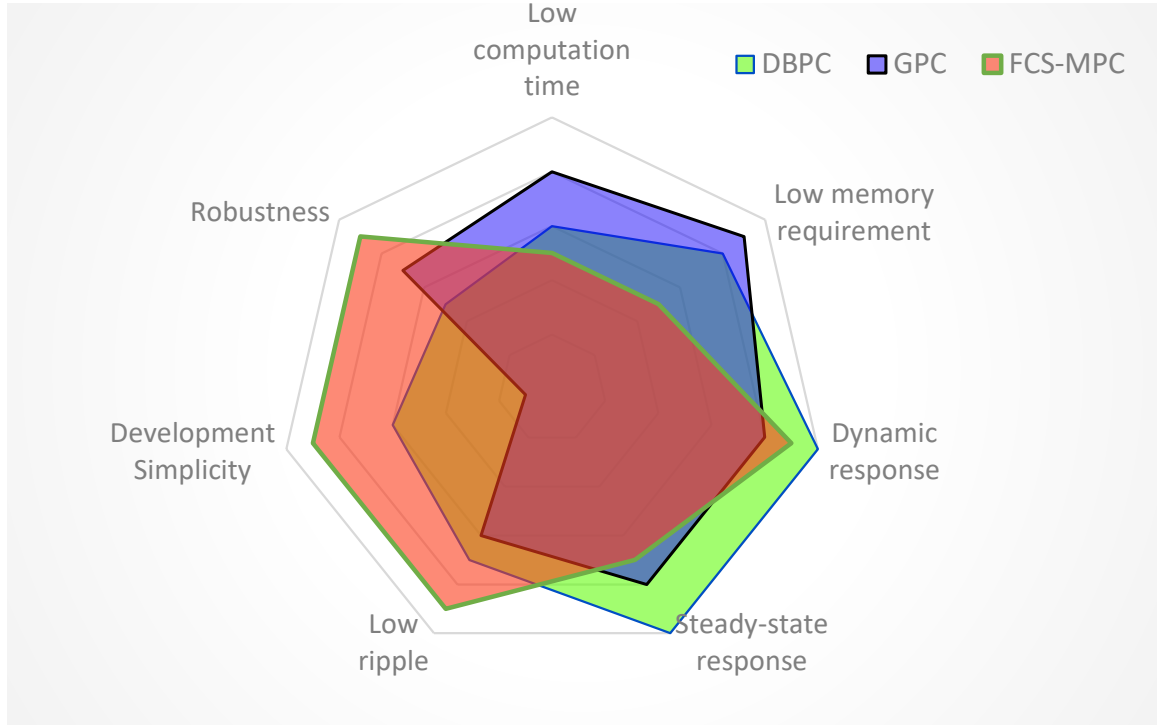
Figure 3.14: Estimated comparison between predictive control features in terms of performance and computational requirements

is increased. In addition, being the use of static maps a preferred option in SRMs, the use of FCS-MPC calls for an increased memory allocation of lookup tables, required to evaluate the model within all possible switching states, thus increasing the computation time as a function of the number of phases. The popularity of FCS-MPC for torque control has risen, initially, due to the simplicity in the CFHOC problem formulation, the robustness of the technique, and the possibility to reduce its computational burden by limiting the search space [145], or by including an equivalence to a reference voltage vector [24].

3.3   Other Predictive Control Objectives

3.3.1   Predictive speed control

Additional to current and torque control, predictive speed control has been targeted for SRM, which finds GPC as the most suitable technique, given the low time constant and relative simplicity of mechanical systems [146–148]. This approach has been improved by considering the nonlinear variations in the model and including dynamic coefficients within a discrete transfer function, later embedded in a commercial DSP [149]. Other applications include the use in lower power SRM for use in smart buildings [150] or the use on SRGs [151]. It is also extended to position control in the machine [152, 153].

3.3.2   Overload control

Beyond the rated values, every drive is able to deliver a peak power for a limited time without risking its integrity. Overload control has applied a predictive model to determine the most efficient limitation for the transient and steady state torque reference. This can be conveniently operated with a DBPC approach, thus guaranteeing maximum efficiency, even in such extreme operating conditions [154, 155].

3.4   Trends and Opportunities

This section presents an analysis on the trends and opportunities of MPC for SRM and their potential applications based on the existing work already reviewed.

There exist also an important number of applications that has not been considered

yet, but which can potentially boost the use of switched reluctance machines as well as improve several innovative applications. A more comprehensive description of this vision of future applications is presented in the next Chapter.

3.4.1   SRM topologies and power rating

The three-phase 12/8 machine adopted for this work has been the most common used SRM topology for low-power applications [9]. In this way, predictive control has been limited to low-power, low-voltage systems, with only a few cases evaluating high-power machines in simulation conditions. To date, the maximum reported power has been 35 kW for current control [75] and 15 kW for PTC [76, 122]. However, there is still potential for predictive control in higher-power machines (> 50 kW) [156], which tend to be designed with a higher pole configuration, such as the 60 kW 24/16 in [101], designed for hybrid vehicles. The increase in the dc-link voltage is also trending in power converters, thus making more attractive the use of SRM, given it enhanced dc-voltage utilization, especially at high-speed [1]. However, the control in the high-speed region becomes more challenging; therefore, the use of predictive control to handle both, high-speed and optimal dc-link voltage utilization is a challenge. Moreover, only conventional SRMs have been analyzed so far, leaving other topologies such as mutually coupled SRM (MCSRM), Segmental rotor SRM or double stator SRM (DSSRM) still open for further research opportunities for predictive control.

Technologies, challenges and potential applications of SRM drives have been already analyzed [157, 158], but the use of new predictive control techniques can accelerate its commercial attractive.

3.4.2 Applications in electrified powertrains

Although SRMs fail to deliver a smooth torque and low NVH levels, its potential to operate in post-fault and high-speed conditions as well as with a high dc-link utilization are far beyond conventional AC drives, making them suitable for electrified powertrains [1]. An unified controller able to handle these diverse operating conditions is a challenge that fits predictive control features.

SRMs are ideal candidates for post-fault operation because their phases are independently controlled and the torque depends on the contribution of each of them; therefore, the machine can easily operate, with a reduced torque, in case of phase disconnections. This feature is important for electrified vehicles, especially since they are related to safety issues [159]. Besides, the non-active phases can be exploited for other functions such as sensorless control, thus improving the drive robustness. This variety of operations and structural differences would require several modifications in the control strategy, which can be simplified with predictive control and strategically designed cost functions.

Another integration factor with electrified vehicles is the possibility to empower the particular topology of SRM and operate it also as an on-board battery charger [160]. This would require a especial configuration and controller, which can be managed by predictive techniques. This area has been already explored in SRM, with particular applications of MPC [85].

3.4.3 Power electronics and converter topologies

The trend in automotive sector is going towards 800 V dc-link [161]. This represents a challenge in SRM control given the low inductance at unaligned rotor position.

This phenomenon is discussed in detail in the part I of this survey *fundamentals and current control.* The use of multi-level converters as proposed in [162] is an alternative to alleviate this condition. Given the enhanced complexity in control that multi-level topologies would mean, predictive control techniques will be highly suitable to handle this task. Besides, increasing the switching frequency might be possible with the new generation of wide band-gap devices such as gallium nitride (GaN) or silicon carbide (SiC) [163], which represents a boost for the application of predictive control.

3.4.4   Control strategies

Despite the advances in predictive control for power electronics and drives, it is still the beginning for its application in SRM drives. Multiple strategies have been already implemented in conventional drives to guarantee predictive control optimal performance under a wide operating range with high robustness and reduced computational burden [164]. It is also a promising controller for new-coming complex drives [165]. Based on the literature presented in this work, the first steps in improving the applications in SRMs is to identify accurate models to improve the accuracy and properly design cost functions and weight factors. A totally different alternative has been the elimination of both of them, with model-free predictive control [54] and the elimination of weight factors with nested predictive control [53].

3.5   Summary

Predictive control has recently been of interest for researchers due to their enhanced performance for controlling power electronics and AC drives, especially improving the

dynamic response. Predictive control has also shown the ability to handle nonlinearities and multiple objectives of systems with high complexity. These characteristics make predictive control strategies suitable for switched reluctance machine drives, given their highly nonlinear behaviour.

The first part of this two-part survey presented the fundamentals of predictive control, its classification, the nonlinear model of the SRM drives and their predictive current control strategies in the literature. These strategies were classified according to the particular technique, the modelling approach, switching behaviour and calculation of the optimal input.

The use of Fourier approximation and discrete equations with static maps are the most used modelling techniques. The first ones compromise accuracy and increase offline computational effort, while the second option increases memory usage. Also, although the use of cost function adds flexibility to the control task, the direct computation of the deadbeat predictive control is a commonly adopted technique for current control given the fixed switching frequency, simplicity and proper tracking. Its performance also offers reduced ripple, but it fails in flexibility for disturbance rejection and four-quadrant operation, unlike CCS- and FCS-MPC. The review unveiled a vast potential for improvement in the high-speed and four-quadrant operation of PCC, where MPC-based strategies might be more suitable. The performance of these techniques can also be enhanced by using multilevel converter topologies or reducing the average terminal voltage in the machine. The application on high-power SRMs can also be further explored, especially for cutting-edge technologies such as automotive applications, where the use of the simple magnet-free structure of SRMs is most attractive.

Chapter 4

Vision, Challenges and Future Trends of Predictive Control in SRM Drives

In Chapter 3, a literature review of how predictive control has been implemented in SRM drives was presented. The analysis allowed to understand the current trends in predictive current and torque control as well as emerging applications like overload (thermal) control and the use of predictive techniques for self-commissioning and on-board charging applications.

In this Chapter, the analysis goes further, and the different uses of model predictive control that have not been considered for SRM drives are discussed. In this way, this Chapter presents a vision on how the use of predictive control can boost the operation of SRMs and defines a road-map of research objectives to do so. The analysis is founded on the basis of successful applications of MPC in other electrical drives and how these might improve the performance of the current techniques used

for SRM. The content is divided as follows: initially, recent developments and applications of MPC in conventional AC drives are presented. Next, control objectives of interest for SRMs are presented, as well as a brief explanation and review of the current techniques to handle them. Besides, some applications of predictive control to solve the same objectives in other systems are mentioned, and the challenges and benefits of adapting them to SRMs are discussed. Finally, a vision on how different applications of interest for high-performance MPC-driven SRMs are presented.

4.1   Recent developments of MPC

The design process of an MPC algorithm considers its performance in terms of the predictive model, cost function, prediction horizon and frequency characteristics to guarantee stability with the lowest memory use and computational load [166]. The predictive model dictates the accuracy of the control action, which would allow a reduction on the sampling. It must consider both the precision of the model and the discretization procedure, as it is implemented in a digital platform. SRMs electromagnetic modelling is a well-studied field, and options for an accurate estimation are available. A comprehensive review of electromagnetic models is presented in [167]. In terms of discretization, the most common approach is the forward Euler approximation due to its simplicity and good performance. A more complex but accurate option considers Taylor approximation instead [168]. Other techniques involve more accurate results but require extensive or multi-step computations [169]. Recent trends have also considered model-free predictive control [170], which has been applied to SynRMs for current control [54], guaranteeing high-performance without concerns on parameter mismatch or nonlinearities.

The cost function defines the behaviour of the control action. Their main feature is the ability to handle multiple variables from different units and magnitude, thus improving the flexibility. However, depending on the impact on the system performance, a weight on these variables is required. The process to calculate these factors is usually based on heuristic techniques [166], thus increasing the development time and effort, plus the additional simulation and testing. Alternatives for tuning have been explored as multi-objective optimization of multiple cost functions with priority coefficients, or cascaded (or sequential) cost functions [171]. The latest presents promising performance with reduced computational burden and simple development time, omitting the use of weight factors or priority coefficients. An alternative is the simplification of the cost function by analytically calculating an equivalent reference voltage vector [24, 172] or a group of virtual voltages [173].

The switching frequency can be fixed using CCS-MPC, but recent alternatives have also evaluated the use of modulated model predictive control (MMPC) [174], which adds a modulation stage to the output of the FCS-MPC. An alternative has been the adaptation of vector control for AC drives within the predictive control [175], also considered for SRMs with a deadbeat approach [176]. The output frequency can be also limited by increasing the prediction horizon, but it usually involves a much higher computational load. This has been recently addressed by techniques such as the sphere decoding algorithm [177], and successfully implemented for AC drives for a horizon up to four steps ahead [38]. Other advanced techniques include the use of higher computational power to increase the prediction horizon with simpler strategies, as the case of using cloud robotics [178].

Finally, as any control technique, MPC must be able to guarantee robustness and

stability. Recent works have proposed a Lyapunov-based MPC on both CCS and FCS that proves stability for a given cost function and any prediction horizon applied to power converters and PM drives [98, 179].

4.2   Challenges and future trends

The full potential of SRM drives for different operating conditions and applications have been already discussed and comprehensively analyzed throughout different works [1, 157, 180, 181]. The main takeaway points converge in their advantage to operate with a natural field-weakening mode due to their high-speed back-EMF, as well as their fault tolerant and DC-link voltage utilization capabilities. Fig. 4.1 summarizes some of the main features of SRMs with respect to conventional induction motor (IM) and permanent magnet synchronous motor (PMSM) drives. The higher the value presented in the figure, the better the machine is on that particular objective. For instance, SRMs get the lowest score in NVH given their high acoustic noise and vibrations. Unlike the comparison presented in [1], this paper separates the efficiency according to the speed range, as evaluated in [2]. Therefore, although SRMs cannot compete in performance at low speed, their outstanding high-speed efficiency give them benefits in this region, and their capability to go beyond ultrahigh speed limits enhances its field weakening score.

Current SRM technology cannot replace IM and PMSM for industrial and automotive applications, respectively. However, if their main drawbacks are regulated up to the minimum requirements of certain applications, it is possible to enhance their comparative advantages and define a potential cluster of interest. In fact, most of the targets for SRM designs and prototypes, as well as existing commercial applications,
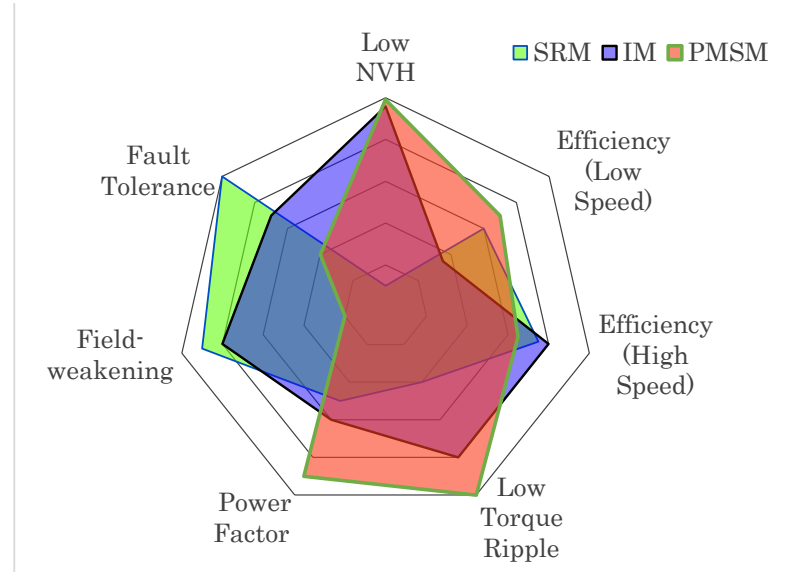
Figure 4.1: Comparison based on reported SRM performance [1, 2]

aim for medium- and high-speed. Fig. 4.2 shows a comparison of IMs and PMSMs targets [182], as well as the maximum power and speed capabilities of SRMs in the literature, both in design and tested prototype stages [183]. It is noticeable how SRMs are complementary to other drives and thus should not be targeted to replace them but to enhance their operative range [184–193].

However, at medium- and high-speed, the control becomes more challenging as nonlinear effects such as iron losses gain more relevance. Rotor position sensing becomes also a problem, which adds-on the already existing nonlinear characteristics of SRMs. It is clear that real physical phenomena contain nonlinearities, and assuming linear control objectives for high-performance systems nowadays is outdated. In addition, an unified control strategy is required for SRMs simultaneously accomplish a minimum performance while it can exceptionally cover certain objectives for particular applications.
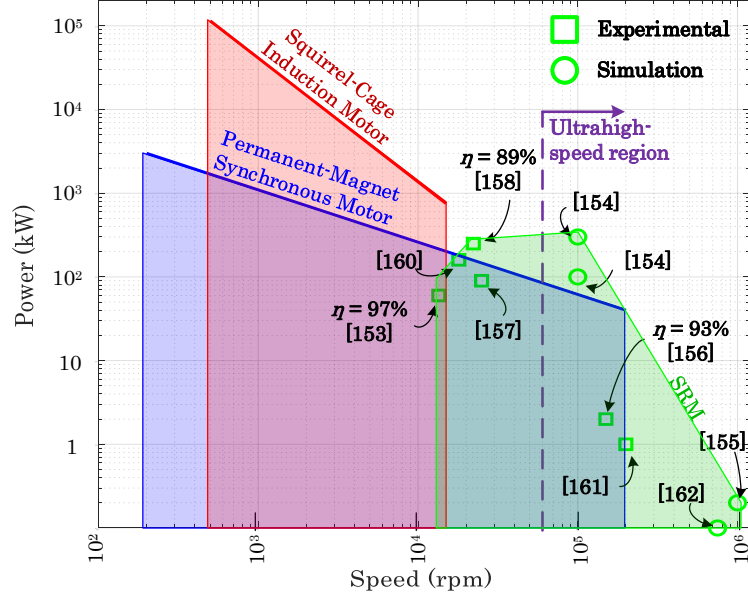
Figure 4.2: Target power levels and designs of SRM drives with respect to conventional AC drives

Therefore, MPC is a relevant response to these nonlinearities and flexibility requirements. It has been already considered for some applications in SRMs, as summarized in Chapter 3. However, this field can be still considered to be at an early stage, as several relevant control objective have not been considered while they have been fully addressed in conventional drives. The conventional techniques and the current challenges are discussed in this section, as well as a brief explanation on how MPC have handled each objective in other systems.

4.2.1   Current and torque

The idea of torque and current control as the fundamental control strategies in SRMs have been addressed in Chapter 3. The implementation of highly innovative MPC

strategies can enhance the basic machine operation. The focus should be not only to improve tracking but also to release some processor memory and computational burden to allocate additional control objectives.

In current control, the use of virtual-flux brings several advantages in terms of local linearization of the predictive model [86]. This concept has not been fully exploited, as it improves systems robustness by simplifying the general formulation of the control problem [194]. At the same time, the concept of stability of the current loop using predictive technique has not been considered, yet important for positioning the machine. In addition, the use of long prediction horizon can be helpful to reduce parameter sensitivity and improve efficiency [38]. Ultimately, the trend in SRM is to use the current to *shape* certain waveforms that allow minimizing torque ripples and NVH issues. The control algorithm should be extended to shape these currents online.

The online torque sharing has been already considered for torque control, developing high performance strategies based on finite set predictive control (FCS-MPC) at low [116] and high-speed [121]. However, the feasibility of these techniques has not been demonstrated for four-quadrant operation, and there is still room to improve torque ripple at medium speed to meet the standard in automotive applications of 5% [6]. The main challenge is to develop an accurate model that allows calculating optimized conduction angles in real-time with low computational burden.

4.2.2   Acoustic noise and vibrations (radial force control)

Torque ripple is relatively easy to analyze and compensate through direct measurement or using static maps. However, a smooth torque waveform does not guarantee

the elimination of acoustic noise in SRMs. Stator vibration is usually the primary source of acoustic noise in electric machines. The acoustic noise reduction has been addressed through design techniques, aiming to develop a mechanical structure that can mitigate these vibration levels, some of them summarized and analyzed in [195–197]. In contrast, it becomes challenging to include acoustic noise as a control objective as it is a more complex variable.

Apart from the bearings and ventilation system, the vibrations result from the interaction between electromagnetic forces. The use of a power converter to feed a machine leads to applied voltages rich in harmonic components; these harmonics also appear in the stator currents and produce electromagnetically-excited-vibrations [198]. This is worse in SRMs due to the trapezoidal shape of phase currents in conventional controls. Unlike the torque ripple, which is generated by the tangential components of those forces, the acoustic noise is originated from the radial force component, which causes deformations in the machine structure In this way, the control solutions have initially aimed the current shaping to reduce the radial force ripple [196], with more specific attention on the current transient during turn-off as the origin of most of the radial force peaks [199] or a closed loop control of the radial force [200]. However, a smooth radial force waveform might not be sufficient to eliminate unpleasant noise for human ears. The phase currents produce an equivalent radial force density waveform per pole, which, decomposed through 2D FFT, produces temporal and spatial harmonic components. The spatial orders resonate with the machine stator's vibration modes at a frequency determined by the temporal orders [201]. The latest frequency depends on the rotor mechanical frequency. Depending on the mechanical characteristics of the frame, these vibrations can be dissipated

as sound pressure, which is usually used as the base to measure the acoustic noise through the sound pressure level (SPL) in decibels [198]. Therefore, smoothing the radial force ripple compensates only for the harmonics affecting the spatial order zero, but it neglects the temporal orders affecting higher vibration modes.

The temporal orders of higher circumferential orders have been considered in [3] within an offline optimization, compromising the acoustic noise reduction and the torque ripple minimization in radial force shaping (RFS) technique. The iterative process is represented in Fig. 4.3, where the temporal orders are manually discarded, and inverse FFT allows obtaining a reconstructed radial force static map and a current profile. The control is then reduced to a current tracking problem.

Given the high complexity required to solve the iterative process, it is not easy to include operating variables within the RFS algorithm. In this case, the adaptation of such control techniques to a method with an online selection of the optimal switching, such as MPC, would improve real-time performance. MPC has already been used for acoustic noise control in induction motor drives, with a technique that takes advantage of the cost function flexibility and predictive models to directly influence the phase currents as a function of the SPL [202]. It also considers the reduction in the tonality, which can decrease the most disturbing temporal orders from the acoustic noise; however, this is based on an empirical linear model, which might compromise the accuracy and should be adjusted for different motors.

The challenge is then defining a proper predictive model that can be easily adjusted to consider the most prominent temporal orders depending on the SRM pole configuration. It would allow MPC to configure a unified control algorithm with the ability to decide the optimal trade-off between efficiency, torque ripple and acoustic
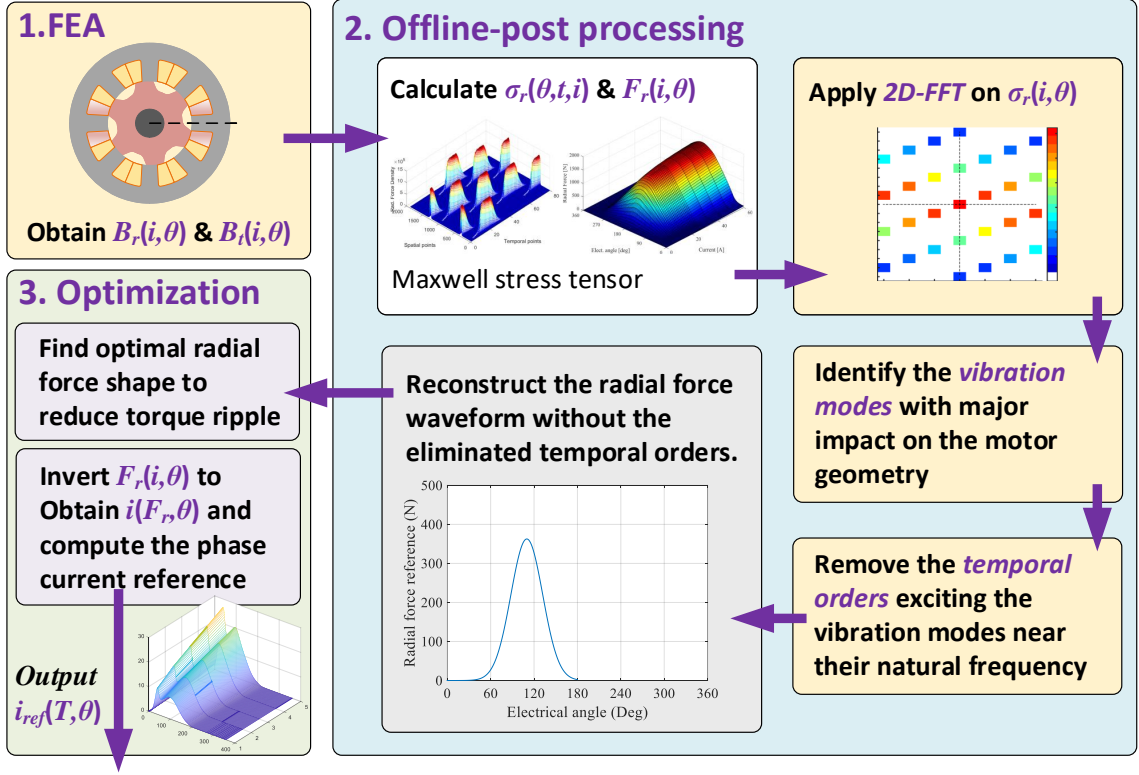
Figure 4.3: Radial force shaping for indirect reduction of acoustic noise and torque ripple in SRMs [3]

noise, depending on the application and operating condition.

4.2.3 High- and ultrahigh-speed operation

The main comparative advantage of SRMs is their capability for reliable and efficient operation at high-speed [157]. Currently, electric drives tend to operate at higher speeds, reducing weight and volume, which benefits systems with high power density requirements such as automotive applications [5].

High-speed control in SRM is a challenging condition as the increased back-EMF limits the current regulation capability. It limits the possibility of current shaping for

multi-objective control such as torque ripple and acoustic noise [9]. The control in the high-speed region is only possible through a single voltage pulse, and the regulation problem is reduced to calculating the conduction angles. Some approaches have considered using sinusoidal excitation and vector control, but the required voltage and switching frequencies are still impractical [203]. Another alternative is the combination of multiple techniques depending on the operating condition. DITC for current build-up with constant phase current control and demagnetization as a function of the electrical position and speed finds a stable control over a wide speed range [204]; However, the transition between different techniques might compromise stability and average torque tracking.

MPC has been already implemented for a similar condition in conventional AC drives, where the field weakening operation presents additional challenges. It solves the issue in IMs, avoiding weight factors with a cascaded MPC strategy and guaranteeing stability, but it increases the computational burden [205]. In [24], this is solved by calculating an equivalent reference voltage vector, thus simplifying the cost function. It also improved the low-speed control by including LUT-based parameters, which are updated online and demonstrate its robustness against parameter variation.

There is another operating condition shown in Fig. 4.2 as the ultrahigh-speed, which is usually defined for shaft speeds over the 60000 rpm and is useful for specific applications such as vacuum cleaners [206] and turbochargers [207]. Theoretical designs for SRM drives have reached up to one million rpm [186], but experimental evidence of a proper control has been provided for operating speeds up to 150000 rpm [187]. Although this operating region also allows only single-pulse control, the problem arises from the limitation in the position sensing technology, which does not

go beyond 60000 rpm. It is usually solved either using multiple Hall-effect sensors or sensorless control [208]. Therefore, an optimal unified control strategy, including ultrahigh-speed, requires the ability to include sensorless and self-sensing techniques, which can also be implemented within predictive control algorithms.

4.2.4   Self-sensing and parameter estimation

The use of parameter estimation and sensorless control techniques has become a focus of research in electric drives to reduce cost, improve performance and guarantee reliability of the system [180]. Self-sensing techniques in SRM have the advantage of using the idling phases to inject perturbations and the strong relationship between the flux linkage, current and rotor position [157] The latest is more convenient for position sensorless control, but it has been exploited for online parameter estimation. These techniques can be generally classified according to the phase state used, the requirement of external hardware [209] and even the speed range [210].

Voltage equations and model-based approaches make the estimation techniques compatible with the principle of MPC. It has already been proposed through some online estimation [79] where the CCS-MPC continuously updates the inductance and back-EMF characteristics through an optimization algorithm that guarantees high performance of the control technique itself. However, this has not been implemented using FCS-MPC.

The use of FCS with self-sensing techniques is interesting for SRM, given the advantages that skipping the modulation stage has. Although some of the well-known self-sensing techniques for conventional AC drives are not compatible with modulator-free controls such as FCS-MPC, it has been proven the feasibility of new

estimation algorithms for such control methods. For instance, position estimation in IPM drives could be computed from the current ripple, inherent to FCS-MPC [211]. A similar approach has also been considered for an optimization algorithm with a co-estimation of speed and position [212]. The algorithm has been extended even to multi-parameter estimation avoiding the use of high-frequency current injection [213]. These techniques result not only in a reliable estimation but also on a high-performance predictive control as the model-based algorithm counts with a real-time update of the parameter information while guaranteeing a constrained computational burden [214].

The next generation of SRM controllers must contain such estimation algorithms as a unified MPC technique that guarantees reliable, robust, and efficient operation. Although the current ripple in SRM does not directly provide position information, it can estimate it through the voltage equation and a standard optimization algorithm. Similar estimation approaches consider simplified convex spaces such as in [215] that can be adapted either to CCS or FCS MPC on SRM. The challenge in multiple estimations is to overcome the highly nonlinear inductance, which depends on the rotor position, making it difficult to estimate both. An extra challenge appears at high and ultra-high-speed since there are no more idling phases, and the simultaneous activation of phases in the single pulse operation modifies the model, forcing to consider mutual coupling.

4.2.5 Fault-tolerance

One of the main advantages of SRMs in terms of fault-tolerant operation is their capability to independently operate their phases. Of course, this would not prevent

the occurrence of a fault, but it allows the machine to be functional even after a fault. Their capability to operate at higher speeds makes SRM attractive for high-speed safety-critical applications [216].

The so-called post-fault operation has been operated by Several methods including current profiling [217], Fuzzy logic control, and position signal assistance have been implemented. In general, the most common faults in electrical drives are open-circuit faults [180]. The short-circuit fault usually leads into an open-circuit. However, in SRMs, the reality might differ from conventional AC drives. As mentioned in section 4.2.4, position sensor fault is the main threat at high- and ultrahigh-speed operation. A comprehensive literature review on both fault diagnosis and control algorithms for SRM drives is provided in [216].

To date, predictive fault tolerant control has not been applied to SRM drives. However, predictive control is quite popular to handle post-fault control in highly complex machines. That is the case of multi-phase machines, which provided an increased number of degrees of freedom, usually represented by an additional subspace in the rotating frame, implement predictive control to compensate for faults. An example of implementing FCS-MPC minimizes the total current harmonic content [218]. In addition, a fixed switching frequency fault tolerant control can be achieved by integrating the virtual voltage vectors with predictive method [219].

4.2.6   Overload control

Overload control takes advantage of the overloading capabilities of the machine to produce a short-term peak torque. The control strategy evaluates the magnitude and time of the overload condition to produce the maximum torque without compromising

the motor safety. Overload control also allows preventing oversizing during the motor design process. Although conventional overload limitations were obtained based on static thermal limits [220], recent works have demonstrated the importance of considering the transient thermal response for inverter-driven machines [221]. This feature has been initially explored on induction motors where the time ratings for its operation are defined [222]. However, a controller with good dynamic response to fully consider the real-time thermal behaviour along with the machine transient response is required. MPC has been proposed as the solution given the simple adaptation to the control loop by adopting the appropriate predictive model. The model predicts the instantaneous operating temperature within the next sampling periods and determines the optimal torque/current reference limitation. It has been considered for induction [223], PM, DC motors [224], and even SRMs [154].

The application in SRMs gains more relevance because they can withstand thermal stress better than AC machines. It led to predictive control to handle the highly nonlinear characteristics and predict the winding temperature online, thus limiting the maximum torque to maintain a defined level of copper losses [154]. The iron losses have not been considered given the little impact they have on the low-speed copper losses. However, in high-speed operation, iron losses gain relevance, and improvement of such predictive control technique requires their inclusion into the limitation considerations.

4.2.7   Topological improvements

Machine topologies

Beyond the control objectives, certain applications could find benefit on different SRM topologies. Design procedures have come up with several variations in the structure or operating principle of the machine. The most promising in literature deals with mutually-coupled SRM (MCSRM) drives, which take advantage of the variable self- and mutual-inductance with respect to the rotor position to generate torque [225]. Therefore, MCSRMs are especially designed with a winding distribution that considerable increases the mutual coupling between phases. Their most attractive feature is the claimed improvement in terms of acoustics.

Recent approaches have considered the sinusoidal excitation of MCSRMs, which not only would further reduce its acoustic noise and vibrations but also allows using well-known vector control [225]. Besides, this enables the machine to operate with conventional two-level voltage source inverters.

This is a relatively new research trend and, despite the potential applications, a deep analysis on current shaping for this topology has not been investigated. This has opened a window for predictive control to optimally evaluate the performance of the machine. Deadbeat predictive control has been implemented within unipolar current control for a MCSRM [226]. The potential of the bipolar 2L-VSI-fed machine has also been evaluated within a FCS-MPC approach with promising results for current control [227]. The latest research can be further expanded to torque regulation and all control objectives mentioned in this Chapter.

Other topology alternative include the segmental rotor SRM and double-stator SRM (DSSRM). The first one has presented improvements on the machine torque

density, while the DSSRM offers a better energy conversion ratio, torque production, and utilization of the machine volume [1]. Both of them show potential to enhance performance objectives with MPC, depending on the target application.

Power electronics

One drawback in SRM drives is the use of the unconventional asymmetric power converter, which offers flexibility for the individual phase operation thus allowing improved fault tolerant control. The use of sinusoidal-excited MCSRM brings the chance to use conventional two-level voltage source inverters, but it reduces the attractive of the machine for post-fault operation. Other topologies for the SRM drive include $(N+1)$-switch, C-dump, N-switch, split AC and split DC converters. A detailed evaluation of these topologies is presented in [29], bringing up the compromise they present regarding performance, control complexity and the number of switching devices.

Furthermore, the use of multilevel converters have also been introduced for SRMs, given their potential to enhance high-power and high-voltage machine performance [30, 228]. It is also an alternative to deal with the relative low inductance of the machine at unaligned position during control. This, along with the upcoming wide bandgap (WBG) technology, represents an overall improvement in robustness, controllability, and reduction of cost and volume of these drives [6, 163].

4.3 Vision and Potential Applications

Previous section stated the main challenges regarding SRM control objective and how MPC has the potential to overcome them. Therefore, a high-performance SRM with
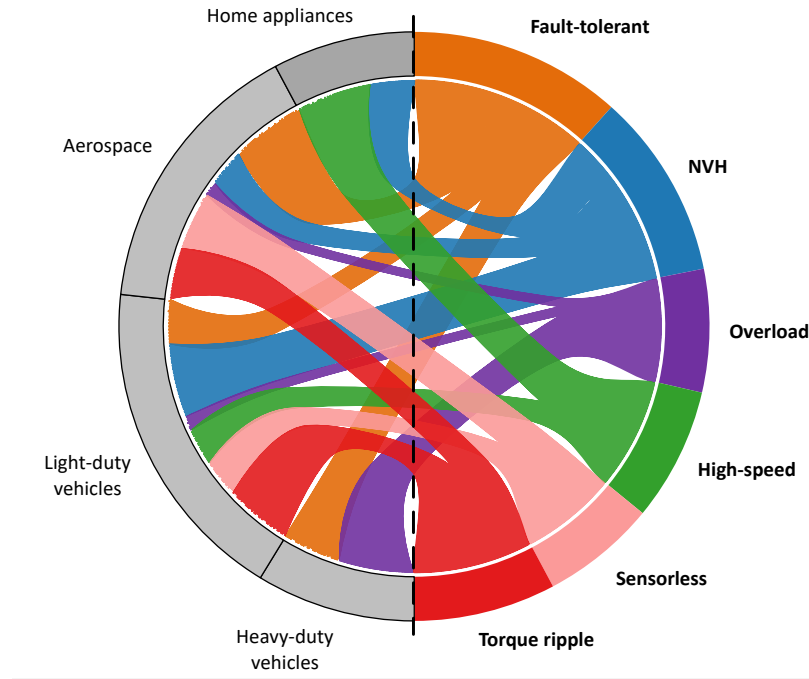
Figure 4.4: Potential usage of SRM control objectives for practical applications

an unified algorithm for simultaneous optimal control can make these machines suitable for different applications. These are primarily applications with high potential for SRM usage which has seen a limited or nonexistent practical scenarios due to the limitations previously discussed.

Beyond current and torque control, which are common for all applications, Fig. 4.4 illustrates the impact of the described control objectives into some highly appealing applications for SRMs. The first and most important thing to notice is the fact that all require more than one control objective to guarantee high-performance of the electric drive. It also allows noticing how diverse applications might differ in priorities. This allows proposing a vision of how these applications can not only adopt SRMs are main electric machine but also be enhanced by their use among MPC.

Beyond home appliances, where low-power high-speed with reduced NVH levels

is required [181, 195], automotive applications require more diversity of control objectives. However, these applications can also be subdivided. In the case of light duty vehicles, although there exist SRMs which is able to reproduce the behaviour of automotive IPMSMs in dimensions and torque-speed envelope [184, 229], the control technique can still be improved to offer a high-performance outcome. Important trends in automotive applications lead to new challenges such as the integration with other vehicle systems, more traction motors per powertrain, higher power, and higher voltage [6, 230] as well as integrated battery chargers. The latest utilizes the machine's winding as a filter and the inverter as a bidirectional converter to connect the EV battery to the grid [231]. It has been considered in [85], where a FCS-MPC for current tracking is proposed for SRM-based integrated charging. Further developments in dual-functionality MPC-based controllers are still proposed for future works.

Alternatively, hybrid heavy-duty harsh vehicles have already implemented SRMs as the noise, torque ripples and vibrations do not represent a significant restriction. Instead, efficiency, robustness and overload capability dictate the best performance for applications like earth-moving vehicles [232]. As these vehicles use an engine to generate electricity for the motors, an unified control might also increase the robustness of the generator-motor SRM drives as a whole, thus improving efficiency and fuel consumption.

Research and industry trends are also pushing aerospace technology towards the more-electric era. Commercial flights tend to use more electric aircraft (MEA) technology, which attempts to replace mechanical, hydraulic and pneumatic systems for electrical ones as much as possible [233]. The more electrified system needs then

additional generating capabilities and, therefore reliable starter/generators. This application has seen SRMs as a potential solution for the rough conditions the high temperature and pressure levels of commercial and military flights [197], thus offering enhanced robustness and fault-tolerant capability. Alternatively, SRMs have been considered as part of electromechanical actuators replacing hydraulic systems such as fuel pumps, surface actuators for flight control, and flap and rudder actuators [157].

4.4   Summary

Considering the different control objectives and limitations of SRM drives, and the potential to overcome these issues with the latest advances in predictive control, the future market attractive of SRM is promising. The main drawbacks of this machine can be overcome if the machine non-linear behaviour is handled. This behaviour limits the use of predefined control laws, leaving the room for using algorithms that can determine the optimal law online. Model predictive control has proven its capability to be a high-performance and reliable multi-objective control technique in several machine drives and power electronics systems. The main challenge is then the definition of accurate predictive models according to the control needs. Additional concerns such as parameter sensitivity, stability, multi-objective optimization and so on, have already been addressed in the literature of predictive control.

The room is then open for the innovation through the implementation of existing high-performance predictive techniques to the most challenging control objectives of SRM. The main takeaway point from this Chapter is then a road-map for future projects, studies, applications, and analysis to be done with respect to the implementation of MPC on SRM. Torque ripple, overcurrents, acoustic noise, high speed

control and position estimation, fault tolerance are only few among several objectives that would position SRM between the candidate machines for high performance applications. Although these applications might compromise the simplicity of the control technique, upcoming technologies demand higher performance from electrical drives, and the migration to higher computational power is a fact.

Chapter 5

Experimental Setup
Implementation

In this Section, the design and implementation of the experimental setup used in this thesis is detailed. The switched reluctance machine and asymmetric converter characteristics are described, and the selection process for the correspondent loading machine is presented. Furthermore, the flux linkage and torque characteristics are identified experimentally based on current injection and the co-energy method, respectively.

5.1   SRM Drive components

The test bench was designed based on the available 5.5 kW, 72 V, 12/8 three-phase SRM in Fig. 5.1(a). The machine has a base speed of 5000 rpm with 81.7 A rated phase current. The power converter in Fig. 5.1(b) is also available for use, which is a four-phase asymmetric converter designed for high-power SRM applications [234].
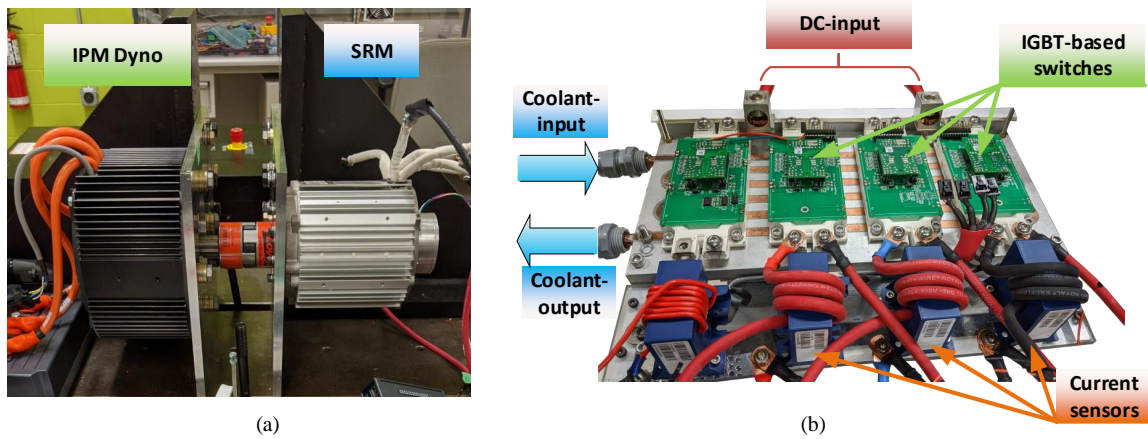
Figure 5.1: Experimental Setup (a) switched reluctance machine and IPM dyno for speed control (b) Asymmetric converter

The converter has IGBT-based switching devices rated at 1200 V and 400 A. The converter is driven by a DSP TI28335, with 1.5 MHz of processing capability. The existing current transducers are rated for 300 A, and three turns are considered for the phases to reduce noise sensitivity.

The SRM is controlled to track a torque reference while a constant speed is provided by a prime mover. This emulates the operation of electric drives in electrified vehicles, where the high-level vehicle controller regulates the speed and sets the torque reference. The dynamometer that maintains the speed is selected based on the maximum torque and voltage level requirements, detailed in the next section.

5.2   Dynamometer selection

The selection of the dynamometer depends on the torque-speed characteristics of the available SRM. Considering the base speed of 5000 rpm, the 5.5 kW SRM has a theoretical rated torque of 10.5 N.m. The machine should be able to provide a slightly

higher torque than the motor under testing in order to hold the commanded speed. An alternative is the use of a dynamometer with different ratings, which should be coupled through a belt-pulley system. This, however, would involve higher costs and increase the assembling time.

The operating voltage should be considered too. The dynamometer can be chosen with a different rated voltage from the SRM, but it would require the use of an additional power supply during testing. Moreover, the selected dynamometer will operate in generating mode, requiring either a bi-directional power supply or a resistance bank to dissipate the generated power. An alternative is to choose a machine with the same 72 V rated voltage and connect both drives to the same dc-link. The connection allows operating in back-to-back mode, thus requiring a power supply only for starting and to feed the system losses. The last scenario represents the most efficient option, and it is, therefore, the chosen one.

Fig. 5.1(a) shows the selected dyno machine mechanically coupled to the SRM. It is a 13 kW interior permanent magnet machine with the characteristics shown in Table 5.1. It has an operating voltage in the range of 48 to 100 Vdc, thus being suitable for the current application. Due to the intended limitation of 72 V operation, the output power is restricted to 7.5 kW. It is acquired as a part of a drive system which includes a 15 kW inverter with a six-switch MOSFET bridge and a predefined speed control loop based on a 15 kHz PWM strategy.

The mechanical supports for both the SRM and dynamometer are designed and custom-manufactured. Both machines are suspended by face-plates allowing direct coupling as shown in Fig. 5.2. The final assembled setup is shown in Fig. 5.1(a).

Table 5.1: Comparison of machine characteristics

Rated values	Power (kW)	Voltage (V)	Current (A)	Speed (rpm)	Number of phases	Stator and rotor poles
SRM	5.5	72	81.7	5000	3	12/8
Converter	60	up to 800	400	n/a	4	n/a
IPM Dyno	7.5	72	116	6000	3	n/a
Inverter	15	72	210	n/a	4	n/a

SRM

Power: 5.5 kW
Peak Power: 11 kW
Torque: 10.5 N.m.
Speed: 5000 rpm
Max. Speed: 10000 rpm
Voltage: 72 V
Current 81.7 A

IPMSM (Dyno)

Power: 15 kW
Torque: 37 N.m.
Speed: 4500 rpm
Maximum Speed: 8000 rpm
Voltage: 48 – 120 V
Phase Current 220 A
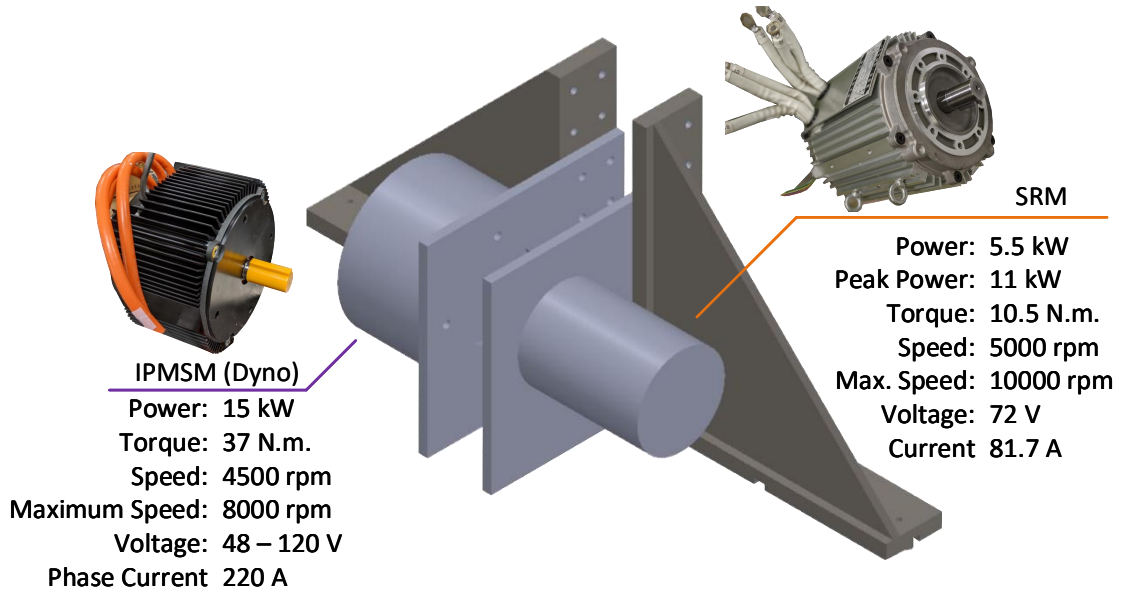
Figure 5.2: Design of the face plates for the motor and load IPM

5.3   SRM Characterization

5.3.1   Flux linkage characteristics

Once the system is assembled, and the SRM current and position sensors are properly calibrated, it is important to determine the SRM parameters, as no manufacture details of FEA model are provided. As described in Section 2, the flux linkage characteristic in an SRM is a function of both the electrical angle and the current. The complexity involving the dependence on two variables can be simplified by assuming

a fixed rotor position; therefore, the flux linkage can be computed from the voltage equation in (2.2a) as,

$$\lambda(i,\theta) = \int_0^t \left[v(t) - Ri(t) \right] dt \Big|_{\theta=const} , \qquad (5.1)$$

where v, i, λ, and R are the the phase voltage, current, flux linkage and resistance, respectively.

At a fixed angle, a single voltage step can be applied to build up the phase current up to its rated value. Considering the different phase inductance per electrical angle, the time-span required for the applied voltage to reach the desired current will vary. Once the voltage and current transients are obtained, (5.1) can compute the flux linkage. The same procedure is repeated at each electrical position. There exists other approaches for the characterization and self-commissioning of SRM drives, but these are out of the scope of this thesis.

The characterization process described above has an additional degree of complexity, as the injected current results in an electromagnetic torque that tried to move the motor shaft. This makes the task of fixing the electrical angle more challenging, specially for values around 90°-electrical where the torque is maximum. In fact, even at the aligned position (180°), the current might cause an oscillation, thus reducing the accuracy of the measurements.

To solve this issue, the shaft should be coupled to a stiff load which can handle $\approx$ 10N.m rated torque of the SRM. Fig. 5.3(a) shows a rotary plate with a lathe chunk that allows keeping the rotor static. Fig. 5.3 illustrates the coupling to the SRM shaft.

The rotary table is initially adjusted at 0° with respect to the phase A. Using a

(a)   (b)
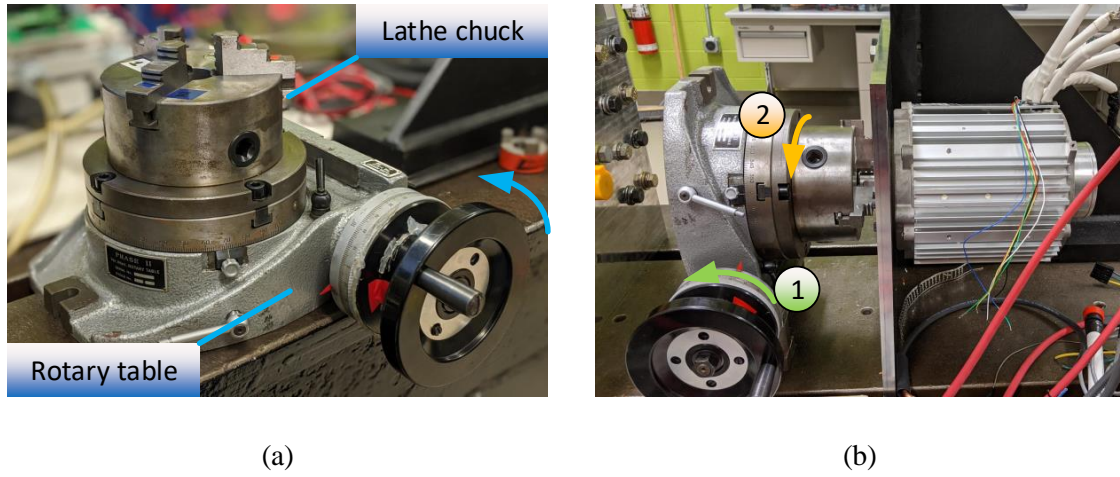
Figure 5.3: (a) Rotary table to fix and change the shaft position of the SRM during machine characterization (b) Rotary table coupled to SRM shaft - 1 controls the rotation of the load, while 2 rotates the shaft for the position variation

power supply with current regulation, a 72 V (rated voltage) pulse is used to inject up to the rated current (82 A). Although the machine is rated at 81.7 A as its rms value, the maximum value is can reach might be around 180 A peak. However, due limitation in the supply and wiring, the characterization is performed up to 82 A only. Next, the transient response is saved using the oscilloscope to be processed offline. The shaft is then rotated in steps of 2°-electrical, and the process is repeated up to 358°-electrical. It is worth noticing that an angle span of 180° is enough to fully characterize the flux linkage profile, given the symmetry of the plot, as shown in Fig. 2.2 in Section 2, but it is done considering the 360° for verification purposes.

The phase flux linkage is calculated from the voltage equation in (5.1). R_{ph} is obtained from the same test by Ohm's law and using the applied voltage and phase current at steady-state. This results in an average resistance of 8.26 mΩ. The results for the flux linkage in the phase A as a function of the current are shown in Fig.
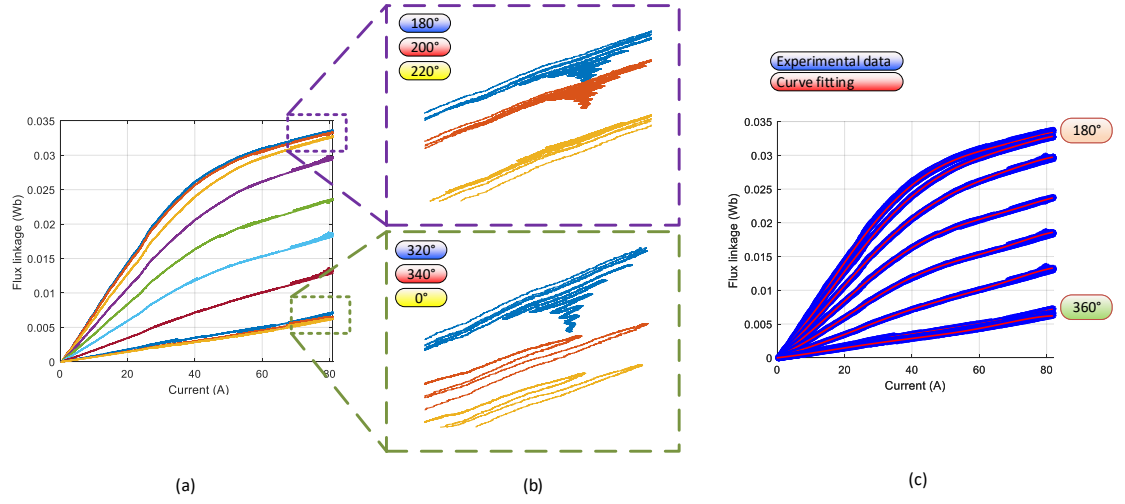
Figure 5.4: (a) Experimental flux linkage curves for phase A (b) Inaccuracies in flux caused by shaft oscillation (c) Curve fitting to obtain fluk LUT

5.4(a)-(c). Although the test was performed for an electrical angle step of 2°, results in Fig. 5.4 show 20° to facilitate its visualization.

It is worth noticing that the curve presents inaccuracies caused by the oscillations in voltage and current. These inaccuracies are zoomed in the Fig. 5.4(b). In practice, it was found that the applied voltage causes an oscillation in the SRM shaft at any fixed position. It is also due to the transient response of the current itself. This error still does not present an overshoot greater than 1°-electrical (0.25°-mechanical), which is accurate enough for characterization purposes. However, the occurrence of several flux points at the same current makes impossible to store the results in Fig. 5.4)(a) as a lookup table; therefore, a curve fitting and polynomial approximation is applied to store the average of these curves. The approximation is used as a linear fitting the flux curves at each rotor position. Fig. 5.4(c) shows the results of this curve fitting.

The flux linkage static map as a function of the phase current and electrical angle is then depicted in Fig. 5.5 and stored as a look-up table to be used in the
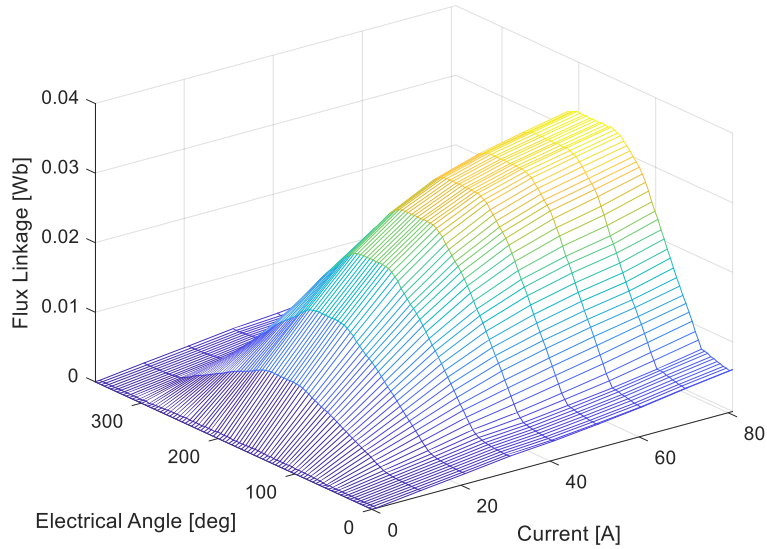
Figure 5.5: Experimental flux linkage characteristic of the 12/8 SRM

simulation and experimental stages of this thesis. This allows computing the torque characteristics from offline computations.

5.3.2   Inductance profile

From the flux linkage characteristics, it is possible to compute the phase inductance of the machine as depicted in Fig. 5.6. The process follows a simple division between the obtained flux and each current for a fixed electrical angle. It is worth noticing that the zero current is not defined, and therefore assumed to be constant and equal to the first current value.

It is important to highlight, from the results in Fig. 5.6, that the testing machine has an exceptionally low inductance, even at its maximum value. This makes the control task more challenging as, for instance, at unaligned position, it might be lower than 0.1 mH, meaning that the minimal voltage transient causes considerable
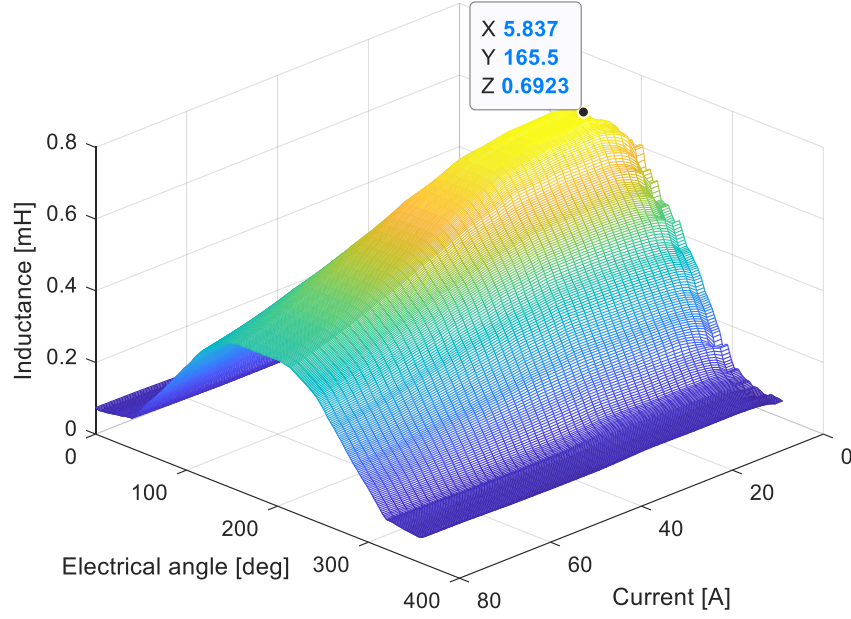
Figure 5.6: Experimental phase inductance characteristics of the 12/8 SRM

current spikes.

5.3.3 Electromagnetic torque

The electromagnetic torque produced by one phase can be represented as:

$$T = \left.\frac{dW_c(i,\theta)}{d\theta}\right|_{i=const} = \left.\frac{dW_e(i,\theta)}{d\theta}\right|_{\lambda=const}, \tag{5.2}$$

where $W_s = \int_0^\lambda i\, d\lambda$ is the stored energy in the airgap and $W_c = \int_0^i \lambda\, di$ is the co-energy. Therefore, as the flux linkage as a function of the current is known, the torque can be obtained from the co-energy calculation in (5.2). The method is illustrated considering the curve in Fig. 5.7, where the flux linkage as a function of current is shown for two electrical positions. As the flux in 5.5 is a discrete variable instead of
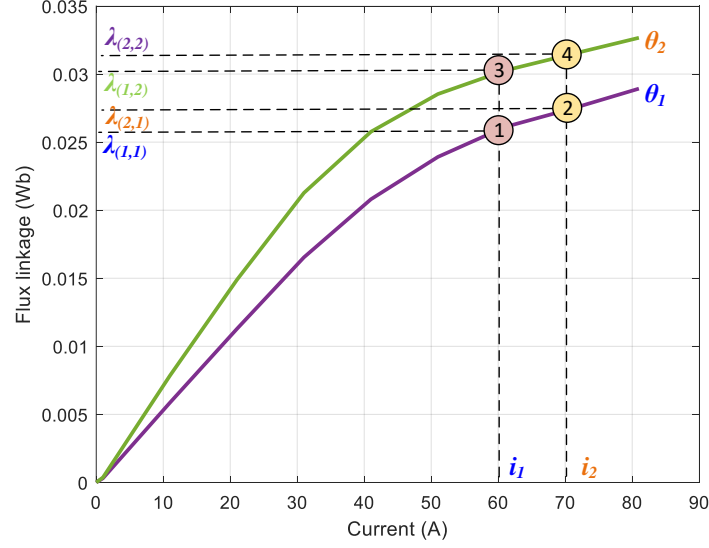
Figure 5.7: Principle of torque calculation from the phase flux linkage

a continuous function, an approximation to compute the co-energy can be done as,

$$W_c(k,j) = \sum_{p=2}^{k} \left(\frac{\lambda_{j,p} + \lambda_{j,p-1}}{2} \right) (i_p - i_{p-1}), \tag{5.3}$$

where $W_c(k,j)$ is the stored co-energy at the current i_k and electrical angle θ_j. Therefore, for a fixed electrical angle θ_j, the flux at two adjacent currents are used (points 1 and 2 in Fig. 5.7) and accumulated to solve the integration. From this, the discrete torque values can be obtained as,

$$T_e(k,j) = \left(\frac{W_c(k,j) - W_c(k,1)}{\theta(j) - \theta(j-1)} \right), \tag{5.4}$$

Fig. 5.8 shows the obtained electromagnetic torque static map. This map is
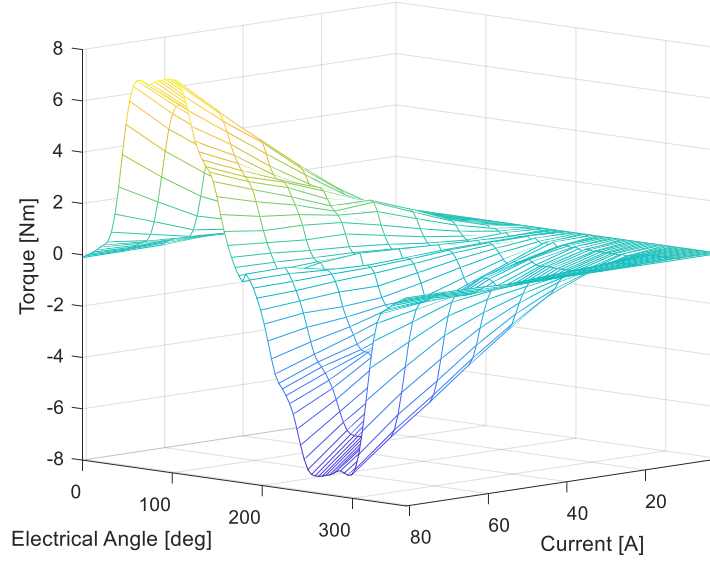
Figure 5.8: Experimental phase torque characteristic of the 12/8 SRM

experimentally validated by running the SRM with a torque sensor. The dynamome-
ter is run at a fixed speed of 1000 rpm and a current reference of 50 A is set to
the SRM. A simple hysteresis current control is run with random conduction angles
($\theta_{on} = 30, \theta_{off} = 150$). The phase currents are then stored, and the shaft torque is
measured with a torque sensor. The available torque sensor for this setup is a NCTE
2200-75, which is rated for 75 Nm with a resolution of 23 mV/Nm. Although it is
oversized for the current application, it is used for validation purposes only, given
the high costs of a torque sensor. Besides, the resolution would not allow to evaluate
torque ripples, but it is used to compare the produced average torque.

Fig. 5.9 shows the results for the experimental validation. The upper figure shows
the phase currents, followed by the resultant torque from the Fig. 5.8 map with these
currents and the electrical angle as an input. Finally, the bottom figure in Fig. 5.9
compares the total torque from the LUTs with the average torque measured from the
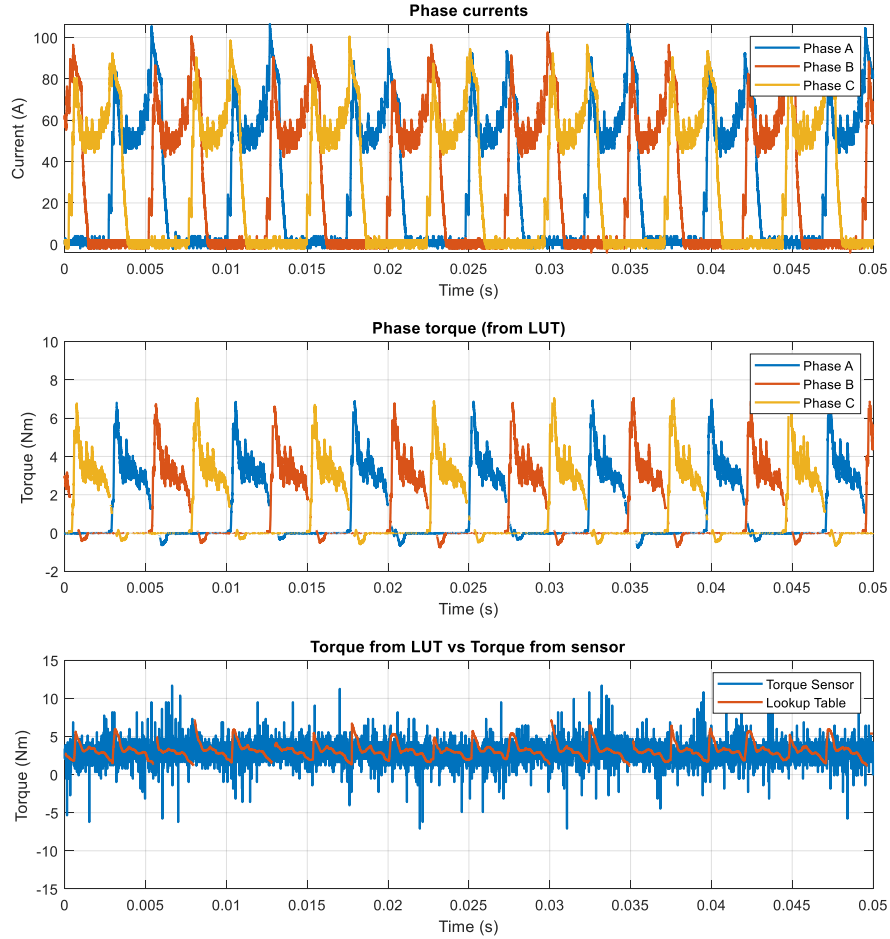
Figure 5.9: Experimental validation of torque static maps for the 12/8 SRM torque sensor. It can be seen these values match for the given operating condition.

5.4 Summary

Technical details of the selection and implementation of the experimental setup were presented in this Section. As the SRM, power converter and DSP for this thesis were already available, the procedure focused on selecting a loading machine to work as a

dyno in the speed loop, as well as designing the mechanical face-plates and couplings for them.

In addition, a test to obtain the flux linkage characteristics based on imposing voltage pulses and measuring phase currents was implemented. A lookup table with the flux linkage static characteristics was obtained, and it served as a base to obtain the phase inductance and torque profiles. These lookup tables allow not only to simulate the machine behaviour, but also to develop the MPC techniques based on online static maps.

Chapter 6

Predictive Current Control (PCC) of SRM Drives

Current tracking in SRM has been discussed in Chapter 3, especially regarding the latest predictive current control techniques in the literature. From the review, the advantages of mapping the current into the virtual flux domain were highlighted, but this Chapter explains deeper the concept of virtual-flux and proposes a predictive current control (PCC) technique based on this concept.

On a predictive control scheme, the selection of either CCS-MPC or FCS-MPC depends on the application as they have different control properties. Differences are related to the current ripple of the power converter and getting either a constant or variable switching frequency. In general, CCS-MPC has been used for current control considering advanced features such as online inductance calibration [79], but FCS-MPC has not been fully explored for current tracking in SRM drives. From its applications in AC drives, the advantages of FCS-MPC in terms of dynamic response and the consideration of nonlinear constraints are evident [37].

In addition, the inclusion of the virtual-flux concept, initially introduced for PMSM drives [97], is possible. This concept allows linearizing the MPC problem using static flux maps that transform the nonlinear current control problem into a linear virtual flux control problem. In PMSM, this is important to deal with saturation and other non-ideal behavior. Therefore, it results in a useful technique for the SRM highly nonlinear characteristics. Given the potential of using the virtual-flux approach, a virtual-flux FCS-MPC for current control in SRM is proposed in this Chapter.

6.1 Proposed Virtual-Flux Predictive Current Control (VF-PCC) Strategy

Fig. 6.1 shows the block diagram of the proposed virtual-flux PCC of SRM drive. The execution of the proposed algorithm works as follows. First, the current and rotor position are measured at the instant k. After delay compensation using (3.4), the flux at $(k + 2)$ is obtained, the possible future plant states are predicted for the next sampling periods, with a horizon of 2 step, which means, for the sampling period $k + 2$. The predicted states are compared to the reference flux and evaluated with a cost function. The one with the lowest cost is used as a plant input in the next sampling period. The algorithm is executed per phase, as these are independently managed.

It is worth noticing that this technique is, in reality, an indirect current tracking algorithm. Although it uses a flux-based model to describe the system in a simple way, the stator flux cannot be measured in conventional drives; therefore, a virtual
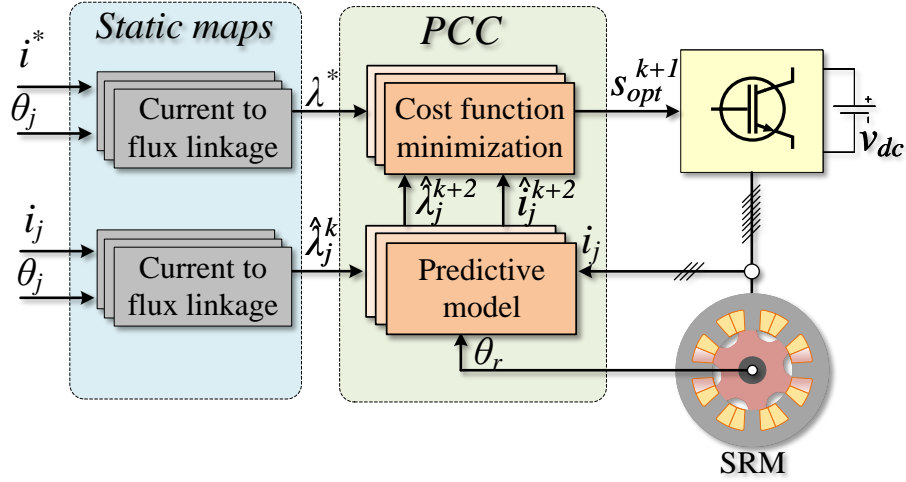
Figure 6.1: Block diagram of the proposed virtual-flux FCS-MPC technique

flux is calculated and used as a state variable. This flux is determined based on static flux maps as the one in Fig. 2.2(b). Therefore, the measurements of current i and rotor position θ allow obtaining the flux λ. The same transformation is applied to the reference currents, thus making the system to behave as a current controller. The advantage of the virtual-flux domain is the independence of the closed-loop behavior of the machine type, as the current-flux map is external. Hence, simple stability and robustness can measure, which give also computational benefits especially if longer horizons are used [98].

6.1.1   Discrete dynamic model, state prediction and runtime compensation

The state prediction of the proposed technique is based on the discretized phase voltage equation in (2.2) considering the forward Euler approximation as in (3.4).

The applied terminal voltage in (3.4) is replaced here by the vector v_g, which

represents all possible discrete switching states of the inverter. Unlike conventional AC drives, this value can be independently evaluated per each phase, thus giving only three possible voltage values to be applied by using an asymmetric converter: V_{dc}, 0 or $-V_{dc}$.

In practice, the calculated voltage is not set instantaneously after the measurements, but after the calculations in the algorithm; therefore, delay compensation is applied. Considering the convention in which measurements are taken at the sampling period k, the delay compensated flux $\lambda(k+1)$ can be determined by:

$$\lambda(k+1) = \lambda(k) + T_s(v(k) - i(k)R) \tag{6.1}$$

where $v(k)$ is stored from the previous control action calculation, and the value $\lambda(k)$ is obtained by the static flux map using the measured phase current $i(k)$ and the electric angle $\theta(k)$. The flux map in Fig. 2.2(b) is inverted and the values of $\lambda(k+1)$ and $\theta(k+1)$ are used as input to obtain the delay compensated current $i(k+1)$. This current is then used to compute the predicted flux $\hat{\lambda}(k+2)$ in (3.4). The compensated electrical angle is calculated using (6.2) and assuming constant speed with respect to the sampling period.

$$\theta(k+1) = \theta(k) + T_s\omega_r(k) \tag{6.2}$$

6.1.2 State limitations

The number of possible discrete states that are considered for the prediction in the next sampling period can be limited as a function of the present state. Fig. 6.2 presents a simple phase switch state graph to limit the v^g inputs of the predicted flux linkage in (3.4). Several benefits can be obtained from such a limitation graph.
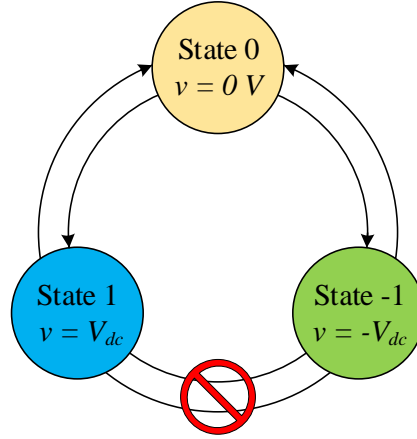
Figure 6.2: Switch state graph with possible state transitions per each phase

Initially, the number of predictions and equations in the cost function are reduced, improving the computational burden. As the application of v^g with opposite polarity is now restricted, the operation leads to a better dv/dt behavior as well as a lower current ripple. Finally, as the transition from state 1 to state -1 requires the simultaneous switching of two devices s_{j1} and s_{j2} (See Fig. 2.3), forcing an intermediate state 0 limits the switch state changes to only one per sampling period, reducing the switching frequency [235].

6.1.3   Cost function

The cost function is the stage where the voltage to be applied in the next sampling time is decided. For each possible switching state, the cost is calculated, and the one producing the lowest cost is selected. Since the proposed controller is based on the virtual-flux tracking, a cost function using the phase flux linkage is proposed in (6.3). First, the reference current is transformed into a reference flux based on the flux maps like the one in Fig. 2.2(b). The electrical angle used for this transformation has to

be considered at the same sampling period than the predicted phase flux; this is at the instant $k + 2$. To compute $\theta(k + 2)$ the same expression (6.2) is adapted.

$$\min_{v_0 \ldots v_{N-1}} G_1 = \left| \hat{\lambda}_j^{\ ref} - \hat{\lambda}_j^{\ v_g} (k + 2) \right|^2 \tag{6.3}$$

6.1.4 Control limitations

Drives thermal constraints are commonly associated with a maximum absolute current. As the proposed technique does not directly regulate the current, additional considerations must be defined for the maximum current limitation. The idea is to prevent a control action that causes a current larger than the maximum current i_{max}. For this, a limitation term I_m is added to the cost function as defined in (6.4):

$$I_m (k + 1) = \begin{cases} 0 & \left| \hat{i} (k + 2) \right| \leq |i_{max}| \\ \delta \gg 0 & \left| \hat{i} (k + 2) \right| > |i_{max}| \end{cases} \tag{6.4}$$

The cost function is then modified to include the limitation term as (6.5). The value of I_m depends on the predicted phase current. If the current is predicted to go beyond the limit, the value of I_m will make the cost to be the highest possible number, thus preventing that switching state to be applied.

$$\min_{v_0 \ldots v_{N-1}} G = \left| \hat{\lambda}_j^{\ ref} - \hat{\lambda}_j^{\ v_g} (k + 2) \right|^2 + I_m (k + 2) \tag{6.5}$$

6.2   Simulation Results

The simulation results were obtained based on a 5 kW, four-phase 8/6 SRM drive with flux linkage characteristics shown in Fig. 2.2(b). The motor was driven by an asymmetric converter with 300 V dc-link voltage. It is assumed that the SRM drive is operated in torque control mode while driven by a dyno, guaranteeing a constant speed. Although in practice the dyno would not be able to avoid speed fluctuations due to the torque transients or the SRM inherent torque ripple at low speed, it is assumed smooth speed transition for simulation results. To produce the reference currents, two different current shaping techniques were used, TSF and RFS. Given a reference current, the steady state and dynamic response were evaluated and compared to the benchmark technique, HCC operating in both soft-switching and hard-switching modes. The sampling interval was set to $f_{samp} = 50$ kHz so that a maximum switching frequency of 50 kHz results. The simulation considers the transient response for variations in the speed and torque commands.

6.2.1   Four-phase, 8/6, 5kW SRM

Reference generation procedure

The reference currents are based on two current shaping techniques for torque ripple and acoustic noise reduction, torque sharing function and radial force shaping, respectively.

The TSF reduces the torque ripple by minimizing the torque dips caused by the phase commutation. It guarantees that the sum of the individual phase torque contributions is equal to the commanded torque. The commutation between one phase

and the next one can be done using different approaches such a linear, quadratic or cubic reference. The distribution of the phase torque between the independent phases can also be optimized, considering the dynamics of the machine itself. Further information TSF and its optimization can be found on [236]. In this paper, a simple cubic TSF is considered.

In the case of RFS, an offline multi-objective optimization process shapes the phase current to produce an equivalent Gaussian-shaped radial force and to reduce the torque ripple. These waveforms are stored in a 2D-look-up table (LUT) and are defined as a function of the torque and electrical angle. This LUT is then used to obtain the current reference based on a torque reference and the information of the electrical angle. The detailed process on the current shaping for acoustic noise reduction can be found on [3].

Results and analysis

Figs. 6.3(a) to 6.3(c) show the performance of the proposed and benchmark controllers for the RFS-based references, while Figs. 6.3(d) to 6.3(f) show the correspondent results for TSF algorithms. Only the currents of phases A and B are shown for simplicity in the visualization. For both cases, an initial speed of 500 rpm with a torque of 1 N.m were set. The speed was then increased to 1000 rpm with a slope limitation of 900 rpm/s, thus emulating the real dynamics of a accelerating dyno machine. Next, torque command is changed to 6 N.m. Finally, under the same load, a speed reversal to -1000 rpm with the same speed ramp limitation was applied, thus making the machine to operate in generating mode. The use of negative speeds and the generating mode is not commonly reported in SRM testing because it requires a
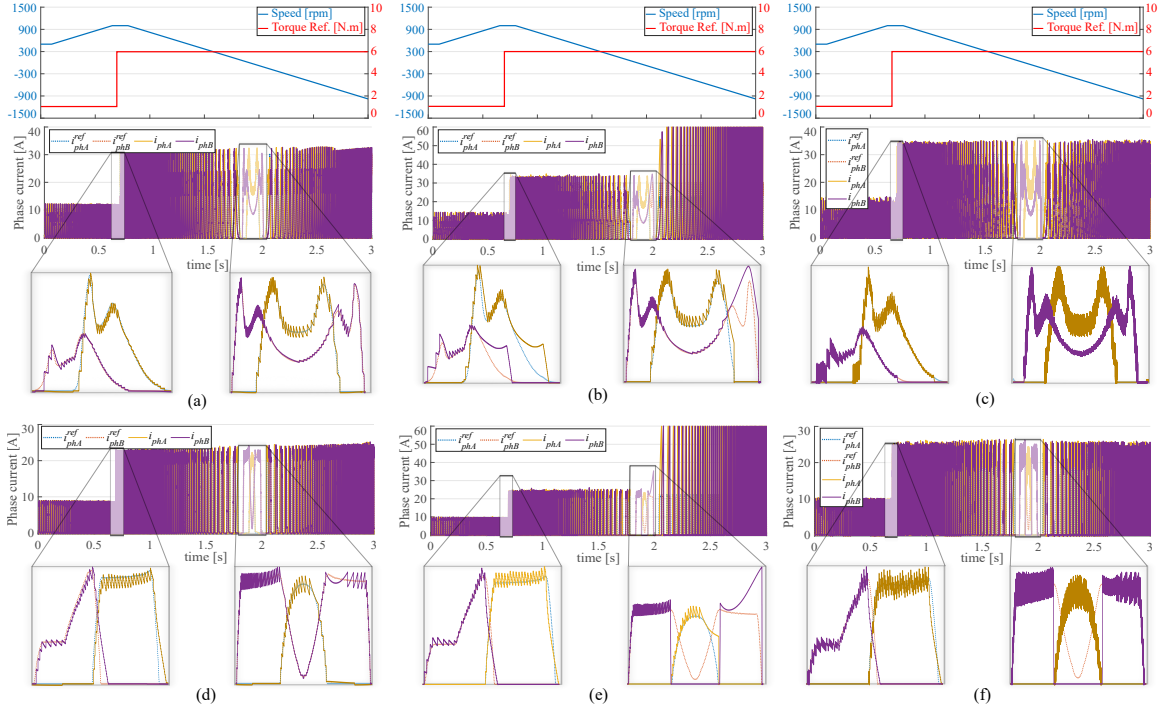
Figure 6.3: Dynamic response to changes in load and dyno speed. (a) RFS reference tracked by MPC (b) RFS reference tracked by HCC-SS (c) RFS reference tracked by HCC-HS (d) TSF reference tracked by MPC (e) TSF reference tracked by HCC-SS (f) TSF reference tracked by HCC-HS

change in the phase excitation sequence. Also, as the equivalent to the field current is generated from the stator currents, it is necessary to keep certain excitation before operating in the generating region of Fig. 2.2(b).

The TSF-based reference currents have a slow transient during the current growing up and down, followed by an approximately constant value, shaping a trapezoidal-wise waveform. The proposed technique in Fig. 6.3(d) evidences a satisfactory tracking in all the operating conditions. It suffers a delay during the outgoing current of the turning-off phases, but this phenomenon is related to the machine limitations in terms of the maximum rate of change of flux linkage. This can be solved by offline optimization techniques [17]. The response for HCC-SS is shown in Fig. 6.3(e). The

dynamic response to the torque step offers better average tracking as the conduction angles are synchronized with the TSF conduction angles; however, for speed reversal, this method loses tracking as the electrical angle oscillates outside the activation interval. In addition, HCC-SS cannot operate in generating mode for current tracking as the 0 state keeps the current flowing due to the back-EMF. Therefore, the current tends to keep increasing. On the other hand, HCC-HS offers good tracking but increases the current ripple and commutations. It is also limited by the conduction angles interval in the speed reversal.

The current waveform from RFS technique does not present a region of constant value, providing a dynamic change of current as a function of the rotor position. Fig. 6.3(a) shows the response of the proposed technique, with a major tracking error at the beginning of the curve. This error is explained by the flux characteristic in Fig. 2.2(b). For small θ_e, the rate of change of flux linkage is low, which represents a small inductance; therefore, for small variations in the terminal voltage, high changes in the phase current are obtained, making more difficult the control, especially for high power machines. In this model, however, the proposed technique can be adapted without additional constraints. In the case of HCC-SS in Fig. 6.3(b), the same problem is evidenced around the unaligned position, but only two states are considered during the conduction interval and the dynamics is slower. This is more noticeable around the aligned position. As the θ_e is still in the conduction interval, the conduction signal G_j remains active, and the current is slowly reduced by freewheeling operation; however, it cannot be reduced as fast as the reference current due to the higher inductance at aligned position. Finally, in the case of HCC-HS, the reference current is successfully tracked, but the current ripple increases.

Table 6.1: Estimated rms error and average switching frequency

Operating point	$\epsilon_{rms}(A)$			$f_{sw}^{av}(kHz)$		
	MPC	HCC-SS	HCC-HS	MPC	HCC-SS	HCC-HS
$T_{ref} = 1Nm$ $\omega = 500rpm$	0.5323	1.6867	1.1257	3	5	5.5
$T_{ref} = 1Nm$ $\omega = 1000rpm$	0.5844	1.8373	1.1217	3	5.5	5
$T_{ref} = 6Nm$ $\omega = 1000rpm$	1.0324	2.8234	1.3298	6	9.5	6
$T_{ref} = 6Nm$ $\omega = -1000rpm$	1.0116	N/A	1.3340	5	N/A	8

To compare the performance of the algorithms, the rms error and the maximum average switching frequency per operating point of RFS are shown in Table 6.1. The switching frequency is estimated per switching device and considering the number of commutations within a time window of 1 ms. It can be seen how the proposed technique offers more accurate results with a reduced switching frequency for all operating points.

6.2.2 Three-phase, 24/16, 60 kW SRM

As discussed in Chapter 4, current control techniques have been comprehensively investigated for different SRM configurations, but a proper comparison between their application into low- and high-power machines has not been presented. As an additional contribution, this section investigates how commonly used current control techniques behave in a 60 kW, three-phase 24/16 SRM used for traction applications [101]. Simulations of different current control techniques are then completed for the 60 kW motor using an asymmetric bridge converter. Table 6.2 shows the characteristics of this SRM, with the flux linkage and torque characteristics obtained from FEA, in a similar way as the ones from the 8/6 SRM.

Table 6.2: 60 kW - 24/16 machine characteristics

Stator/rotor poles	Power rating (kW)	Base speed (rpm)	Rated voltage (V)	Stator outer diameter
24/16	60	2750	650	264

It is important to note that for a high-power motor, mutual coupling between the phases cannot be ignored and must be included in the model, as discussed in [10]. It is done through the integration between the Finite Element Analysis (FEA) software JMAG and Simulink, by using the JMAG-RT Simulink interface.

Figs. 6.4-6.6 show the simulation results. The machine is rotated at a constant speed of half of the base speed, with a sampling frequency of 100 kHz and switching frequency of 20 kHz. The results include the high power 24/16 SRM at 1375 rpm with reference currents of 50 A, 100 A, and 150 A. The main takeaway from this section focuses solely on the current tracking ability of the proposed technique for high power rating machines and therefore a step function reference current is used. Results are also represented in terms of the maximum switching frequency and rms error in Table 6.3.

Figs. 6.4-6.6 provide evidence of a different behaviour with respect to the 8/6 machine. As the effect of mutual coupling is significant, the phase transition becomes a more challenging region for current control. This phenomenon is well reflected in Fig. 6.5, where the controller presents a considerable overshoot once the phase current must be decreased. This phenomenon happens because of both the slow dynamic response of the modulator-based controller and the high phase inductance at aligned position, which is boosted by the mutual inductance effect. Once the rotor pole is aligned with the stator pole, that phase operates as a generator, the back-EMF changes its polarity, thus producing a sudden increase in the current. Alternatively,
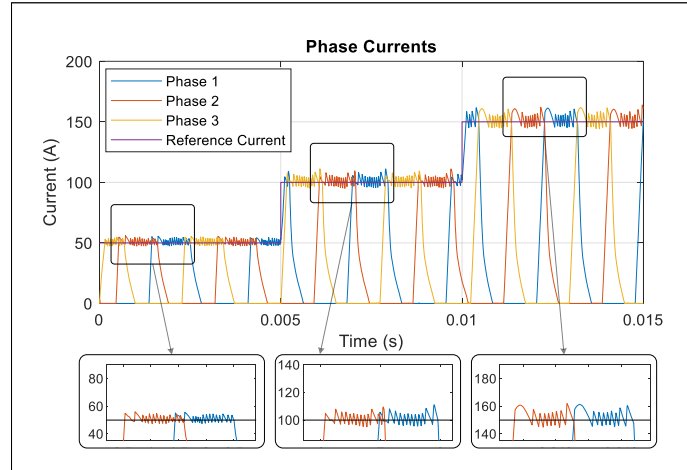
Figure 6.4: 24/16 SRM Phase Currents with Reference Current Steps of 50A, 100A, and 150A at 1375 rpm using hysteresis current control
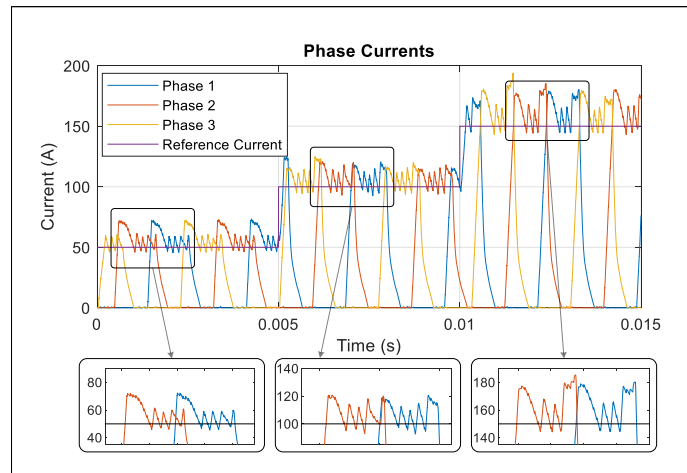
Figure 6.5: 24/16 SRM Phase Currents with Reference Current Steps of 50A, 100A, and 150A at 1375 rpm using delta modulation control
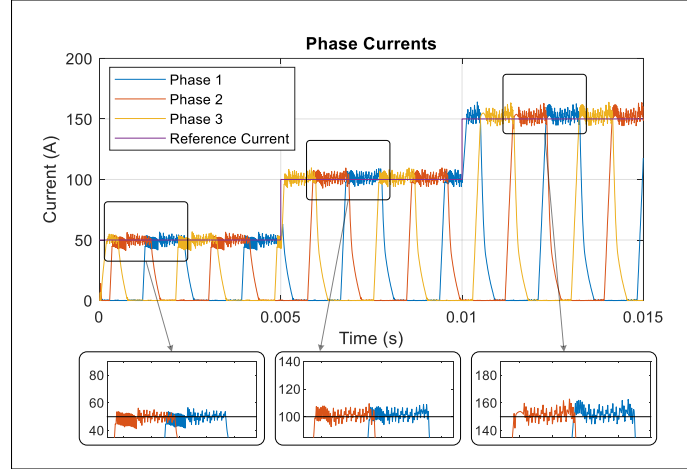
Figure 6.6: 24/16 SRM Phase Currents with Reference Current Steps of 50A, 100A, and 150A at 1375 rpm using the proposed virtual-flux PCC

Table 6.3: Comparison between current controllers for a high-power SRM at low, medium, and high reference currents

	Control technique	Hysteresis	FCS-MPC	Delta modulation
60 kW 24/16 SRM	i_{av} (A)	51.41 , 102.0 , 153.2	49.75 , 101.4 , 151.9	56.26 , 108.6 , 163.6
	i_{rmse} (A)	1.899 , 3.475 , 4.631	2.489 , 2.976 , 3.703	7.960 , 8.435 , 12.01
	$f_{sw,av}$ (kHz)	16	17	20

as seen in Figs. 6.4 and 6.6, the use of direct actuation techniques can solve this issue, but there is the trade-off of having a variable switching frequency especially since with a higher rate of change of current, there is a higher switching frequency at the beginning and end of the conduction period. Although the overall average switching frequency of these techniques in Table 6.3 was below 20 kHz, the maximum frequency could easily go beyond 30 kHz for a transient period, especially during such commutation. This shows promising results for the use of predictive control in SRMs especially when it comes to the use of high-power drive systems. A comparison with other control techniques is presented in [100].
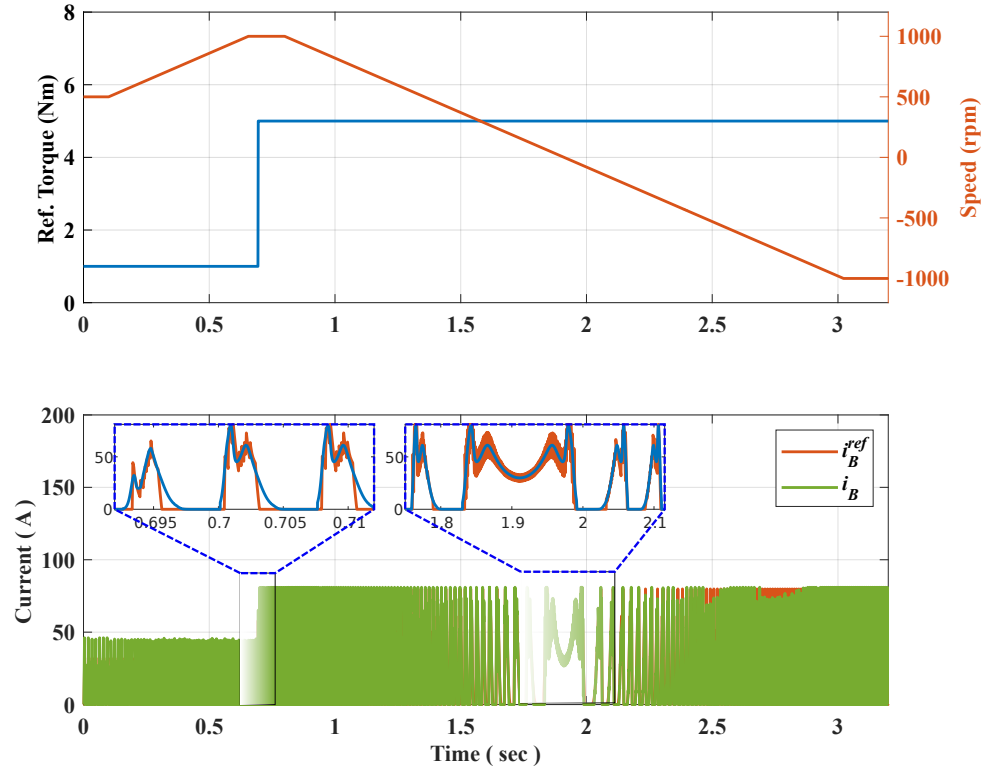
Figure 6.7: Simulation results for the 12/8 three/phase SRM. RFS reference current with a speed sweep 500 rpm to 1000 rpm and 1000 rpm to -1000 rpm using the proposed virtual-flux PCC

Three-phase, 12/8, 5.5 kW SRM

Finally, Fig. 6.7 shows the simulation results for the 12/8 machine, which was experimentally characterized in Chapter 5. The simulation follows a current reference based on the RFS technique, similarly as implemented in the four-phase 8/6 SRM. The simulation is run from 500 to 1000 rpm, with a reference torque step between 1 and 3 Nm, and a posterior reduction in the speed to -1000 rpm. Fig. 6.7 shows the steady-state and dynamic response under such conditions.

Although the three-phase 12/8 machine presents a small inductance with respect

to previous works presented in the literature, the proposed VF-PCC manages to track the reference current at a different speeds and regenerative braking operation. However, considering the ideal scenario of simulation, the technique is also validated experimentally in the next Section.

6.2.3 Experimental Results: 12/8 SRM

The proposed VF-PCC technique is validated experimentally using the setup described in Chapter 5. The speed is set by the dynamometer as 1000 rpm, and the TSF algorithm-based reference currents are used for the initial analysis. Figs. 6.8(a)-(c) show the experimental results at a sampling frequency of 25 kHz. Fig. 6.8(a) shows the results of current tracking using the conventional HCC with soft-switching. Fig. 6.8(b) uses the conventional predictive current control (PCC) implementing the current tracking through a cost function that uses current $i(k+2)$ to track the reference. Finally, Fig. 6.8(c) shows the results for the proposed technique.

Although all the techniques successfully track the reference current, Table 6.4 evidences an improve tracking in terms of the standard deviation or rms error. Using the same sampling frequency, the technique reduces the tracking error and the switching frequency, at the expenses of a higher computational time. However, given that the proposes technique does not compare the currents but flux linkage, the computational time is reduced with respect to conventional PCC. It was found during the experiment that the computational time of PCC is $30\mu s$, while the proposed VF-PCC is executed at around $10\mu s$.

In addition, and similar to the simulation results in the previous section, the
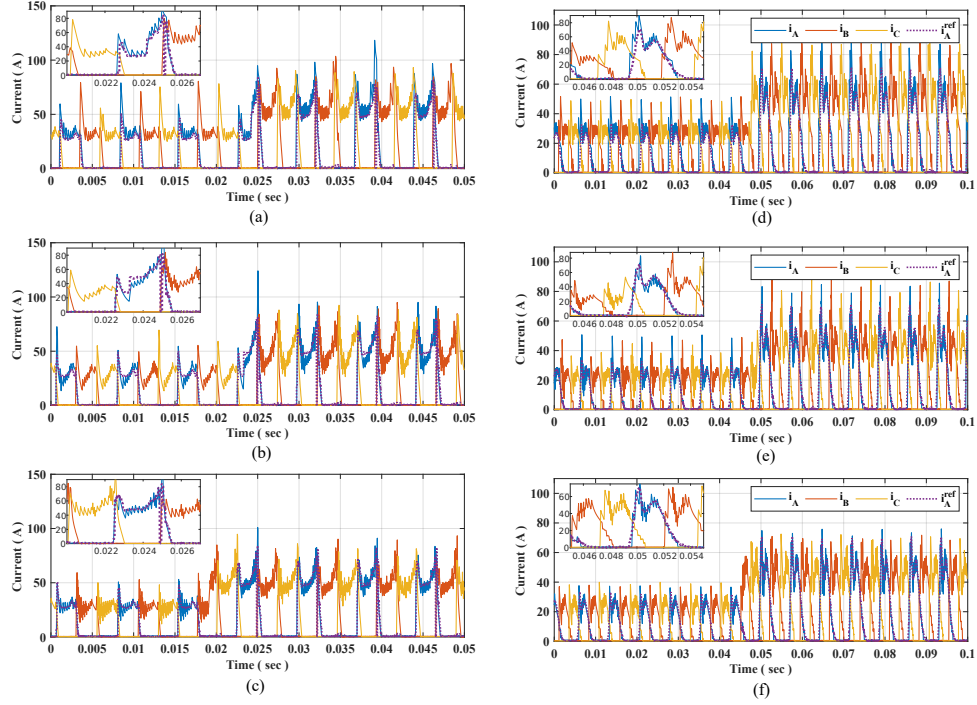
Figure 6.8: Experimental results for the 12/8 three/phase SRM. (a) TSF-based reference currents with HCC (b) TSF-based reference currents with PCC (c) TSF-based reference currents with VF-PCC (d) RFS-based reference currents with HCC (e) RFS-based reference currents with PCC (f) RFS-based reference currents with VF-PCC

RFS-based reference currents are also presented in 6.8(d)-(f), which evidence an outperforming result of the proposed technique over conventional PCC and HCC. Table 6.4 highlights again the improved current tracking with a reduced computational time, thus showing the benefits of the proposed contribution.

Negative speed operation

From Chapters 3 and 4, it is clear that one of the main drawbacks of existing predictive-based techniques is the lack of operation in the four-quadrants. Therefore, the proposed technique is also tested for negative speed operation. Fig. 6.9 shows the results comparing the operation at -1000 rpm of both the conventional PCC and the
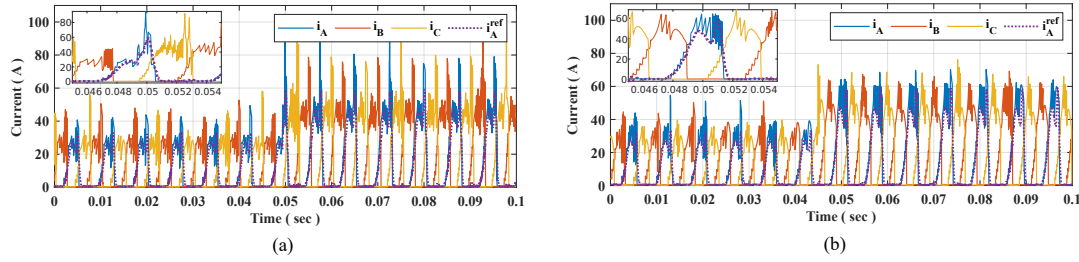
Figure 6.9: Experimental results for the 12/8 three/phase SRM at -1000 rpm. (a) Conventional PCC (b) Proposed VF-PCC

proposed technique. Table 6.4 shows the measurements in terms of current tracking deviation and average switching frequency. Results evidence a better performance of the proposed technique and prove its applicability for different operating conditions.

High-speed operation

Results of the proposed technique are also validated at high-speed. As the SRM has its highest efficiency and market-placing in the high-speed operation, the proposed technique must be able to properly operate in such a speed levels. As the speed increases and the back-EMF becomes more significant, it becomes challenging to inject current into the phase windings. As the proposed VF-PCC utilizes the flux linkage as a state variable, the limitations and rate of change of flux are inherently adopted within the algorithm. Fig. 6.10 shows the operation at 2500 rpm, 3500 rpm and 4500 rpm, proving that the proposed strategy allows current tracking in the mentioned conditions.
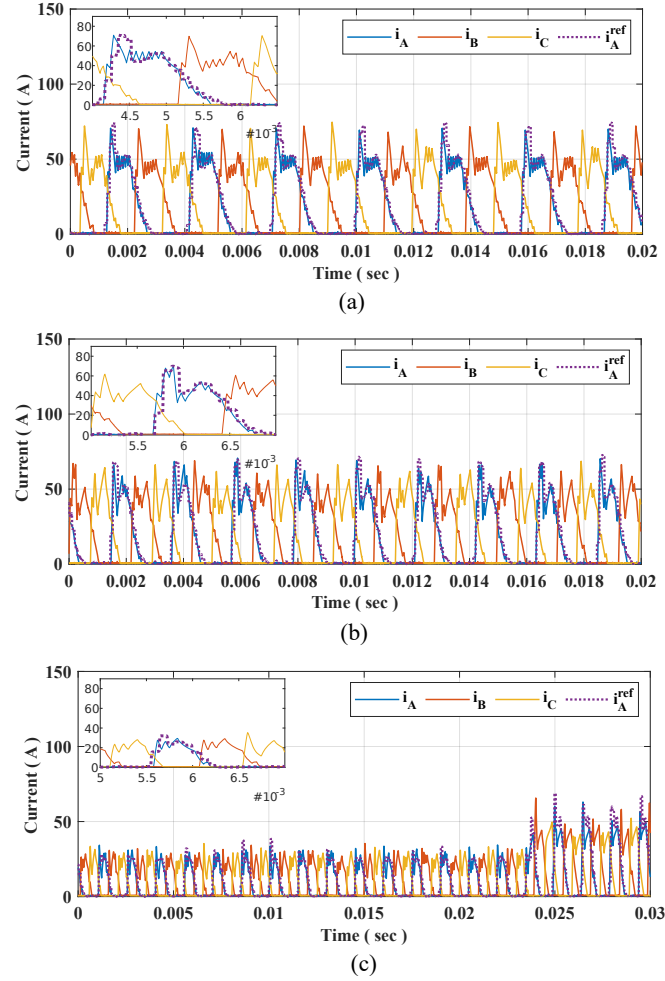
Figure 6.10: Experimental results for the 12/8 three/phase SRM using the proposed VF-PCC. (a) at 2500 rpm (b) at 3500 rpm (c) at 4500 rpm

Parameter sensitivity analysis

One of the main drawbacks claimed in the literature for MPC-related techniques is the high dependence on parameter and measurement accuracy, thus making the operation extremely sensitive to parameter variation. The use of a virtual-flux mapping enhances the robustness of the technique, as evidenced in the results of Fig. 6.11. This figure compares the effect on tracking when the flux linkage static map or resistance present a mismatch. The comparison is achieved by reducing it a 25 % (Fig. 6.11(a),(b)), increasing it a 25 % (Fig. 6.11(c),(d)), or varying its estimated phase resistance by 25 % (Fig. 6.11(e),(f)). Although the latest does not affect any of the techniques significantly, the variations on the flux linkage drastically affect conventional PCC, while the VF-PCC maintains its tracking performance. Table 6.4 summarizes the tracking deviation of the case in which the inductance was reduced by a 25 %.

Robustness against parameter variation might also offer alternative applications such as self-commissioning, in which the drive itself can execute an algorithm to identify machine parameters. Using only a rough estimation of the flux, phase current can be injected and the flux linkage computed.

Operation at a lower sampling frequency

Finally, if SRM points towards a competitive market, its control technique must operate in the lowest possible sampling frequency. It is a common standard in automotive industry, in particular for electrified powertrains, to adopt a maximum of 10 kHz sampling frequency. Fig. 6.12 shows the performance of the proposed technique at the mentioned frequency. Although tracking error in Table 6.4 are higher, the technique
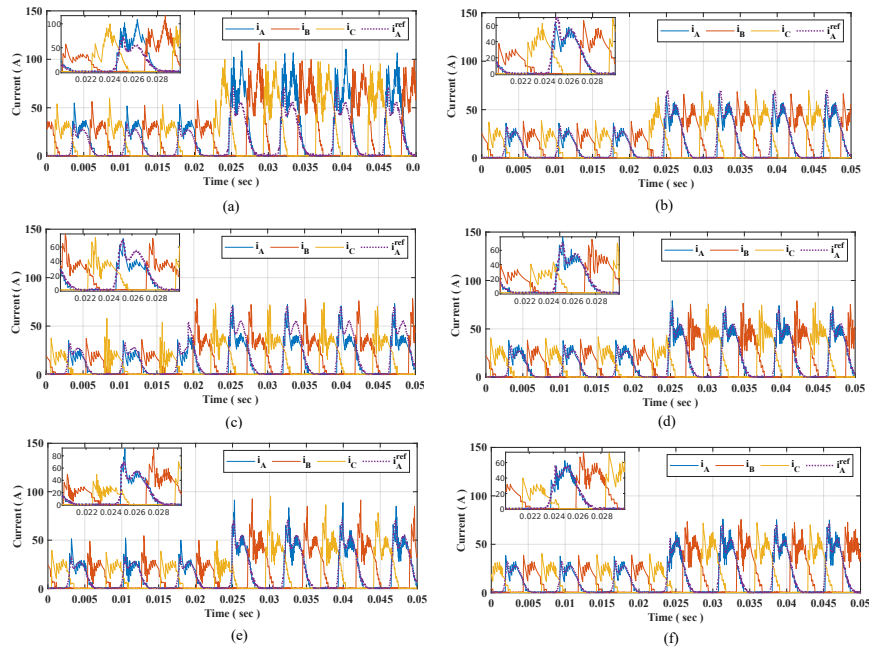
Figure 6.11: Experimental results for the 12/8 three/phase SRM. Parameter sensitivity analysis. (a) PCC performance with 25 % reduction in the flux linkage static map (b) Vf-PCC performance with 25 % reduction in the flux linkage static map (c) PCC performance with 25 % increase in the flux linkage static map (d) V-PCC performance with 25 % increase in the flux linkage static map (e) PCC performance with 25 % reduction in the phase resistance (f) VF-PCC performance with 25 % reduction in the phase resistance
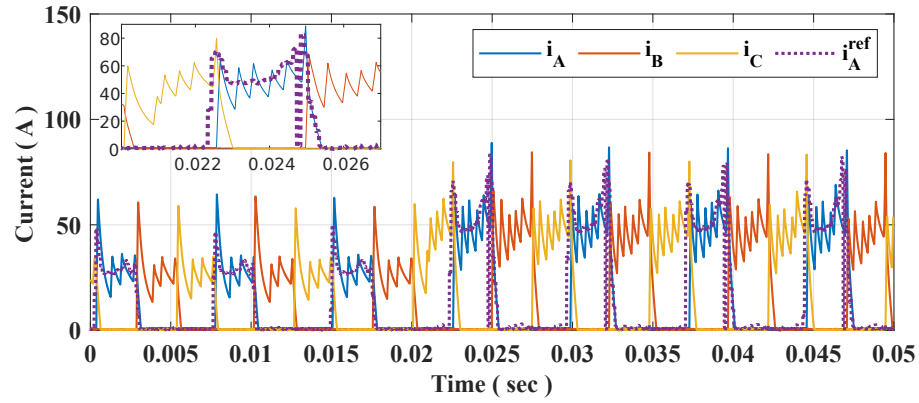
Figure 6.12: Experimental results for the 12/8 three/phase SRM

still tracks the dynamically challenging current.

Assessment

Table 6.4 summarizes the performance results of the proposed techniques with respect to conventional predictive current control and hysteresis current control. The comparison is assumed to keep the same control structure of all operating conditions. In this way, the comparison proposed in Fig. 6.13 evidences the superior performance of the proposed technique for a wide range of conditions. Although HCC get a maximum score in computational time and immunity to parameter mismatch, it cannot handle negative or high speed without additional considerations. On the other hand, the proposed VF-PCC has demonstrated its ability to operate in different operating conditions with robustness and reliability.

Table 6.4: Estimated rms error and average switching frequency of experimentally validated VF-PCC with respect to PCC and HCC

Operating point	$\epsilon_{rms}(A)$			$f_{sw}^{av}(kHz)$		
	VF-PCC	PCC	HCC-SS	VF-PCC	PCC	HCC-SS
1000 rpm (TSF)	7.49	7.896	11.48	3.2	3.8	3.5
1000 rpm (RFS)	3.72	4.465	7.82	3	3.5	3.5
-1000 rpm	5.87	5.93	N/A	4	5.8	N/A
1000 rpm (10 kHz)	11.47	12.45	N/A	2.8	3	N/A
1000 rpm $\lambda = 0.75\lambda(i,\theta)$	5.108	11.73	N/A	6	4.8	N/A

6.3   Summary

A virtual-flux FCS-MPC method for the SRM drives has been developed. The control is based on a virtual-flux tracking algorithm which predicts the phase flux linkage using the machine voltage equation and flux static characteristics. A cost function is then used to evaluate the switching states that produce the lowest flux linkage error with respect to a flux reference. A state limitation graph was also proposed to limit the number of commutations and computational burden. This controller indirectly tracks the provided phase current.

Simulation results evidenced the improved performance of the proposed technique with respect to the benchmark HCC methods. For this, two current shaping strategies were used: TSF, with trapezoidal-wise waveforms, and RFS, with more dynamically challenging waveforms. It was found that the HCC methods presents drawbacks related to different operating points, while the proposed technique can work consistently
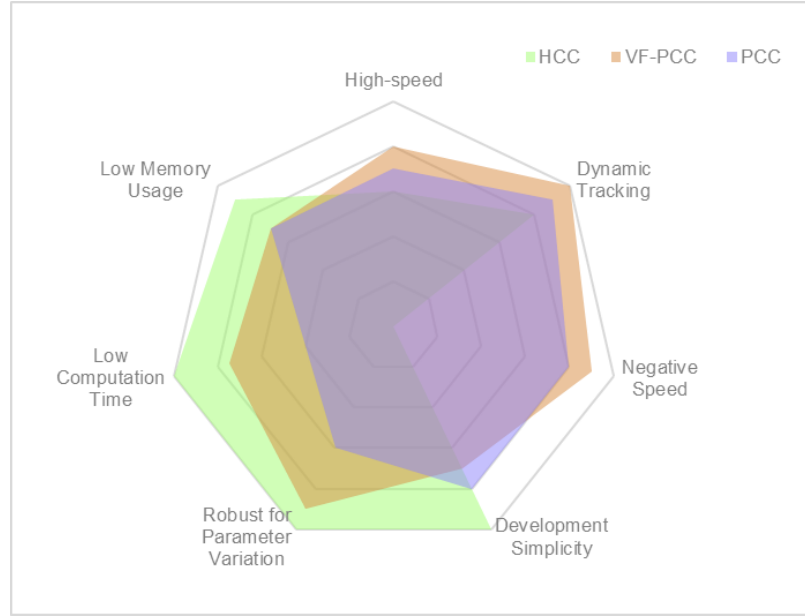
Figure 6.13: Assessment

through all of them. The main benefits of the proposed method are: the current tracking accuracy is improved, and the estimated switching frequency is lower. Moreover, the FCS-MPC can operate in the four quadrants tracking current even for generating mode. In addition, simulation results evidenced the benefits of variable switching frequency on high-power SRMs to handle the additional effect of non-negligible mutual coupling. This was simulated through a 60 kW automotive-based SRM in comparison with hysteresis current control and delta modulation based control.

The proposed technique was validated experimentally in a three-phase 12/8 SRM with small phase inductance. Multiple tests evidence the superiority of the proposed technique to adapt into different operating conditions with no further modification of the control algorithm. A parameter sensitivity analysis also demonstrated the robustness of the proposed technique and its potential with respect to other predictive-based techniques.

Chapter 7

Predictive Torque Control (PTC) of SRM Drives

A comprehensive analysis on predictive torque control applied to SRM drives was presented in Chapter 4, along with the discussion on the torque sharing, modelling and modulation techniques adopted in the literature. From the above, it was concluded the possibility to improve the torque control by taking advantage of the online optimal-search nature of MPC.

In this Chapter, two predictive-based torque control algorithm are proposed. Both of them rely on the use of a static-map-based predictive model and a FCS-approach. The first one proposes an improved prediction based on a Kalman filter. The second, adopts the concept of virtual-flux in order to define the torque sharing online. The algorithms are simulated in the 5.5 kW 8/6 and the 12/8 SRMs previously analyzed in Chapters 5 and 6. The virtual-flux-based PTC algorithm is also validated experimentally in the 12/8 SRM previously discussed.
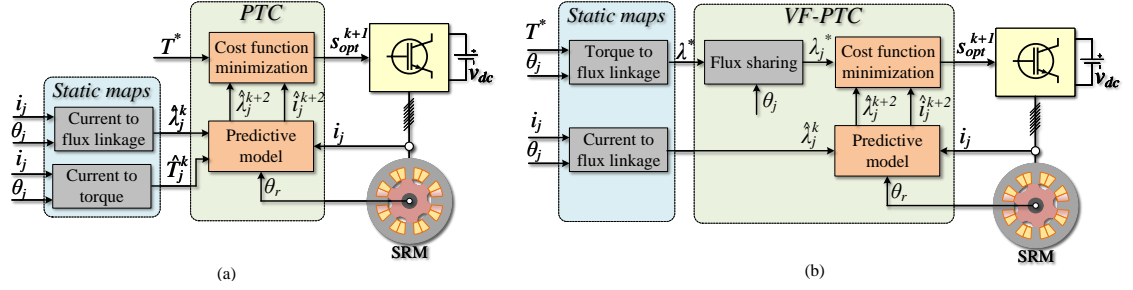
Figure 7.1: Block diagram of the proposed strategies (a) PTC-KF and (b) VF-PTC

7.1   Proposed predictive torque control techniques

7.1.1   Predictive torque control with Kalman Filter (PTC-KF)

Fig. 7.1(a) shows the block diagram of the proposed PTC. The algorithm works as follows: the phase current and rotor position are measured from the machine and, after a delay compensation stage, they are fed into the predictive model. The predictive model then computes the predicted flux linkage $\lambda(k + 2)$ based on all possible converter states: These values of flux are then mapped for each phase as a predictive torque $T(k + 2)$, and the algebraic sum of all of them gives all possible values of total torque $T_{tot}(k + 2)$. Finally, the cost function chooses the switching states that minimized the cost. As shown in Fig. 7.1(a), the torque sharing is not predefined, and the algorithm itself selects the phase that best contributes to the total torque. Additional restrictions are added to the selection criteria in order to reduce the computational load. Details of the different stages of the proposed technique are given next.

Predictive model

The predictive model combines the concept of virtual-flux from Chapter 6 with a simple but reliable prediction technique and the use of static maps. As only phase currents are position are known, the flux linkage at the instant of measurement can be estimated.

As it is assumed that a good control strategy has been delay-compensated, the measurement is considered to be executed one instant of time before the algorithm execution, that is, at the instant k. The variables $i(k)$, $\theta(k)$ and $\lambda(k)$ are known at the motor stage in Fig. 7.1(a). A simple approach uses the forward Euler approximation to estimate the variables at the next sampling time, but it depends on both the measurements and the accuracy of the static maps.

To improve the robustness of the proposed technique, a linear Kalman filter is implemented in the compensation stage. As the variables are already mapped into the virtual-flux domain, they can be represented by the model 2.3, which is locally linear at the given sampling time. The method proposed in [79] for delay compensation is followed. The current-based model can be represented by,

$$\dot{\lambda}(k+1) = \frac{-R_s\lambda(k)}{L)} + v(k) \tag{7.1a}$$

$$i(k) = \frac{\lambda(k)}{L(k)}, \tag{7.1b}$$

where $L(k)$ is the inductance profile, obtained from the flux linkage static maps. The simplest Kalman filter algorithm relies on a set of *time-update* (or prediction) and *measurement update* equations [237]. These equations are fed by the parameters from (7.1) and measurements, and they compare the measurements at the instant $k+1$ with

the ones at k and the estimations. This process delivers a clean, filtered noise-free prediction, which is trustful to use in the predictive model.

Next, the compensated equivalent current $i(k + 1)$ is obtained from the inverse static map using $\lambda(k + 1)$ and the estimated electrical angle $\theta(k + 1)$. To obtain the latest, Lagrange approximation is applied to determine the electrical angles at $k + 1$ and $k + 2$ based on [238],

$$\theta(k + 2) = 6\theta(k) - 8\theta(k - 1) + 3\theta(k - 2), \tag{7.2}$$

Once the compensated variables are obtained, the prediction of all possible control actions and their behaviour on the machine is computed. Under the concept of FCS-MPC, the switching states of all phases are considered, and the total torque is calculated for every combination. If this is applied to a three-phase SRM, considering soft-switching operation, then there are 27 possible combinations, which elevate to 81 for a four-phase machine.

In the previous chapter, the number of possible combinations was not a severe issue, since the current tracking is done per each phase, individually. However, as the torque control involves the contribution of all phases (or maximum two at the same time, ideally), additional restrictions must be considered.

Restrictions

Fig. 7.2 shows the restrictions prior the calculations of the predicted flux and torque, $\lambda(k + 1)$ and $T(k + 2)$, respectively. In torque control of SRMs, at least one of the phases will be contributing to the torque generation. Fig. 7.2(a) shows the state restriction applied in this case, which is exactly the same one implemented for PCC

(a)   (b)
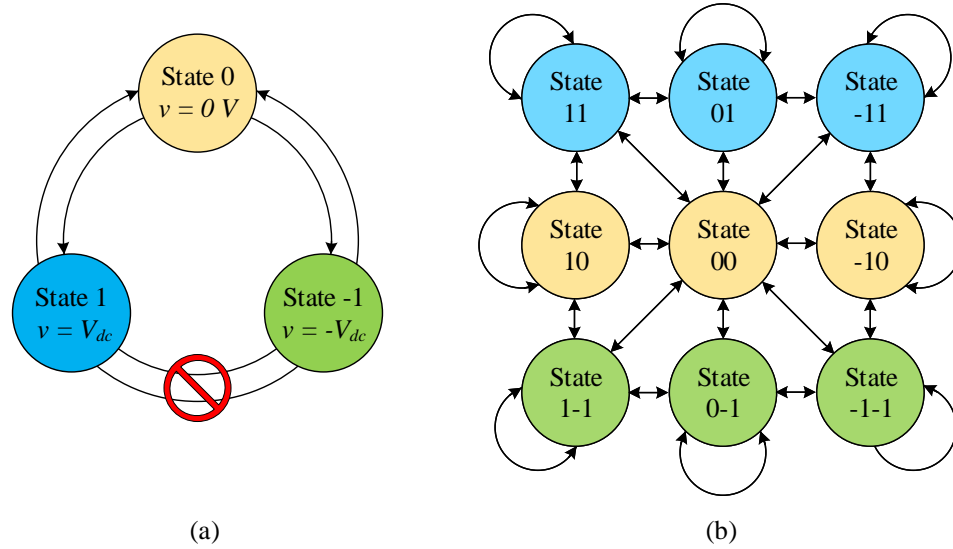
Figure 7.2: Limitation in the state transition

in Chapter 6 in order to reduce the number of commutations of the switching devices. This restriction is then extended to the case when two phases are active during a transient: one incoming phase, building up current, and one outgoing phase, reducing the current to zero. 7.2(b) illustrates this consideration, where each of the phases can produce only one commutation per switch [239].

It is also worth noticing that maximum two simultaneous phases are considered for the algorithm. It can be extended to the case when three phases are simultaneously active, which might happen in case of SRMs with more phases and working at high-speed. However, this particular applications is out of the scope of this thesis.

Cost function

From Fig. 7.1(a), once the delay compensation and predictive model are defined, the cost function evaluates the optimal control action $v(k + 1)$ to be applied within the next sampling period. In this way, depending on the components of the cost function,

the outputs of the predictive model are defined.

Initially, as the main objective is to control torque with a reduced ripple, the torque error $T^* - T_{tot}$ is considered. It is important that the total torque $T_{tot} = \sum\limits_{j=0}^{m} T_j$, where T_j is the phase torque and m is the number of phases. The value of T_{tot} is computed for every possible combination of allowed switching states.

Next, the regulation on the phase currents is considered. The objective is to achieve the minimum torque ripple, while tracking the reference torque with the minimum phase currents. This is included in the cost function as a simple algebraic sum of all phase currents. In addition, as this is a secondary objective, a weight factor $\sigma_i = 0.015$ is included. This factor has been heuristically tuned for this applications; however, there exist several techniques for calculating this factor and even to completely omit it. These techniques have been reviewed in Chapter 4.

The proposed cost function is shown in (7.3). Similarly to the technique proposed for current tracking, an additional safety factor is included, which would make the cost infinity if the current goes beyond a defined threshold.

$$\min_{v_0 \ldots v_{N-1}} g = \left| T^{ref} - T_{tot}^{v_g}(k+2) \right|^2 + \sigma_i \sum i_j(k+2) + I_m(k+2), \qquad (7.3)$$

where $I_m(k+2)$ is defined by the predicted current in the same manner as in (6.4).

Finally, it is worth noticing that there is not penalty for switching, as it has already been considered in the restrictions, and such restriction limits the dynamic response of the technique.

7.1.2   Virtual-flux predictive torque control (VF-PTC)

The PTC-KF algortihm offers an enhanced prediction and therefore control action from the MPC technique. However, the use of Kalman filter requires the knowledge of an additional static map as well as a higher computational load. In this section, a variation with lower computational burden is proposed based on the same principle as the VF-PCC discussed in Chapter 6. The virtual-flux predictive torque control (VF-PTC) algorithm is shown in Fig. 7.1(b). The algorithm works as follows: the measured phase current and position use the flux linkage static map to estimate the flux at the time k, which is used for delay compensation obtaining $\lambda(k + 1)$. The compensation uses the forward Euler discretization technique, although other higher-order techniques might be suitable as well. Next, the current at the instant $k + 1$ is computed from the inverse static map and used to predict the $\lambda(k + 2)$. Similarly, the reference torque feeds a static map to obtain an equivalent phase flux linkage. The reference flux is then adopted as the individual phase flux during the span $\theta_j > 0°\&\theta_j < 180°$, with j being the active phase.

It is worth noticing that no torque vs current static map was implemented; therefore, although there is an additional lookup table, another one is omitted not jeopardizing the memory usage of the microprocessor. The new flux linkage versus torque and position static map is presented in Fig. 7.3. It is worth noticing that this map corresponds to the positive torque and half cycle. Given the symmetry of the torque waveform shown in Fig. 7.6, the negative torque would produce zero flux in the range $\theta <= 180°$, while the value is nonzero in the range $\theta > 180°$.
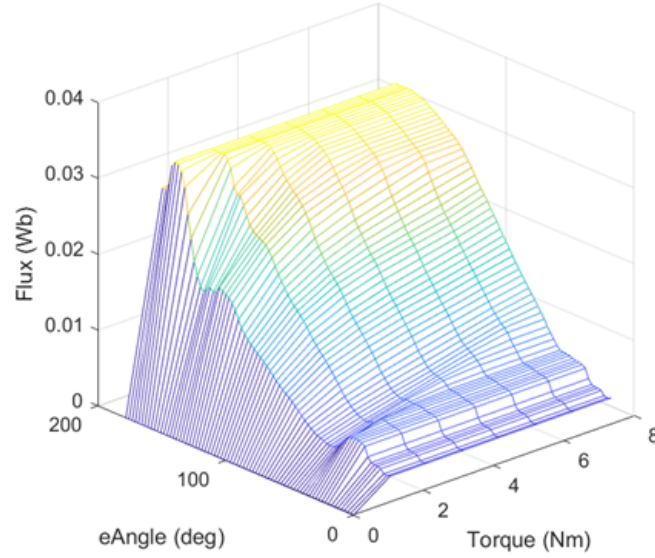
Figure 7.3: Flux linkage as a function of torque and position

Predictive model

The prediction in the VF-PTC technique uses the same model as the PTC-KF, but is does not require the individual calculation of phase torque, thus improving the computational time of the overall technique. Instead, the control action is decided based on the flux linkage as discussed next.

Cost function

The cost function adopted for this technique follows the same principles as the one presented above in (7.3). However, given the control using the variables mapped in the virtual-flux domain, the cost function main objective must be the flux tracking.

Therefore, the cost function can be modified as,

$$\min_{v_0...v_{N-1}} g = \left|\lambda^{ref} - \lambda^{v_g}(k+2)\right|^2 + \sigma_i \sum i_j(k+2) + I_m(k+2), \qquad (7.4)$$

where λ^{ref} is the equivalent reference phase flux linkage, and $\lambda^{v_g}(k+2)$ is the predicted phase flux linkage vector accounting per all the switching states.

7.2   Simulation Results

7.2.1   Four-phase 8/6 SRM

The four-phase 8/6 SRM with characteristics shown in Fig. 2.2 is simulated to evaluate the performance of the proposed PTC-KF technique.

The algorithm was tuned using the procedure from Fig. 7.1 considering an operation at 800 rpm, but the simulation could also run at higher speed up to base speed and beyond with no modifications in the control structure. This evidences the flexibility and robustness of predictive control and the use of a cost function. Simulation results are shown in Figs. 7.4 and 7.5. The PTC-KF is compared with conventional TSF with cubic transition, where the equivalent current reference is tracked with both HCC and the PCC proposed in Chapter 6. For all simulations, the sampling frequency was fixed as 100 kHz.

Fig. 7.4(a) evidences a proper torque tracking of the reference torque for the proposed technique. Although there exist some dips during phase transition, the algorithm successfully decided the optimal behaviour that does not compromise the current. Fig. 7.4(b) shows how there exist higher peaks during phase transitions, as
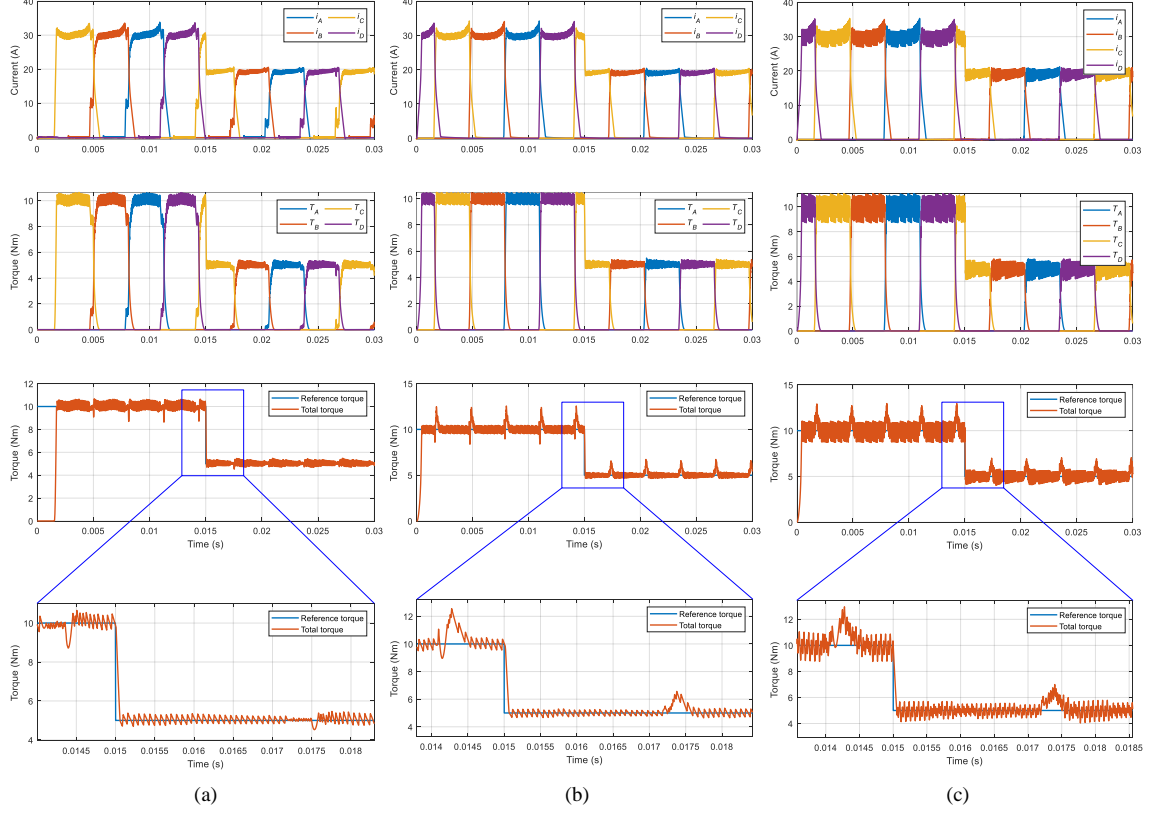
Figure 7.4: Simulation results for the four-phase 8/6 SRM at 800 rpm using (a) TSF and HCC (b) TSF and VF-PCC (c) Proposed PTC with Kalman Filter

the implemented TSF does not consider the maximum rate of change of flux linkage, and therefore, the rate of change of each current to prevent these phenomena [17]. Fig. 7.4(c), although is the simplest, computationally-wise, presents not only the same transition peaks but also a higher ripple during steady state operation of the phase. In the same way, Table 7.1 shows the tracking rms error of each technique. The general trend is to present an easier control at low load, and the proposed PTC-KF achieves the best response in terms of ripple.

Fig. 7.5 shows the results at high-speed (6000 rpm). Given the natural field-weakening that occurs in SRMs, the reference torque in this simulation is reduced

Table 7.1: Estimated rms error and average switching frequency

Operating point	$T_{\epsilon(rms)}$ (Nm)		
	PTC	TSF + VF-PCC	TSF + HCC
$T_{ref} = 10Nm$ $\omega = 800rpm$	0.2736	0.6200	0.8528
$T_{ref} = 5Nm$ $\omega = 800rpm$	0.1486	0.4655	0.5913
$T_{ref} = 1Nm$ $\omega = 6000rpm$	0.0706	0.0884	0.1596
$T_{ref} = 0.5Nm$ $\omega = 6000rpm$	0.0387	0.0603	0.1075

10 times. From Fig. 7.5 and Table 7.1 is can be seen how the proposed technique manages to track the given reference with an acceptable torque ripple, having the lowest rms error. The rms error measures the deviations from the reference. Given that all techniques successfully track the average torque, the rms error becomes a good measure of ripple, which is defined by [9],

$$T_{rms} = \sqrt{\frac{1}{\theta_1 - \theta_2} \int_{\theta_1}^{\theta_2} (T(\theta) - T_{ave})^2 \, d\theta} \tag{7.5a}$$

$$T_{ave} = \frac{1}{\theta_1 - \theta_2} \int_{\theta_1}^{\theta_2} T(\theta) d\theta, \tag{7.5b}$$

7.2.2 Three-phase 12/8 SRM

Proposed PTC-KF

A similar simulation is performed for the 5.5 kW, 12/8 SRM, 72 V SRM described in Chapter 5. This machine is particularly challenging to control because it has a considerable small phase inductance. the inductance was experimentally obtained in Fig.
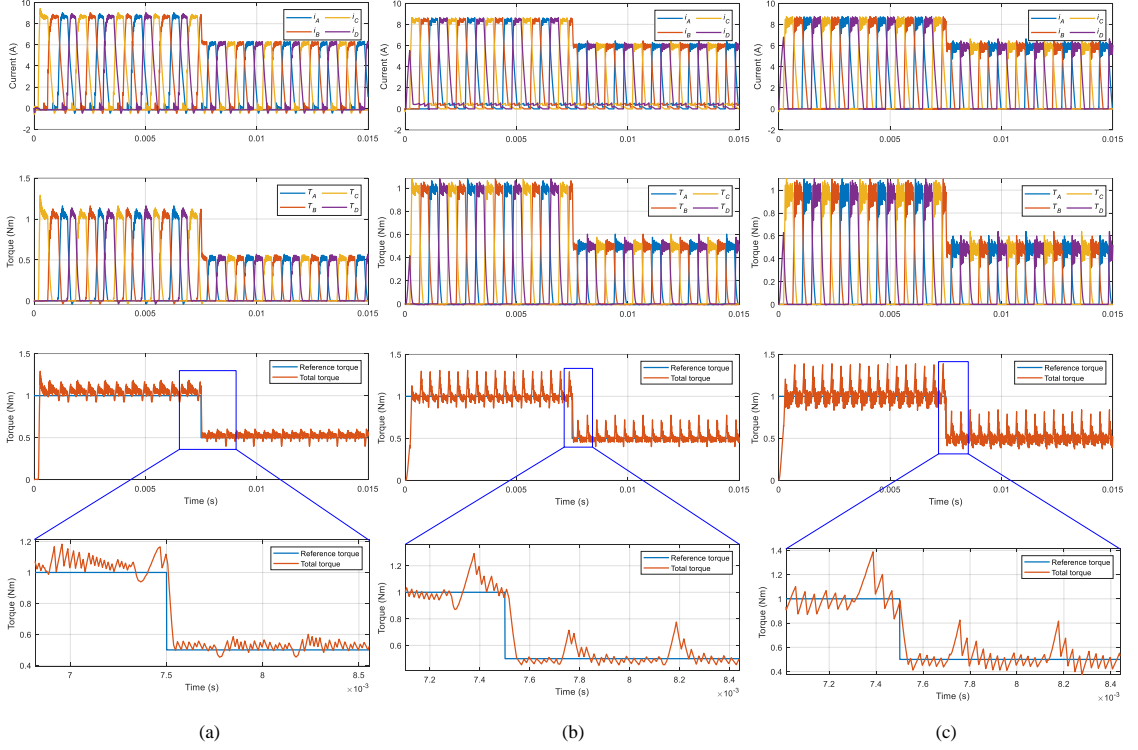
Figure 7.5: Simulation results for the four-phase 8/6 SRM at 6000 rpm using (a) TSF and HCC (b) TSF and VF-PCC (c) Proposed PTC with Kalman Filter

5.6, and it is shown in Fig. 7.6 with the torque profile for convenience of the reader. Previous works using FCS-MPC such as [116] rely on low-speed operation of machines with an inductance up to 40 times more than the maximum inductance in Fig. 7.6. In this section, the proposed technique is validated at low- and medium-speed operation as well as for regenerative braking conditions, thus evidencing its effectivity of controlling low-inductance machines at high speeds. As the static characteristics are based on experimental testing using a TI28335 DSP and IGBT-switched converter, the sampling frequency of all simulations is limited to 40 kHz, which is intended to be validated in such system.
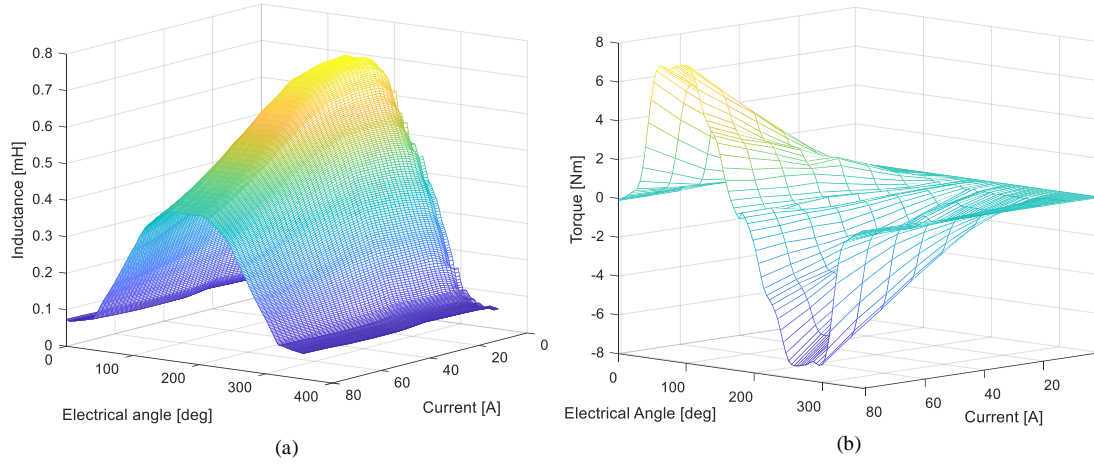
Figure 7.6: Experimental static characteristics of the 12/8 SRM (a) phase inductance (b) phase torque

Fig. 7.7 shows the results at 1000 rpm, which evidences the clear improvement in the torque ripple by using Kalman filter for delay compensation with respect to conventional PTC. A similar behaviour occurs at high speed, where the control becomes more challenging. Conventional PTC in Fig. 7.8 evidences a slightly improvement in the torque ripple, which avoids lower peaks. This can be quantified by calculating the average produced torque and the rms tracking error with Eq. (7.5). The average torque and rms torque error are shown in Table 7.2. As stated, the use of Kalman filter improves both variables.

The control is also tested to operate in more than one quadrant, as shown in Fig. 7.9 where the algorithm is run at negative 5000 rpm. Without any modification in the control structure, the proposed PTC tracks the reference torque, but it fails in providing reduction of the torque ripple. This can still be solved without changing the control basis, just by adapting the cost function gains to allow more or less current to be used within the tracking.
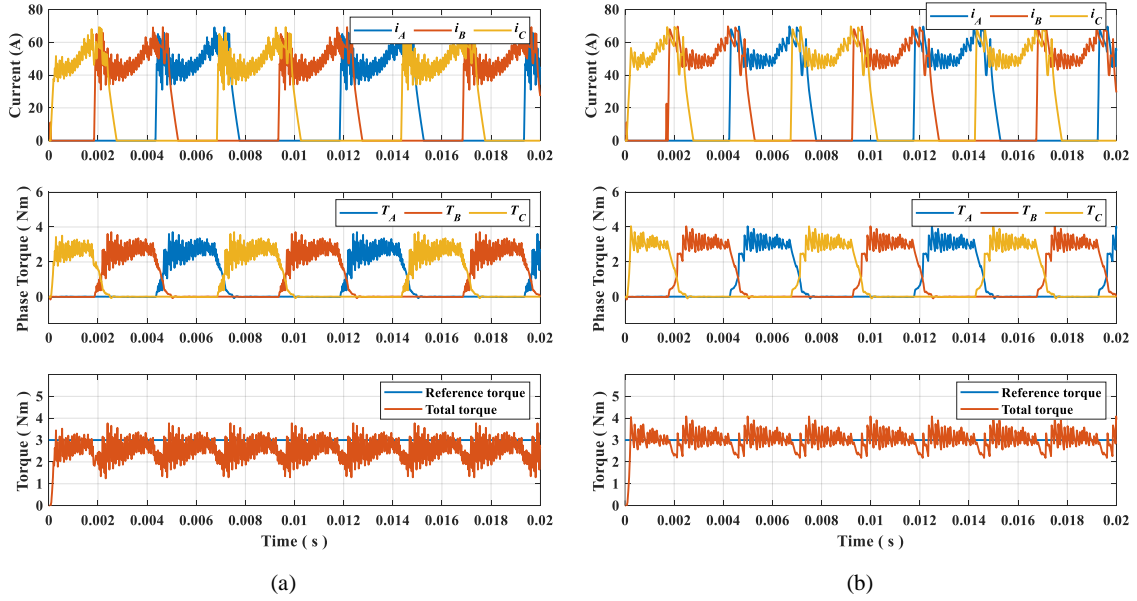
Figure 7.7: Simulation results of the 12/8 SRM at 1000 rpm, 3 Nm using (a) FCS-PTC with simple delay compensation (b) FCS-PTC with Kalman Filter
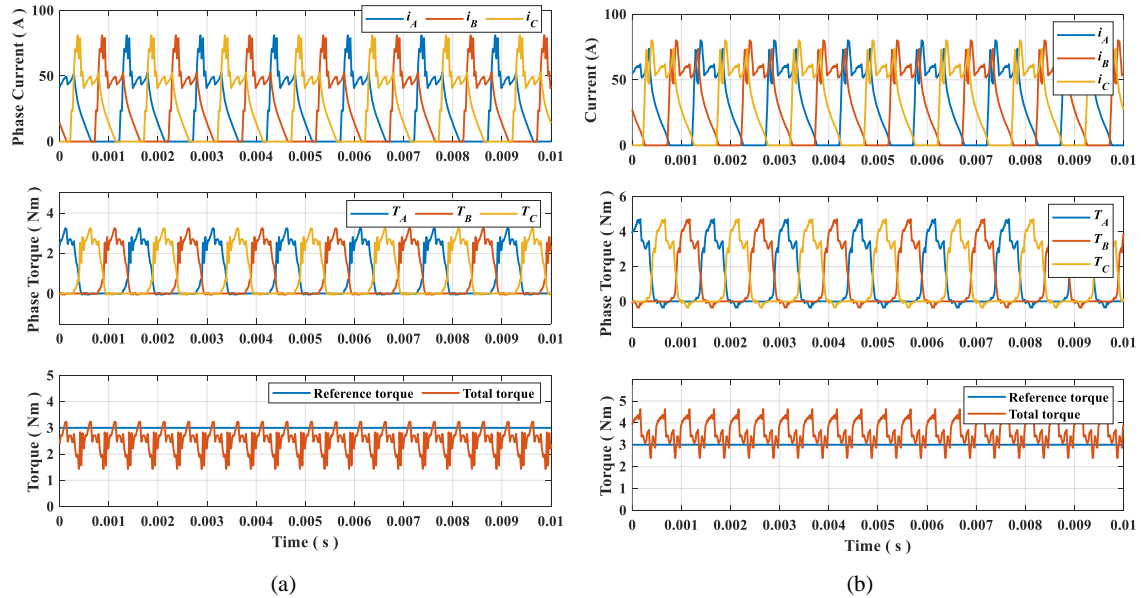
Figure 7.8: Simulation results of the 12/8 SRM at 5000 rpm, 3 Nm using (a) FCS-PTC with simple delay compensation (b) FCS-PTC with Kalman Filter

133
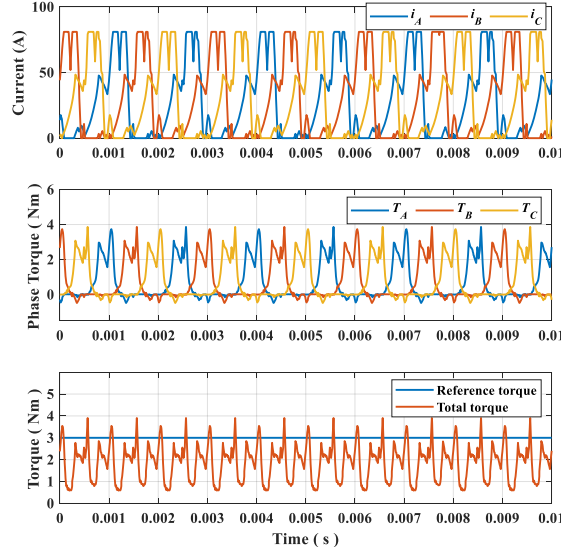
Figure 7.9: Simulation results of the 12/8 SRM at -5000 rpm, 3 Nm using the proposed FCS-PTC with Kalman Filter

Although it is clear that both techniques are able to track the reference torque, the use of the linear Kalman filter seems to require more phase currents to achieve it. To evaluate this claim, the ratio of average torque per ampere is computed, based on the rms current calculation,

$$i_{rms} = \sqrt{\frac{1}{\theta_1 - \theta_2} \int_{\theta_1}^{\theta_2} i(\theta)^2 d\theta}. \tag{7.6}$$

This ratio allows understanding the control efficiency to produce electromagnetic torque from the machine with the minimum phase currents.

Using Eq.s (7.5)-(7.6), Table 7.2 is built. For the results in Fig. 7.7, the use of Kalman filter not only allows obtaining a higher average torque but also a reduced rms error. However, this is done at the expenses of increasing the phase current, thus producing a reduced equivalent efficiency.

Table 7.2: Performance evaluation of the proposed predictive torque control algorithm

			$T^* = 3$ Nm $\omega = 1000$ rpm	$T^* = 3$ Nm $\omega = 5000$ rpm
T_{ave} **(Nm)**	Simulation	PTC	2.61	2.46
		PTC and KF	3.08	3.5
	Experimental	Conventional	3.3	2.84
		PTC	3.28	2.39
		PTC and KF	3.46	2.86
$T_{\epsilon(rms)}$ **(Nm)**	Simulation	PTC	0.5765	0.7335
		PTC and KF	0.4049	0.8750
	Experimental	Conventional	0.5400	1.0800
		PTC	0.6805	1.1273
		PTC and KF	0.6946	0.9242
i_{rms} **(A)**	Simulation	PTC	34.57	33.80
		PTC and KF	36.40	40.72
	Experimental	Conventional	36.24	38.80
		PTC	37.61	34.94
		PTC and KF	38.92	34.93
T_{ave}/i_{rms} **(Nm/A)**	Simulation	PTC	0.076	0.073
		PTC and KF	0.084	0.086
	Experimental	Conventional	0.091	0.073
		PTC	0.087	0.068
		PTC and KF	0.089	0.081

A similar phenomenon occurs at high speed, where the phase current must be increased to compensate for the torque ripples. This demonstrates the relevance in the trade-off tracking versus efficiency in the cost function, by using the weight factors.

Proposed VF-PTC

Fig. 7.10 shows the simulation of the dynamic and steady-state waveforms of the VF-PTC at 1000 rpm. The simulation was executed with a sampling frequency of 20 kHz.

The results in Fig. 7.10 evidence the successful control of a more challenging machine with small inductance values like the 12/8 SRM. This result is further validated through experimental testing in the next Section.
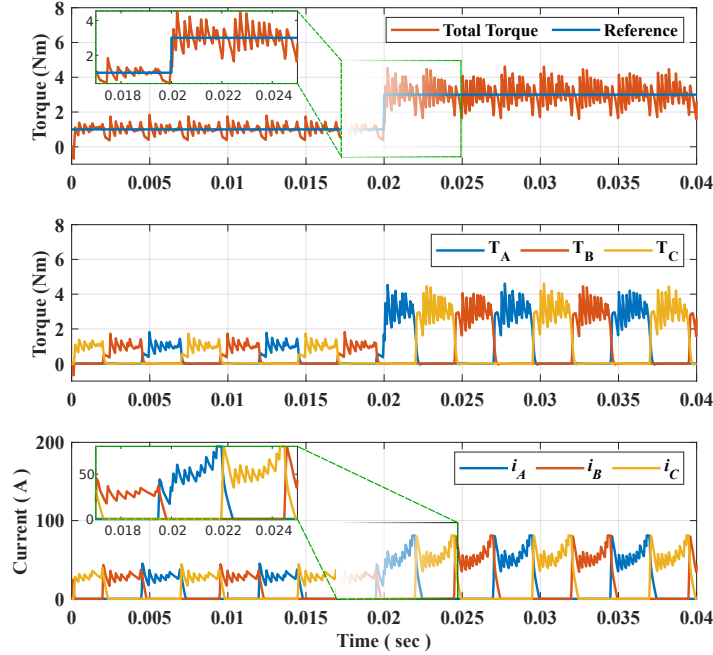
Figure 7.10: Simulation results

7.3 Experimental Results

7.3.1 Proposed PTC-KF

In this section, the torque sharing capability of the proposed PTC-KF technique is evaluated experimentally. The experimental setup has been described in Chapter 5, as well as the machine and dyno characteristics. The machine under test is the three-phase 12/8 SRM previously simulated. The flux linkage, inductance and torque characteristics are obtained experimentally and presented in Figs. 5.5 and 7.6. Given the increased computational burden of the proposed technique, it is not implemented in the available TI F28335 microprocessor. Instead, the equivalent reference current

obtained from the executed simulations in the previous section is implemented experimentally through a current controller at a sampling frequency of 40 kHz for all cases.

Fig. 7.11 shows the experimental results at 3 Nm reference torque and 1000 rpm, which were maintained by the IPM dyno with a commercial speed controller. The phase currents and rotor position were measured in steady state conditions, and their values were used to obtain phase torque and total torque during post-processing. The torque values were obtained using the phase torque static map shown in Fig. 7.6(b).

Results in Fig. 7.11 confirm the behaviour obtained in the simulation from Fig. 7.7, where the torque ripple is considerably reduced by the use of Kalman filter within the predictive torque control strategy. In a similar way, these results are comparable to the ones obtained from conventional torque sharing techniques. The performance evaluation in all cases is shown in Table 7.2. Fig. 7.12 shows the same experiment executed at 5000 rpm. Following the trend from the previous experiment, the proposed technique tracks the reference torque, with the best average torque production and lowest torque ripple. Unlike the simulation results, the PTC with KF presents and improved torque per ampere capacity, which is evident at high-speed with respect to the other two existing methods.

The results evidence its potential to operate the machine in a wide speed range while taking advantage of the machine capabilities at high speed. As concluded in Chapter 4, the target of SRM must be the high efficiency at high-speed; therefore, the proposed torque control algorithm is a step further to position SRMs as a more competitive drive.
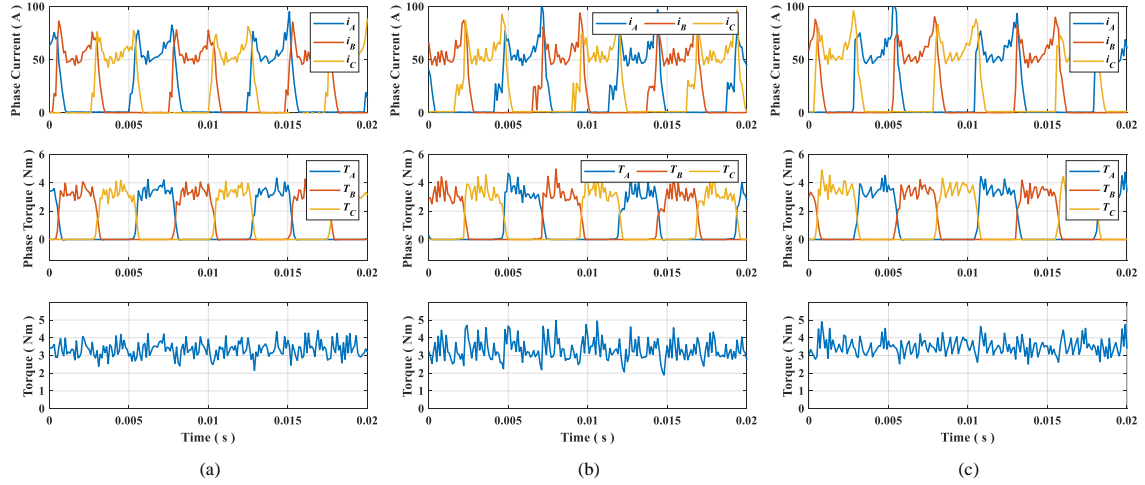
Figure 7.11: Experimental results of the 12/8 SRM at 1000 rpm, 3 Nm using (a) Conventional torque sharing (b) FCS-PTC with simple delay compensation (c) FCS-PTC with Kalman Filter
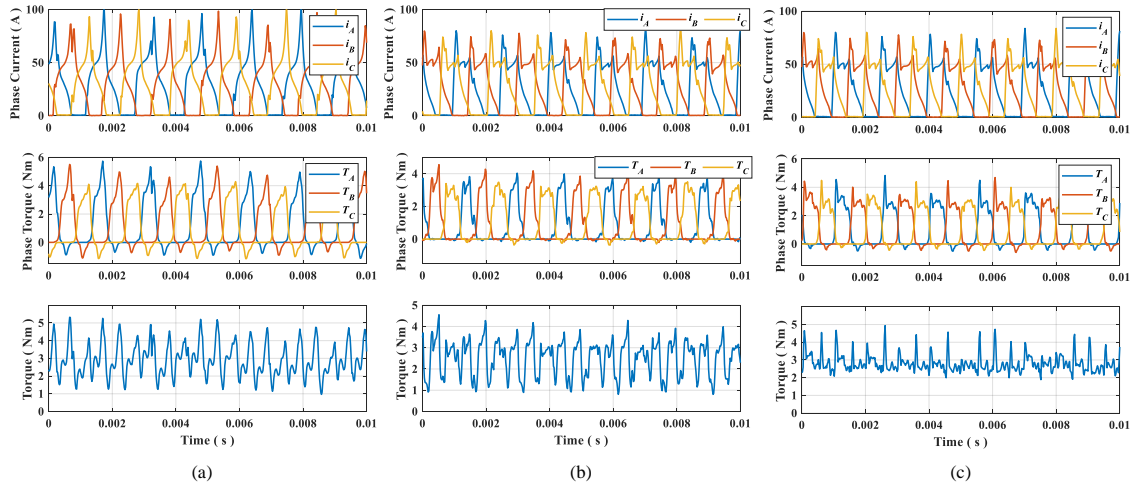
Figure 7.12: Experimental results of the 12/8 SRM at 5000 rpm, 3 Nm using (a) Conventional torque sharing (b) FCS-PTC with simple delay compensation (c) FCS-PTC with Kalman Filter

7.3.2   Proposed VF-PTC

The proposed VF-PTC was implemented in the TI-F28335 microprocessor given its reduced computational burden with respect to the PTC-KF. With the computation time of around $45\mu s$, it is possible to execute this technique at a 20 kHz sampling frequency. For the sake of comparison, a conventional PTC is executed with the same sampling frequency and maximum allowed current.

The technique defines the flux reference by selecting the active phase; therefore, the trigger between one phase and the next is given by the turn on angle θ_{on}. Also, the weight factor associated to the currents in (7.4) is heuristically determined based on experimental work. Fig. 7.13 shows the torque ripple and the average torque per ampere obtained for different variations of θ_{on} and σ_i obtained from several experiments with all these combinations of factors. The resultant parameters are tuned as $\theta_{on} = 29°$ and $\sigma_i = 0.1e^{-7}$.

Fig. 7.14 shows the comparison between the performance of the proposed VF-PTC and the conventional PTC, both at a sampling frequency of 20 kHz and a maximum switching frequency of 20 kHz. The conventional PTC does not require the activation angle, but it need the weight factor for the current minimization component in the cost function. In order to maintain similarity in the operation and safety, this is tuned to maintain a current below the 90 A. Fig. 7.14(b) shows how this limitation penalizes the torque production, thus providing a low torque ripple, a minimum use of currents but an average torque below the reference. On the other hand, the proposed technique in Fig. 7.14(a) provides a better average torque with a slightly higher phase current during the phase transition. This is compared in terms of the standard deviation or rms torque deviation in Table 7.3. It is evident that the proposed technique offers
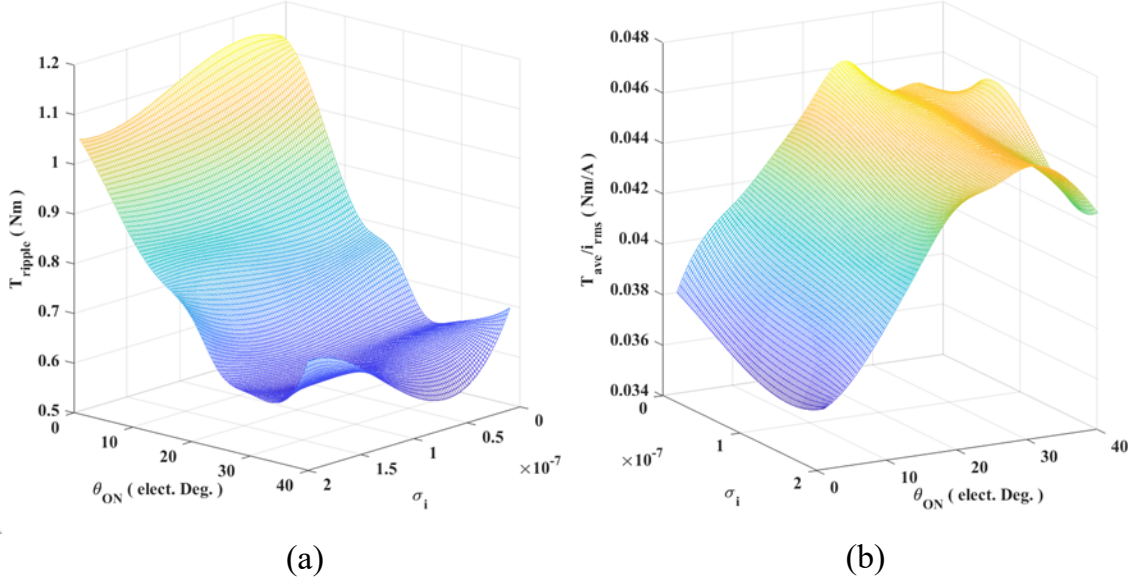
Figure 7.13: Cost function tuning for the optimal VF-PTC technique (a) Torque ripple (b) Average torque per ampere

the best performance with a maximum torque per ampere. The conventional PTC minimizes the current usage, but reduces the average torque production per ampere, thus making the drive less efficient.

Similarly, Figs. 7.15 to 7.17 evidence the results of the VF-PTC outperforming the conventional technique in a similar manner. Although conventional PTC minimizes the peak-to-peak variations of torque, its rms error is higher and the torque production is less efficient. This is also confirmed from the results in Table 7.3.

7.3.3 Parameter sensitivity

As the proposed technique uses a Kalman filter for the delay compensation, it mitigates the potential errors coming from the measurements. However, it relies also on lookup-tables, which vary with conditions such as aging or temperature. It affects the
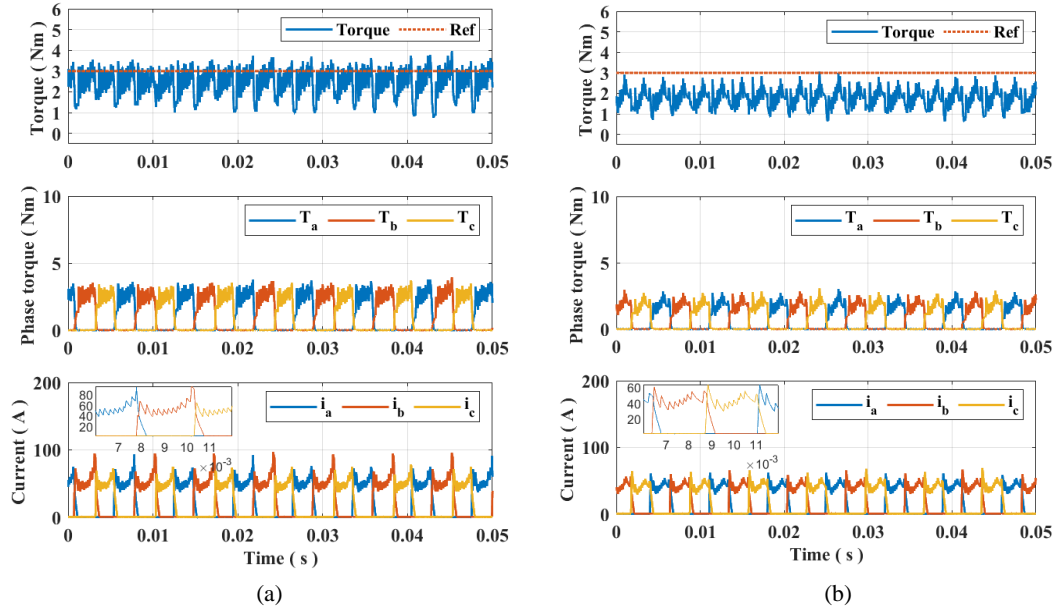
Figure 7.14: Experimental results of the 12/8 SRM at 1000 rpm. (a) Proposed VF-PTC (b) Conventional PTC
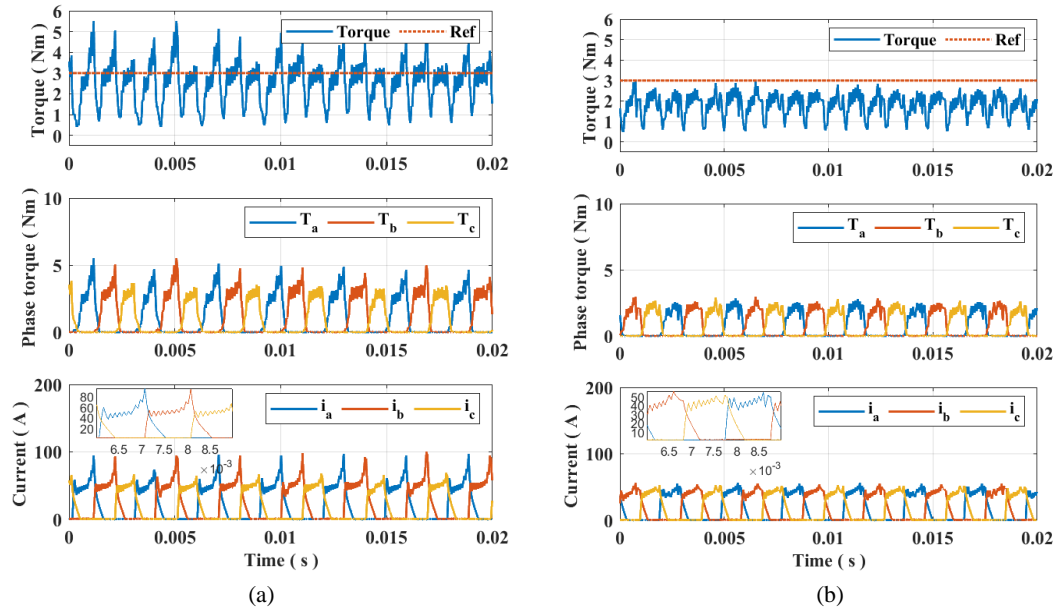
Figure 7.15: Experimental results of the 12/8 SRM at 2500 rpm. (a) Proposed VF-PTC (b) Conventional PTC

141
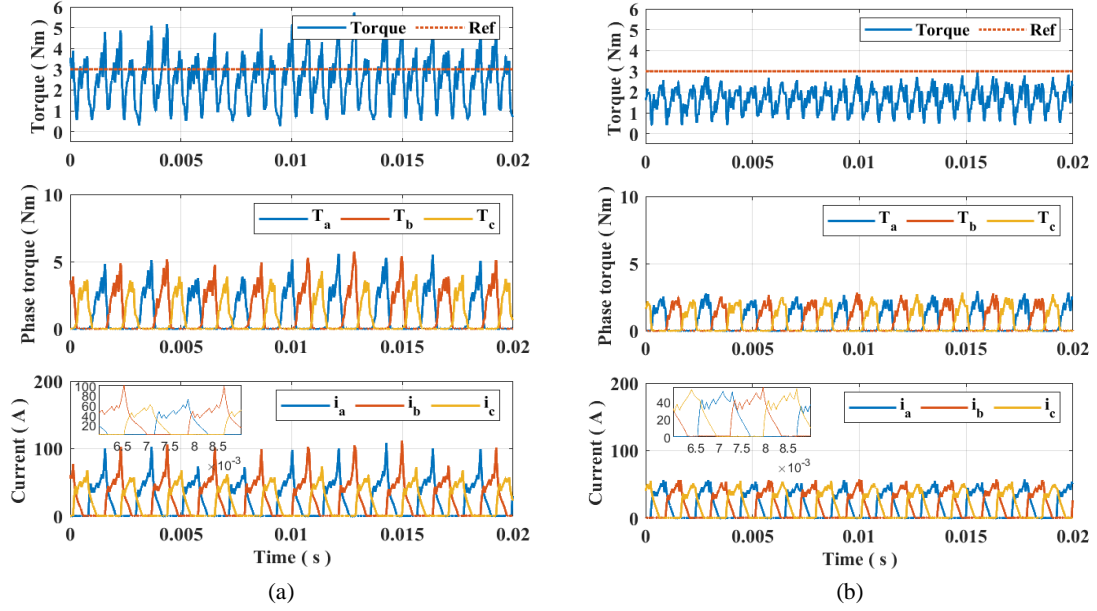
Figure 7.16: Experimental results of the 12/8 SRM at 3500 rpm. (a) Proposed VF-PTC (b) Conventional PTC
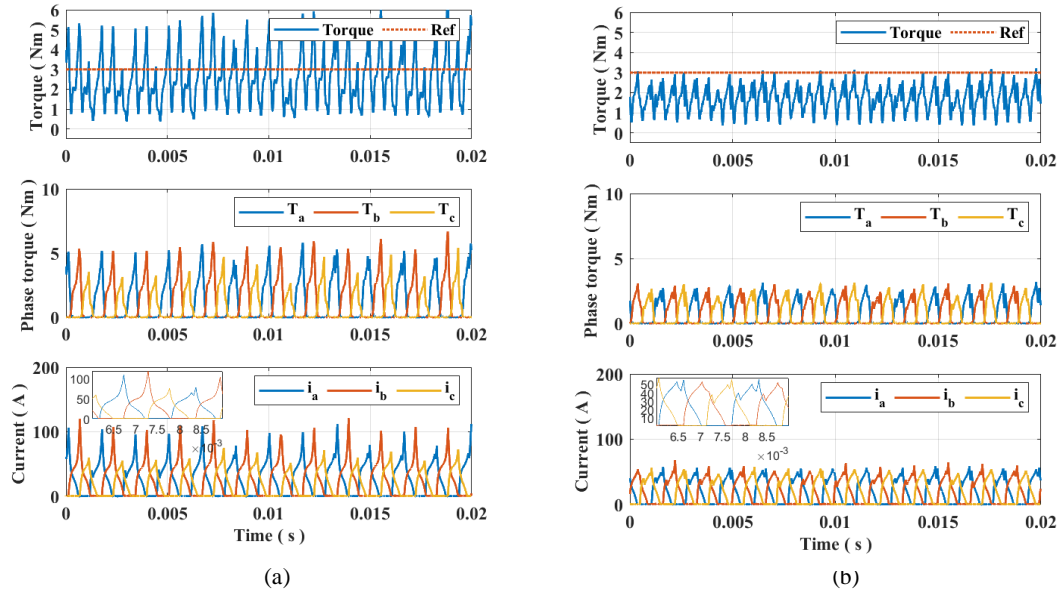
Figure 7.17: Experimental results of the 12/8 SRM at 4500 rpm. (a) Proposed VF-PTC (b) Conventional PTC

Table 7.3: Performance evaluation of the proposed VF-PTC

		VF-PTC	PTC
T_{ave} **(Nm)**	1000 rpm	2.61	2.46
	2500 rpm	2.51	1.74
	3500 rpm	2.48	1.66
	4500 rpm	2.54	1.72
$T_{\epsilon(rms)}$ **(Nm)**	1000 rpm	0.85	0.1.32
	2500 rpm	0.94	1.33
	3500 rpm	1.21	1.43
	4500 rpm	1.36	1.41
i_{rms} **(A)**	1000 rpm	59.65	49.12
	2500 rpm	63.92	50.91
	3500 rpm	65.49	53.15
	4500 rpm	71.31	55.44
T_{ave}/i_{rms} **(Nm/A)**	1000 rpm	0.0402	0.0355
	2500 rpm	0.0393	0.0351
	3500 rpm	0.0380	0.0313
	4500 rpm	0.0356	0.0311

produced average torque but leaves the torque ripple at the minimum with respect to other techniques.

The use of virtual-flux approach offers robustness against flux linkage variations. However, the variation on the torque maps with respect to the variations on the flux linkage should be further investigated to guarantee proper immunity against parameter variation.

7.4   Summary

Two FCS-PTC methods for SRM drives have been proposed. The first control is based on a two-step estimation where Kalman filter serves as a first stage for delay compensation. The next estimation predicts the flux linkage and torque based

on static maps. A cost function evaluates the switching states that produce the lowest instantaneous torque error with the minimum phase current, thus reducing torque ripple at the highest possible efficiency. Additional restrictions assure a limited number of switching commutations and reduce computational burden. A second technique based on the virtual-flux predictive torque control was also proposed to simplify the computational burden and provide robustness against parameter variations. The technique relies on an additional lookup table that replaces the torque vs current map.

Simulation results evidenced the improved performance of the proposed techniques with respect to the use of TSF with inner control loops or even conventional PTC techniques. For the benchmark, the reference currents were generated with conventional cubic TSFs, and two current tracking techniques were implemented: hysteresis and virtual-flux predictive control as well as the conventional PTC.

The results showed that the use of TSF has drawbacks on the reference current generation, even if the inner loops tracks them well, as the PCC did. TSF should be enhanced with further offline optimizations and considerations to presented a better performance, while the proposed PTC is intuitive, easy to implement and robust for a wide range of speeds. The results were also simulated with a low-inductance three-phase SRM, with characteristics obtained from experimental testing. The results in the last simulation is also evaluated in terms of the capability of the controller to produce torque per ampere beyond the torque ripple reduction.

Finally, the proposed techniques were evaluated experimentally in terms of the torque sharing capability, demonstrating its ability to reduce torque ripple while producing a high average torque and maintaining a good torque production per ampere

capability. The techniques can be still further improved in terms of parameter sensitivity analysis and regenerative region ripple minimization.

Chapter 8

Conclusions and Future Work

8.1 Conclusions

This thesis presented a comprehensive evaluation of model predictive control techniques for switched reluctance machine drives. SRM drives have been in the aim of researchers for several years already because their design is a promising competitor in terms of cost, efficiency and robust operation. However, their drawbacks associated to uncontrollable variables have kept SRMs away of the market. MPC has recently gained popularity among the researchers and a few industry representatives due to its intuitive development process as well as facility to handle nonlinearities. This places MPC as a favorable candidate to solve, through control algorithms, the drawbacks of SRM drives.

Although MPC has already been considered in the literature for SRM control, is it still in an early stage compared to applications in power electronics and drive systems. Therefore, possibilities tend to be unlimited, considering the different scenarios and operating condition in which an SRM can potentially replace (or complement)

conventional AC drives. The main barrier of MPC has been its high computational requirements. However, it is slowly getting into the past as everyday higher micro-processing capabilities as well as improved power electronics and switching devices are coming.

Current challenges of MPC, particularly for SRMs, are delimited as the predictive models. Fourier approximations and discrete equations with static maps are usually the proposed solution, but they define a trade-off between accuracy, memory allocation and computational effort. New modelling strategies are also being under research, opening possibilities to improve this stage. The cost functions are usually defined through basic control objectives, limiting switching and targeting efficiency while accomplishing the primary task. One of the main features of MPC is the flexibility of the cost function, which can be further exploited by considering adaptive or variable cost components. The limitation comes usually from the switching frequency, which is intended to be constant; however, for some applications it might be beneficial to vary the frequency within a range. For MPC, this might affect positively the control under the variable inductance of the machine, which can push its operation to the high-speed and four-quadrant operation, usually missing in the current literature. Besides, the trend in power electronics going towards the use of wide-band gap devices, which can handle higher switching frequencies, and therefore improve MPC performance.

This thesis proposes then a road-map for future applications of MPC, considering both the lack of controlled objectives in SRM, and the newest approaches that the control algorithm has implemented. Through the analysis of SRM target applications, and the comparison of other electrical drives, it is discussed how SRMs should

be targeted as a complement for the existing technology. High speed and ultrahigh-speed operation become then the aim of the control, along with advanced techniques such as sensorless and parameter estimation. Out of this road-map, two simple control approaches for current and torque regulation have been proposed. The first one guarantees an improve tracking in the four-quadrants and for high-power SRMs. On the other hand, the proposed torque control simplifies the modelling by using static maps and improves the torque sharing development by letting the algorithm decide it online. Both techniques have been validated through simulation and experimental testing at a wide range of speeds. The predictive torque control has also been compared with other techniques in terms of performance and online torque sharing. Results show how the MPC-based technique not only improves torque ripple but also enhances the torque production per ampere capability, this at low-and high-speed. In this way, the proposed methods are the base for an unified control technique with easy adaptation of extra control objectives, restrictions and limitation, being the first step to a future with high-performance SRM drives.

8.2   Future Work

This thesis has been one of multiple pioneers on implementing predictive control in switched reluctance drives, and it is the first one to fully disclose their potential. The proposed control techniques configure the base of an unified control technique, which can be easily adapted to different control strategies or restrictions by modifying it cost function. The proposed methods rely on the use of finite sets, leading to a variable switching frequency; if the inductance profile of the machine does not change much, this strategy can be either migrated to a continuous approach or adapted to

a modulated MPC. The latest would also allow to consider virtual voltages, being optimal for its applications in machines with low phase inductance, as the equivalent applied voltage will be reduced.

The proposed predictive torque control in Chapter 7 uses Kalman filter and Lagrange interpolation within their predictive model. The use of Lagrange is the simplest based of the so called model-free predictive control. There is an opportunity to improve robustness and memory usage by migrating to a model-free predictive control approach. Along the thesis, important references on how these techniques have been successfully applied in SynRM are discussed.

Finally, Chapter 4 presented a whole scenario of possible applications and future projects that combine MPC and SRM. Control objectives that can be implemented go from fault-tolerance to ultrahigh speed and sensorless predictive control. The most relevant for this machine topology is the consideration of predictive acoustic noise under the analysis of the vibration modes of a certain topology. The online compensation given by MPC presents a tremendous potential to improve this complex issue, subject to the proper definition of a predictive model and feedback control.

8.3   Publications

8.3.1   Journals

D. F. Valencia, R. Tarvirdilu-Asl, C. García, J. Rodriguez, and A. Emadi, "A Review of Predictive Control Techniques for Switched Reluctance Machine Drives. Part I: Fundamentals and Current Control," submitted to *IEEE Transactions on Energy Conversion*.

D. F. Valencia, R. Tarvirdilu-Asl, C. García, J. Rodriguez, and A. Emadi, "A Review of Predictive Control Techniques for Switched Reluctance Machine Drives. Part II: Torque Control, Assessment and Challenges," submitted to *IEEE Transactions on Energy Conversion.*

D. F. Valencia, R. Tarvirdilu-Asl, C. García, J. Rodriguez, and A. Emadi, "Vision, Challenges and Future Trends of Predictive Control in SRM Drives," (To be submitted).

D. F. Valencia, C. García, J. Rodriguez, and A. Emadi, "A lookup-table-based predictive torque control for Switched Reluctance Machine Drives," (To be submitted).

J. Rodriguez, C. Garcia, A. Mora, S. Alireza Davari, J. Rodas, **D. F. Valencia**, M. Elmorshedy, K. Zuo, F. Wang, L. Tarisciotti, F. Flores-Bahamonde, W. Xu, Z. Zhang, Y. Zhang, M. Norambuena, A. Emadi, T. Geyer, R. Kennel, T. Dragicevic, D. Khaburi, M. Abdelrahem, and N. Mijatovic, "Latest Advances of Model Predictive Control in Electrical Drives. Part II: Applications and Assessment with Classical Control," IEEE Transactions in Power Electronics, (To be submitted).

8.3.2   Book Chapters

D. F. Valencia, and A. Emadi, "Predictive control in a switched reluctance machine", in Predictive control of electrical drives. John Wiley & Sons, Inc., (In progress).

8.3.3   Conference

D. F. Valencia, S. R. Filho, A. D. Callegaro, M. Preindl and A. Emadi, "Virtual-Flux Finite Control Set Model Predictive Control of Switched Reluctance Motor Drives," *45th Annual Conference of the IEEE Industrial Electronics Society (IECON)*, Lisbon, Portugal, 2019, pp. 1465-1470.

J. Taylor, **D. F. Valencia**, B. Bilgin, M. Narimani and A. Emadi, "Comparison of Current Control Strategies for Low- and High-Power Switched Reluctance Motor Drives," *IEEE Transportation Electrification Conference and Expo (ITEC)*, 2020, (To be published).

References and Bibliography

[1] E. Bostanci, M. Moallem, A. Parsapour, and B. Fahimi, "Opportunities and Challenges of Switched Reluctance Motor Drives for Electric Propulsion: A Comparative Study," *IEEE Transactions on Transportation Electrification*, vol. 3, no. 1, pp. 58–75, Mar. 2017.

[2] Z. Yang, F. Shang, I. P. Brown, and M. Krishnamurthy, "Comparative Study of Interior Permanent Magnet, Induction, and Switched Reluctance Motor Drives for EV and HEV Applications," *IEEE Transactions on Transportation Electrification*, vol. 1, no. 3, pp. 245–254, Oct. 2015.

[3] A. D. Callegaro, B. Bilgin, and A. Emadi, "Radial force shaping for acoustic noise reduction in switched reluctance machines," *IEEE Transactions on Power Electronics*, vol. 34, no. 10, pp. 9866–9878, 2019.

[4] IEA, "World energy outlook 2019," International Energy Agency (IEA), Tech. Rep., 2019.

[5] B. Sarlioglu, C. T. Morris, D. Han, and S. Li, "Driving Toward Accessibility: A Review of Technological Improvements for Electric Machines, Power Electronics, and Batteries for Electric and Hybrid Vehicles," *IEEE Industry Applications*

Magazine, vol. 23, no. 1, pp. 14–25, Jan. 2017.

[6] "U.S. DRIVE electrical and electronics technical team roadmap," U.S. Department of Energy, Oct. 2017.

[7] W. Rippel, "Induction versus dc brushless motors," 2007, accessed 2020-10-01. [Online]. Available: https://www.tesla.com/blog/induction-versus-dc-brushless-motors

[8] K. Rajashekara, "Present Status and Future Trends in Electric Vehicle Propulsion Technologies," *IEEE Journal of Emerging and Selected Topics in Power Electronics*, vol. 1, no. 1, pp. 3–10, Mar. 2013.

[9] B. Bilgin, J. W. Jiang, and A. Emadi, *Switched Reluctance Motor Drives: Fundamentals to Applications.*   CRC Press, 2019.

[10] S. E. Schulz and K. M. Rahman, "High-Performance Digital PI Current Regulator for EV Switched Reluctance Motor Drives," *IEEE Transactions on Industry Applications*, vol. 39, no. 4, pp. 1118–1126, jul 2003.

[11] H. Li, E. Fairall, B. Bilgin, and A. Emadi, "Performance evaluation of a high-speed high-power switched reluctance motor drive," in *2015 IEEE Applied Power Electronics Conference and Exposition (APEC)*, Mar. 2015, pp. 1337–1342.

[12] H. Li, B. Bilgin, and A. Emadi, "An improved torque sharing function for torque ripple reduction in switched reluctance machines," *IEEE Transactions on Power Electronics*, vol. 34, no. 2, pp. 1635–1644, 2019.

[13] R. Mikail, I. Husain, M. S. Islam, Y. Sozer, and T. Sebastian, "Four-Quadrant Torque Ripple Minimization of Switched Reluctance Machine Through Current Profiling With Mitigation of Rotor Eccentricity Problem and Sensor Errors," *IEEE Transactions on Industry Applications*, vol. 51, no. 3, pp. 2097–2104, 2015.

[14] C. Gan, J. Wu, Q. Sun, S. Yang, Y. Hu, and L. Jin, "Low-cost direct instantaneous torque control for switched reluctance motors with bus current detection under soft-chopping mode," *IET Power Electronics*, vol. 9, no. 3, pp. 482–490, 2016.

[15] B. Bilgin, B. Howey, A. D. Callegaro, J. Liang, M. Kordic, J. Taylor, and A. Emadi, "Making The Case for Switched Reluctance Motors for Propulsion Applications," *IEEE Transactions on Vehicular Technology (Early access*, pp. 1–1, 2020.

[16] S. Mehta, P. Pramod, and I. Husain, "Analysis of dynamic current control techniques for switched reluctance motor drives for high performance applications," in *2019 IEEE Transportation Electrification Conference and Expo (ITEC)*, 2019, pp. 1–7.

[17] J. Ye, B. Bilgin, and A. Emadi, "An Offline Torque Sharing Function for Torque Ripple Reduction in Switched Reluctance Motor Drives," *IEEE Transactions on Energy Conversion*, vol. 30, no. 2, pp. 726–735, 2015.

[18] M. Morari and J. H. Lee, "Model predictive control: Past, present and future," *Computers & Chemical Engineering*, vol. 23, no. 4, pp. 667–682, May 1999.

[19] S. Vazquez, J. I. Leon, L. G. Franquelo, J. Rodriguez, H. A. Young, A. Marquez, and P. Zanchetta, "Model Predictive Control: A Review of Its Applications in Power Electronics," *IEEE Industrial Electronics Magazine*, vol. 8, no. 1, pp. 16–31, 2014.

[20] V. Yaramasu and B. Wu, *Model Predictive Control of Wind Energy Conversion Systems*.   John Wiley & Sons, Dec. 2016.

[21] J. Rodriguez and P. Cortes, *Predictive Control of Power Converters and Electrical Drives*, 1st ed.   Chichester, West Sussex, UK ; Hoboken, N.J: Wiley-IEEE Press, Apr. 2012.

[22] A. A. Ahmed, B. K. Koh, and Y. I. Lee, "A Comparison of Finite Control Set and Continuous Control Set Model Predictive Control Schemes for Speed Control of Induction Motors," *IEEE Transactions on Industrial Informatics*, vol. 14, no. 4, pp. 1334–1346, Apr. 2018.

[23] M. Preindl and S. Bolognani, "Model Predictive Direct Torque Control With Finite Control Set for PMSM Drive Systems, Part 1: Maximum Torque Per Ampere Operation," *IEEE Transactions on Industrial Informatics*, vol. 9, no. 4, pp. 1912–1921, Nov. 2013.

[24] H. Hadla and S. Cruz, "Predictive Stator Flux and Load Angle Control of Synchronous Reluctance Motor Drives Operating in a Wide Speed Range," *IEEE Transactions on Industrial Electronics*, vol. 64, no. 9, pp. 6950–6959, Sep. 2017.

[25] I. Kim, R. Chan, and S. Kwak, "Model predictive control method for CHB multi-level inverter with reduced calculation complexity and fast dynamics," *IET Electric Power Applications*, vol. 11, no. 5, pp. 784–792, 2017.

[26] I. Gonzalez-Prieto, M. J. Duran, J. J. Aciego, C. Martin, and F. Barrero, "Model Predictive Control of Six-Phase Induction Motor Drives Using Virtual Voltage Vectors," *IEEE Transactions on Industrial Electronics*, vol. 65, no. 1, pp. 27–37, Jan. 2018.

[27] D. Winterborne and V. Pickert, "Improving direct instantaneous torque control of switched reluctance machines with predictive flux constraints," in *8th IET International Conference on Power Electronics, Machines and Drives (PEMD 2016)*, 2016, pp. 1–6.

[28] J. Ye, B. Bilgin, and A. Emadi, "Comparative evaluation of power converters for 6/4 and 6/10 switched reluctance machines," in *2012 IEEE Transportation Electrification Conference and Expo (ITEC)*, Jun. 2012, pp. 1–6.

[29] J. Ye and A. Emadi, "Power electronic converters for 12/8 switched reluctance motor drives: A comparative analysis," in *2014 IEEE Transportation Electrification Conference and Expo (ITEC)*, 2014, pp. 1–6.

[30] F. Peng, J. Ye, and A. Emadi, "An asymmetric three-level neutral point diode clamped converter for switched reluctance motor drives," *IEEE Transactions on Power Electronics*, vol. 32, no. 11, pp. 8618–8631, 2017.

[31] V. V. Hadke and M. P. Thakre, "Integrated Multilevel Converter Topology for Speed Control of SRM Drive in Plug in-Hybrid Electric Vehicle," in *2019 3rd*

International Conference on Trends in Electronics and Informatics (ICOEI), Apr. 2019, pp. 1013–1018.

[32] D. Q. Mayne, J. B. Rawlings, C. V. Rao, and P. O. M. Scokaert, "Constrained model predictive control: Stability and optimality," *Automatica*, vol. 36, no. 6, pp. 789–814, Jun. 2000.

[33] C. A. Rojas, J. I. Yuz, M. Aguirre, and J. Rodriguez, "A comparison of discrete-time models for model predictive control of induction motor drives," in *2015 IEEE International Conference on Industrial Technology (ICIT)*, Mar. 2015, pp. 568–573.

[34] S. Bolognani, S. Bolognani, L. Peretti, and M. Zigliotto, "Design and Implementation of Model Predictive Control for Electrical Motor Drives," *IEEE Transactions on Industrial Electronics*, vol. 56, no. 6, pp. 1925–1936, Jun. 2009.

[35] T. Dorfling, H. d. T. Mouton, T. Geyer, and P. Karamanakos, "Long-Horizon Finite-Control-Set Model Predictive Control With Nonrecursive Sphere Decoding on an FPGA," *IEEE Transactions on Power Electronics*, vol. 35, no. 7, pp. 7520–7531, Jul. 2020.

[36] M. Alamir and G. Bornard, "Stability of a truncated infinite constrained receding horizon scheme: The general discrete nonlinear case," *Automatica*, vol. 31, no. 9, pp. 1353–1356, Sep. 1995.

[37] M. Preindl and S. Bolognani, "Comparison of direct and PWM model predictive control for power electronic and drive systems," in *2013 Twenty-Eighth*

Annual IEEE Applied Power Electronics Conference and Exposition (APEC), Mar. 2013, pp. 2526–2533.

[38] A. Andersson and T. Thiringer, "Assessment of an Improved Finite Control Set Model Predictive Current Controller for Automotive Propulsion Applications," *IEEE Transactions on Industrial Electronics*, vol. 67, no. 1, pp. 91–100, Jan. 2020.

[39] S. Vazquez, C. Montero, C. Bordons, and L. G. Franquelo, "Model predictive control of a VSI with long prediction horizon," in *2011 IEEE International Symposium on Industrial Electronics*, Jun. 2011, pp. 1805–1810.

[40] R. Abdel-Fadil and L. Számel, "Predictive control of switched reluctance motors for aircraft electrical actuators applications," *Acta Polytechnica Hungarica*, vol. 17, no. 5, 2020.

[41] S. V. Raković and W. S. Levine, *Handbook of Model Predictive Control.* Springer, Sep. 2018.

[42] P. Karamanakos, E. Liegmann, T. Geyer, and R. Kennel, "Model Predictive Control of Power Electronic Systems: Methods, Results, and Challenges," *IEEE Open Journal of Industry Applications*, vol. 1, pp. 95–114, 2020.

[43] N. Yan, X. Cao, and Z. Deng, "Direct torque control for switched reluctance motor to obtain high torque-ampere ratio," *IEEE Transactions on Industrial Electronics*, vol. 66, no. 7, pp. 5144–5152, jul 2019.

[44] F. Mwasilu, H. T. Nguyen, H. H. Choi, and J. Jung, "Finite Set Model Predictive Control of Interior PM Synchronous Motor Drives With an External

Disturbance Rejection Technique," *IEEE/ASME Transactions on Mechatronics*, vol. 22, no. 2, pp. 762–773, Apr. 2017.

[45] X. Li and P. Shamsi, "Model Predictive Current Control of Switched Reluctance Motors With Inductance Auto-Calibration," *IEEE Transactions on Industrial Electronics*, vol. 63, no. 6, pp. 3934–3941, 2016.

[46] E. F. Camacho and C. B. Alba, *Model Predictive Control*, 2nd ed., ser. Advanced Textbooks in Control and Signal Processing.   London: Springer-Verlag, 2007.

[47] R. Kennel, A. Linder, and M. Linke, "Generalized predictive control (GPC)-ready for use in drive applications?" in *2001 IEEE 32nd Annual Power Electronics Specialists Conference (IEEE Cat. No.01CH37230)*, vol. 4, 2001, pp. 1839–1844 vol. 4.

[48] S. Vazquez, C. Montero, C. Bordons, and L. G. Franquelo, "Model predictive control of a VSI with long prediction horizon," in *2011 IEEE International Symposium on Industrial Electronics*, Jun. 2011, pp. 1805–1810.

[49] A. Linder, R. Kanchan, R. Kennel, and P. Stolze, *Model-Based Predictive Control of Electric Drives.*   Cuvillier, 2010.

[50] J. Castelló, J. M. Espí, and R. García-Gil, "A New Generalized Robust Predictive Current Control for Grid-Connected Inverters Compensates Anti-Aliasing Filters Delay," *IEEE Transactions on Industrial Electronics*, vol. 63, no. 7, pp. 4485–4494, Jul. 2016.

[51] M. G. Judewicz, S. A. González, J. R. Fischer, J. F. Martínez, and D. O. Carrica, "Inverter-Side Current Control of Grid-Connected Voltage Source Inverters

With LCL Filter Based on Generalized Predictive Control," *IEEE Journal of Emerging and Selected Topics in Power Electronics*, vol. 6, no. 4, pp. 1732–1743, Dec. 2018.

[52] A. Sonawane, S. P. Gawande, S. G. Kadwane, and M. R. Ramteke, "Nearly constant switching frequency hysteresis-based predictive control for distributed static compensator applications," *IET Power Electronics*, vol. 9, no. 11, pp. 2174–2185, 2016.

[53] M. Norambuena, J. Rodriguez, Z. Zhang, F. Wang, C. Garcia, and R. Kennel, "A Very Simple Strategy for High-Quality Performance of AC Machines Using Model Predictive Control," *IEEE Transactions on Power Electronics*, vol. 34, no. 1, pp. 794–800, Jan. 2019.

[54] P. G. Carlet, F. Tinazzi, S. Bolognani, and M. Zigliotto, "An Effective Model-Free Predictive Current Control for Synchronous Reluctance Motor Drives," *IEEE Transactions on Industry Applications*, vol. 55, no. 4, pp. 3781–3790, Jul. 2019.

[55] P. F. C. Gonçalves, S. M. A. Cruz, and A. M. S. Mendes, "Predictive Current Control of Six-Phase Permanent Magnet Synchronous Machines Based on Virtual Vectors with Optimal Amplitude and Phase," in *2019 International Conference on Smart Energy Systems and Technologies (SEST)*, Sep. 2019, pp. 1–6.

[56] J. Gao, C. Gong, W. Li, and J. Liu, "Novel Compensation Strategy for Calculation Delay of Finite Control Set Model Predictive Current Control in PMSM,"

IEEE Transactions on Industrial Electronics, vol. 67, no. 7, pp. 5816–5819, Jul. 2020.

[57] P. Cortes, J. Rodriguez, C. Silva, and A. Flores, "Delay Compensation in Model Predictive Current Control of a Three-Phase Inverter," *IEEE Transactions on Industrial Electronics*, vol. 59, no. 2, pp. 1323–1325, Feb. 2012.

[58] Y. Wang, X. Wang, W. Xie, F. Wang, M. Dou, R. M. Kennel, R. D. Lorenz, and D. Gerling, "Deadbeat Model-Predictive Torque Control With Discrete Space-Vector Modulation for PMSM Drives," *IEEE Transactions on Industrial Electronics*, vol. 64, no. 5, pp. 3537–3547, May 2017.

[59] X. Zhang, B. Hou, and Y. Mei, "Deadbeat Predictive Current Control of Permanent-Magnet Synchronous Motors with Stator Current and Disturbance Observer," *IEEE Transactions on Power Electronics*, vol. 32, no. 5, pp. 3818–3834, May 2017.

[60] T. Zhang, C. Li, and Z. Li, "Generalized predictive control and delay compensation for high — Speed EMU network control system," in *2017 6th International Conference on Computer Science and Network Technology (ICCSNT)*, Oct. 2017, pp. 511–515.

[61] A. V. Rajarathnam, K. M. Rahman, and M. Ehsani, "Improvement of hysteresis control in switched reluctance motor drives," in *IEEE International Electric Machines and Drives Conference. IEMDC'99. Proceedings (Cat. No.99EX272)*, 1999, pp. 537–539.

[62] X. Rain, M. Hilairet, and O. Bethoux, "Comparative study of various current controllers for the switched reluctance machine," in *2010 IEEE Vehicle Power and Propulsion Conference, VPPC 2010*, 2010.

[63] G. Gallegos-López and K. Rajashekara, "Peak PWM current control of switched reluctance and AC machines," *Conference Record - IAS Annual Meeting (IEEE Industry Applications Society)*, vol. 2, no. 1, pp. 1212–1218, 2002.

[64] S. S. Ahmad and G. Narayanan, "Linearized Modeling of Switched Reluctance Motor for Closed-Loop Current Control," *IEEE Transactions on Industry Applications*, vol. 52, no. 4, pp. 3146–3158, jul 2016.

[65] R. Mikail, I. Husain, Y. Sozer, M. Islam, and T. Sebastian, "A fixed switching frequency predictive current control method for switched reluctance machines," in *2012 IEEE Energy Conversion Congress and Exposition, ECCE 2012*, 2012, pp. 843–847.

[66] R. Mikail, I. Husain, Y. Sozer, M. S. Islam, and T. Sebastian, "A Fixed Switching Frequency Predictive Current Control Method for Switched Reluctance Machines," *IEEE Transactions on Industry Applications*, vol. 50, no. 6, pp. 3717–3726, 2014.

[67] X. Li and P. Shamsi, "Adaptive model predictive current control for DSSRM drives," in *2014 IEEE Transportation Electrification Conference and Expo (ITEC)*, 2014, pp. 1–5.

[68] S. S. Ahmad and G. Narayanan, "Predictive control based constant current injection scheme for characterization of switched reluctance machine," in *2016*

IEEE International Conference on Power Electronics, Drives and Energy Systems (PEDES), 2016, pp. 1–6.

[69] S. S. Ahmad and G. Narayanan, "Predictive Control Based Constant Current Injection Scheme for Characterization of Switched Reluctance Machine," *IEEE Transactions on Industry Applications*, vol. 54, no. 4, pp. 3383–3392, Jul. 2018.

[70] C. Liu, X. Cao, R. Yuan, Z. Deng, and J. Zhou, "Torque sharing and predictive current control of dual-winding bearingless switched reluctance motors for torque ripple reduction," in *2016 19th International Conference on Electrical Machines and Systems (ICEMS)*, 2016.

[71] C. Hui, M. Li, W. Hui, S. Q. Shen, and W. Wang, "Torque ripple minimization for switched reluctance motor with predictive current control method," in *2017 20th International Conference on Electrical Machines and Systems (ICEMS)*, 2017, pp. 1–4.

[72] B. Li, X. Ling, Y. Huang, L. Gong, and C. Liu, "An Improved Model Predictive Current Controller of Switched Reluctance Machines Using Time-Multiplexed Current Sensor," *Sensors (Basel, Switzerland)*, vol. 17, no. 5, 2017.

[73] S. Mehta, M. A. Kabir, and I. Husain, "Extended speed current profiling algorithm for low torque ripple srm using model predictive control," in *2018 IEEE Energy Conversion Congress and Exposition (ECCE)*, 2018, pp. 4558–4563.

[74] S. Mehta, I. Husain, and P. Pramod, "Predictive current control of mutually coupled switched reluctance motors using net flux method," in *2019 IEEE Energy Conversion Congress and Exposition (ECCE)*, 2019, pp. 4918–4922.

[75] M. Ma, Q. Yang, X. Zhang, F. Li, and Z. Lin, "A switched reluctance motor torque ripple reduction strategy with deadbeat current control," in *2019 14th IEEE Conference on Industrial Electronics and Applications (ICIEA)*, 2019, pp. 25–30.

[76] X. Zhang, Q. Yang, M. Ma, Z. Lin, and S. Yang, "A Switched Reluctance Motor Torque Ripple Reduction Strategy With Deadbeat Current Control and Active Thermal Management," *IEEE Transactions on Vehicular Technology*, vol. 69, no. 1, pp. 317–327, jan 2020.

[77] A. Anuchin, A. Bogdanov, G. Demidova, E. Stolyarov, D. Surnin, and Y. Vagapov, "Online Magnetization Surface Identification for a Switched Reluctance Motor," in *2020 55th International Universities Power Engineering Conference (UPEC)*, Sep. 2020, pp. 1–5.

[78] B. C. Torrico, R. N. d. C. Almeida, d. Reis, Laurinda L. N., W. A. Silva, and R. S. T. Pontes, "Robust Control Based on Generalized Predictive Control Applied to Switched Reluctance Motor Current Loop," *Journal of Dynamic Systems, Measurement, and Control*, vol. 136, no. 3, pp. 031 021–031 021–7, 2014.

[79] X. Li and P. Shamsi, "Inductance Surface Learning for Model Predictive Current Control of Switched Reluctance Motors," *IEEE Transactions on Transportation Electrification*, vol. 1, no. 3, pp. 287–297, 2015.

[80] B. Li, X. Ling, Y. Huang, L. Gong, and C. Liu, "Predictive current control of a switched reluctance machine in the direct-drive manipulator of cloud robotics," *Cluster Computing*, vol. 20, no. 4, pp. 3037–3049, 2017.

[81] K. Hu, L. Guo, and J. Ye, "Model Predictive Current Control of Mutually Coupled Switched Reluctance Machines using a Three-Phase Voltage Source Converter," in *2020 IEEE Applied Power Electronics Conference and Exposition (APEC)*, Mar. 2020, pp. 704–710.

[82] R. Pupadubsin, P. Somsiri, N. Chayopitak, K. Tungpimolrut, P. Jitkreeyan, and S. Kachapornkul, "Simple predictive delta-modulation current regulator for switched reluctance motor drive," in *2008 International Conference on Electrical Machines and Systems*, 2008.

[83] M. Kiani, "Model predictive control of stator currents in Switched Reluctance Generators," in *2014 IEEE 23rd International Symposium on Industrial Electronics (ISIE)*, 2014, pp. 842–846.

[84] R. Abdel-Fadil and L. Számel, "Enhancement Of the Switched Reluctance Motor Performance for Electric Vehicles Applications Using Predictive Current Control," in *2018 International IEEE Conference and Workshop in Óbuda on Electrical and Power Engineering (CANDO-EPE)*, Nov. 2018, pp. 000 195–000 200.

[85] J. Saeed, M. Niakinezhad, N. Fernando, and L. Wang, "Model Predictive Control of an Electric Vehicle Motor Drive Integrated Battery Charger," in *2019 IEEE 13th International Conference on Compatibility, Power Electronics and Power Engineering (CPE-POWERENG)*, 2019, pp. 1–6.

[86] D. F. Valencia, S. R. Filho, A. D. Callegaro, M. Preindl, and A. Emadi, "Virtual-Flux Finite Control Set Model Predictive Control of Switched Reluctance Motor Drives," in *IECON 2019 - 45th Annual Conference of the IEEE*

Industrial Electronics Society, vol. 1, 2019, pp. 1465–1470.

[87] R. Abdel-Fadil and L. Számel, "Predictive Control of Switched Reluctance Motors for Aircraft Electrical Actuators Applications," *Acta Polytechnica Hungarica*, vol. 17, no. 5, pp. 209–227, 2020.

[88] M. Pereira and R. E. Araújo, "Model Predictive Current Control of Switched Reluctance Motor Drive: An Initial Study," in *Technological Innovation for Life Improvement*, ser. IFIP Advances in Information and Communication Technology, L. M. Camarinha-Matos, N. Farhadi, F. Lopes, and H. Pereira, Eds. Cham: Springer International Publishing, 2020, pp. 256–264.

[89] E. Kiani, B. Ganji, and S. A. Taher, "Model predictive control of switched reluctance generator based on Z-source converter for wind power applications," *International Transactions on Electrical Energy Systems*, vol. n/a, no. e12578, 2020.

[90] C. Labiod, K. Srairi, B. Mahdad, M. T. Benchouia, and M. Benbouzid, "Speed Control of 8/6 Switched Reluctance Motor with Torque Ripple Reduction Taking into Account Magnetic Saturation Effects," *Energy Procedia*, vol. 74, pp. 112–121, Aug. 2015.

[91] H. K. Bae and R. Krishnan, "Study of current controllers and development of a novel current controller for high performance SRM drives," in *Conference Record - IAS Annual Meeting (IEEE Industry Applications Society)*, vol. 1. IEEE, 1996, pp. 68–75.

[92] G. Schroder and J. Bekiesch, "Current control for the switched reluctance motor with enhanced performance," in *2005 European Conference on Power Electronics and Applications*, Sep. 2005, p. 8.

[93] H. Hannoun, M. Hilairet, and C. Marchand, "Gain-scheduling PI current controller for a switched reluctance motor," in *IEEE International Symposium on Industrial Electronics*, 2007, pp. 1177–1182.

[94] Z. Lin, D. Reay, B. Williams, and X. He, "High-performance current control for switched reluctance motors based on on-line estimated parameters," *IET Electric Power Applications*, vol. 4, no. 1, pp. 67–74, 2010.

[95] L. L. N. dos Reis, A. A. R. Coelho, O. M. Almeida, and J. C. T. Campos, "Modeling and controller performance assessment for a switched reluctance motor drive based on setpoint relay," *ISA Transactions*, vol. 48, no. 2, pp. 206–212, Apr. 2009.

[96] Y. Cho and K.-B. Lee, "Virtual-Flux-Based Predictive Direct Power Control of Three-Phase PWM Rectifiers With Fast Dynamic Response," *IEEE Transactions on Power Electronics*, vol. 31, no. 4, pp. 3348–3359, Apr. 2016.

[97] M. Preindl, "Novel Model Predictive Control of a PM Synchronous Motor Drive; Design of the Innovative Structure, Feasibility and Stability Analysis, Efficient Implementation, Experimental Validation," Ph.D. Thesis, University of Padova, 2014.

[98] M. Preindl, "Robust Control Invariant Sets and Lyapunov-Based MPC for IPM Synchronous Motor Drives," *IEEE Transactions on Industrial Electronics*, vol. 63, no. 6, pp. 3925–3933, Jun. 2016.

[99] X. D. Xue, K. W. Cheng, and S. L. Ho, "Optimization and evaluation of torque-sharing functions for torque ripple minimization in switched reluctance motor drives," *IEEE Transactions on Power Electronics*, vol. 24, no. 9, pp. 2076–2090, 2009.

[100] J. Taylor, D. F. Valencia, B. Bilgin, M. Narimani, and A. Emadi, "Comparison of Current Control Strategies for Low- and High-Power Switched Reluctance Motor Drives," in *2020 IEEE Transportation Electrification Conference Expo (ITEC)*, Jun. 2020, pp. 198–203.

[101] J. W. Jiang, B. Bilgin, and A. Emadi, "Three-Phase 24/16 Switched Reluctance Machine for a Hybrid Electric Powertrain," *IEEE Transactions on Transportation Electrification*, vol. 3, no. 1, pp. 76–85, 2017.

[102] X. D. Xue, K. W. Cheng, J. K. Lin, Z. Zhang, K. F. Luk, T. W. Ng, and N. C. Cheung, "Optimal control method of motoring operation for SRM drives in electric vehicles," *IEEE Transactions on Vehicular Technology*, vol. 59, no. 3, pp. 1191–1204, mar 2010.

[103] A. Krasovsky, S. Vasyukov, and S. Kuznetsov, "Design of Speed Regulator at Direct Torque Control of Switched Reluctance Motors," in *2019 International Conference on Industrial Engineering, Applications and Manufacturing (ICIEAM)*, Mar. 2019, pp. 1–5.

[104] R. B. Inderka and R. W. De Doncker, "DITC - Direct Instantaneous Torque Control of Switched Reluctance Drives," *IEEE Transactions on Industry Applications*, vol. 39, no. 4, pp. 1046–1051, jul 2003.

[105] I. Ralev, F. Qi, B. Burkhart, A. Klein-Hessling, and R. W. De Doncker, "Impact of Smooth Torque Control on the Efficiency of a High-Speed Automotive Switched Reluctance Drive," *IEEE Transactions on Industry Applications*, vol. 53, no. 6, pp. 5509–5517, nov 2017.

[106] Q. Sun, J. Wu, and C. Gan, "Optimized Direct Instantaneous Torque Control for SRMs with Efficiency Improvement," *IEEE Transactions on Industrial Electronics*, pp. 1–1, 2020.

[107] M. Shirahase, S. Morimoto, and M. Sanada, "Torque ripple reduction of SRM by optimization of current reference," in *The 2010 International Power Electronics Conference - ECCE ASIA -*, Jun. 2010, pp. 2501–2507.

[108] C. R. Neuhaus, N. H. Fuengwarodsakul, and R. W. D. Doncker, "Predictive PWM-based direct instantaneous torque control of switched reluctance drives," in *2006 37th IEEE Power Electronics Specialists Conference*, 2006, pp. 1–7.

[109] H. Wen and Z. Pan, "A novel dead-beat torque control of switched reluctance machines," in *2011 International Conference on Electrical Machines and Systems, ICEMS 2011*, 2011.

[110] H. J. Brauer, M. D. Hennen, and R. W. D. Doncker, "Multiphase Torque-Sharing Concepts of Predictive PWM-DITC for SRM," in *2007 7th International Conference on Power Electronics and Drive Systems*, 2007, pp. 511–516.

[111] H. J. Brauer, M. D. Hennen, and R. W. D. Doncker, "Control for Polyphase Switched Reluctance Machines to Minimize Torque Ripple and Decrease Ohmic Machine Losses," *IEEE Transactions on Power Electronics*, vol. 27, no. 1, pp. 370–378, 2012.

[112] W. Zhang, A. Xu, L. Han, and S. Wang, "Minimising torque ripple of SRM by applying DB-DTFC," *IET Electric Power Applications*, apr 2019.

[113] A. D. Pierre, A. R. Gilles, H. K. Théophile, and V. Antoine, "Torque ripple minimization in switch reluctance motor using model predictive control for water pumping application," *Current Journal of Applied Science and Technology*, pp. 1–9, 2019.

[114] H. Peyrl, G. Papafotiou, and M. Morari, "Model predictive torque control of a Switched Reluctance Motor," in *2009 IEEE International Conference on Industrial Technology*, 2009, pp. 1–6.

[115] H. Goto and O. Ichinokura, "Model prediction based instantaneous torque control of switched reluctance motor," in *2014 International Conference on Electrical Machines (ICEM)*, 2014, pp. 810–815.

[116] C. Li, G. Wang, Y. Li, and A. Xu, "An improved finite-state predictive torque control for switched reluctance motor drive," *IET Electric Power Applications*, vol. 12, no. 1, pp. 144–151, 2018.

[117] S. Song, R. Hei, R. Ma, and W. Liu, "Model Predictive Control of Switched Reluctance Starter/Generator with Torque Sharing and Compensation," *IEEE Transactions on Transportation Electrification (early access)*, pp. 1–1, 2020.

[118] Y. Li, R. Wang, G. Wang, C. Li, Y. Fan, and J. Liu, "Predictive Direct Torque Control for Switched Reluctance Motor Drive System," in *2018 37th Chinese Control Conference (CCC)*, 2018, pp. 3871–3876.

[119] A. Anuchin, V. Podzorova, V. Popova, I. Gulyaev, F. Briz, and Y. Vagapov, "Model predictive torque control of a switched reluctance drive with heat dissipation balancing in a power converter," in *2019 IEEE 60th International Scientific Conference on Power and Electrical Engineering of Riga Technical University (RTUCON)*, 2019, pp. 1–6.

[120] H. Hu, X. Cao, N. Yan, and Z. Deng, "A new predictive torque control based torque sharing function for switched reluctance motors," in *2019 22nd International Conference on Electrical Machines and Systems (ICEMS)*, 2019, pp. 1–5.

[121] R. Tarvirdilu-Asl, S. Nalakath, B. Bilgin, and A. Emadi, "A Finite Control Set Model Predictive Torque Control for Switched Reluctance Motor Drives with Adaptive Turn-off Angle," in *IECON 2019 - 45th Annual Conference of the IEEE Industrial Electronics Society*, vol. 1, Oct. 2019, pp. 840–845.

[122] C. Shang, A. Xu, L. Huang, and J. Chen, "Flux linkage optimization for direct torque control of switched reluctance motor based on model predictive control," *IEEJ Transactions on Electrical and Electronic Engineering*, vol. 14, no. 7, pp. 1105–1113, 2019.

[123] A. Xu, C. Shang, J. Chen, J. Zhu, and L. Han, "A New Control Method Based on DTC and MPC to Reduce Torque Ripple in SRM," *IEEE Access*, vol. 7, pp. 68 584–68 593, 2019.

[124] J. Villegas, S. Vazquez, J. M. Carrasco, and I. Gil, "Model Predictive Control of a switched reluctance machine using discrete Space Vector Modulation," in *2010 IEEE International Symposium on Industrial Electronics*, 2010, pp. 3139–3144.

[125] P. K. Reddy, D. Ronanki, and P. Parthiban, "Direct torque and flux control of switched reluctance motor with enhanced torque per ampere ratio and torque ripple reduction," *Electronics Letters*, vol. 55, no. 8, pp. 477–478, 2019.

[126] N. Yan, X. Cao, and Z. Deng, "Direct Torque Control for Switched Reluctance Motor to Obtain High Torque–Ampere Ratio," *IEEE Transactions on Industrial Electronics*, vol. 66, no. 7, pp. 5144–5152, Jul. 2019.

[127] S. Song, G. Fang, R. Hei, J. Jiang, R. Ma, and W. Liu, "Torque Ripple and Efficiency Online Optimization of Switched Reluctance Machine Based on Torque per Ampere Characteristics," *IEEE Transactions on Power Electronics*, vol. 35, no. 9, pp. 9608–9616, Sep. 2020.

[128] X. Dang, Y. Shi, and H. Peng, "Torque–flux linkage recurrent neural network adaptive inversion control of torque for switched reluctance motor," *IET Electric Power Applications*, vol. 14, no. 9, pp. 1612–1623, 2020.

[129] S. Wang, Z. Hu, and X. Cui, "Research on Novel Direct Instantaneous Torque Control Strategy for Switched Reluctance Motor," *IEEE Access*, vol. 8, pp. 66 910–66 916, 2020.

[130] J. Fan and Y. Lee, "A Novel Average Torque Control of Switched Reluctance Motor Based on Flux–Current Locus Control," *Canadian Journal of Electrical and Computer Engineering*, vol. 43, no. 4, pp. 273–281, 2020.

[131] T. Husain, A. Elrayyah, Y. Sozer, and I. Husain, "Unified Control for Switched Reluctance Motors for Wide Speed Operation," *IEEE Transactions on Industrial Electronics*, vol. 66, no. 5, pp. 3401–3411, May 2019.

[132] H. Le-Huy and P. Brunelle, "A versatile nonlinear switched reluctance motor model in Simulink using realistic and analytical magnetization characteristics," in *31st Annual Conference of IEEE Industrial Electronics Society, 2005. IECON 2005.*, Nov. 2005, p. 6.

[133] C. P. Weiss, A. Klein-Hessling, and R. W. De Doncker, "Discussion on control structure modifications using an fpga for predictive ditc in switched reluctance machines regarding lut resolution," in *2016 19th International Conference on Electrical Machines and Systems (ICEMS)*, 2016, pp. 1–6.

[134] A. Sadeghzadeh and B. N. Araabi, "Auto-tune predictive control of switched reluctance motor," in *2006 IEEE International Symposium on Industrial Electronics*, vol. 1, 2006, pp. 335–340.

[135] M. Ayala, J. Rodas, R. Gregor, J. Doval-Gandoy, O. Gonzalez, M. Saad, and M. Rivera, "Comparative study of predictive control strategies at fixed switching frequency for an asymmetrical six-phase induction motor drive," in *2017 IEEE International Electric Machines and Drives Conference (IEMDC)*, May 2017, pp. 1–8.

[136] J. Prieto, F. Barrero, C. S. Lim, and E. Levi, "Predictive current control with modulation in asymmetrical six-phase motor drives," in *2012 15th International Power Electronics and Motion Control Conference (EPE/PEMC)*, Sep. 2012, pp. LS1c.1–1–LS1c.1–8.

[137] F. Barrero, M. R. Arahal, R. Gregor, S. Toral, and M. J. Duran, "One-Step Modulation Predictive Current Control Method for the Asymmetrical Dual Three-Phase Induction Machine," *IEEE Transactions on Industrial Electronics*, vol. 56, no. 6, pp. 1974–1983, Jun. 2009.

[138] P. Zanchetta, D. B. Gerry, V. G. Monopoli, J. C. Clare, and P. W. Wheeler, "Predictive Current Control for Multilevel Active Rectifiers With Reduced Switching Frequency," *IEEE Transactions on Industrial Electronics*, vol. 55, no. 1, pp. 163–172, 2008.

[139] M. Rivera, S. Kouro, J. Rodriguez, B. Wu, V. Yaramasu, J. Espinoza, and P. Melila, "Predictive current control in a current source inverter operating with low switching frequency," in *4th International Conference on Power Engineering, Energy and Electrical Drives*, 2013, pp. 334–339.

[140] R. Vargas, U. Ammann, and J. RodrÍguez, "Predictive Approach to Increase Efficiency and Reduce Switching Losses on Matrix Converters," *IEEE Transactions on Power Electronics*, vol. 24, no. 4, pp. 894–902, 2009.

[141] S. Kouro, B. L. Rocca, P. Cortes, S. Alepuz, B. Wu, and J. Rodriguez, "Predictive control based selective harmonic elimination with low switching frequency for multilevel converters," in *2009 IEEE Energy Conversion Congress and Exposition*, 2009, pp. 3130–3136.

[142] M. A. Perez and C. Garcia, "Reduced switching frequency operation of power converters using virtual model based MPC," in *2015 IEEE International Symposium on Predictive Control of Electrical Drives and Power Electronics (PRECEDE)*, 2015, pp. 27–31.

[143] S. Vazquez, J. I. Leon, L. G. Franquelo, J. M. Carrasco, O. Martinez, J. Rodriguez, P. Cortes, and S. Kouro, "Model Predictive Control with constant switching frequency using a Discrete Space Vector Modulation with virtual state vectors," in *2009 IEEE International Conference on Industrial Technology*, 2009, pp. 1–6.

[144] P. Karamanakos and T. Geyer, "Guidelines for the Design of Finite Control Set Model Predictive Controllers," *IEEE Transactions on Power Electronics*, vol. 35, no. 7, pp. 7434–7450, Jul. 2020.

[145] I. Kim, R. Chan, and S. Kwak, "Model predictive control method for CHB multi-level inverter with reduced calculation complexity and fast dynamics," *IET Electric Power Applications*, vol. 11, no. 5, pp. 784–792, 2017.

[146] M. F. Maidana, W. Assuno Da Silva, W. B. Correia, B. C. Torrico, and F. G. Nogueira, "Comparative study of PI-AW and MPC-T controllers, with feedback noise applied for speed control to a switched Reluctance Motor (SRM)," in *14th Brazilian Power Electronics Conference, COBEP 2017*, vol. 2018-January. Institute of Electrical and Electronics Engineers Inc., jul 2017, pp. 1–6.

[147] W. A. Silva, L. L. Dos Reis, B. C. Torrrico, and R. N. Romulo, "Speed control in switched reluctance motor based on generalized predictive control," in *2013 Brazilian Power Electronics Conference, COBEP 2013 - Proceedings*. IEEE Computer Society, 2013, pp. 903–908.

[148] W. A. Silva and L. L. dos Reis, "Phase fault attenuation in srm based on generalized predictive control and filter design," *Electrical Engineering*, vol. 100, no. 3, pp. 1481–1489, 2018.

[149] R. N. C. Almeida, W. B. Correia, W. A. Silva, B. C. Torrico, L. L. N. d. Reis, and V. P. Pinto, "A LMI/MPC embedded controller applied to a switched reluctance machine," in *2013 Brazilian Power Electronics Conference*, 2013, pp. 363–367.

[150] R. McCann, A. T. Le, and D. Traore, "Model predictive control for time-delay compensation of a switched reluctance motor drive in smart building applications," in *2008 IEEE Industry Applications Society Annual Meeting*, 2008, pp. 1–4.

[151] S. Marinkov, B. de Jager, and M. Steinbuch, "Model predictive control of a high speed switched reluctance generator system," in *2013 European Control Conference (ECC)*, Jul. 2013, pp. 4592–4597.

[152] L. Chen, S. D. Huang, J. C. Guo, Z. Y. Hu, X. D. Fu, and G. Z. Cao, "Model predictive position control for a planar switched reluctance motor using parametric regression model," in *Proceedings - PRECEDE 2019: 2019 IEEE International Symposium on Predictive Control of Electrical Drives and Power Electronics*. Institute of Electrical and Electronics Engineers Inc., may 2019.

[153] I. Habeeb and E. K. Ismail, "Adaptive sliding mode and model predictive control of linear variable reluctance motor," in *2014 Annual International Conference on Emerging Research Areas: Magnetics, Machines and Drives, AICERA/iCMMD 2014 - Proceedings*. Institute of Electrical and Electronics Engineers Inc., sep 2014.

[154] F. Qi, A. Stippich, I. Ralev, A. Klein-Hessling, and R. W. De Doncker, "Model Predictive Control of a Switched Reluctance Machine for Guaranteed Overload

Torque," *IEEE Transactions on Industry Applications*, vol. 55, no. 2, pp. 1321–1331, Mar. 2019.

[155] F. Qi, I. Ralev, A. Stippich, and R. W. De Doncker, "Model predictive overload control of an automotive switched reluctance motor for frequent rapid accelerations," in *2016 19th International Conference on Electrical Machines and Systems (ICEMS)*.   IEEE, 2016, pp. 1–6.

[156] T. J. Besselmann, S. Van de moortel, S. Almér, P. Jörg, and H. J. Ferreau, "Model predictive control in the multi-megawatt range," *IEEE Transactions on Industrial Electronics*, vol. 63, no. 7, pp. 4641–4648, 2016.

[157] B. Burkhart, A. Klein-Hessling, I. Ralev, C. P. Weiss, and R. W. D. Doncker, "Technology, research and applications of switched reluctance drives," *CPSS Transactions on Power Electronics and Applications*, vol. 2, no. 1, pp. 12–27, 2017.

[158] I. Kioskeridis and C. Mademlis, "A unified approach for four-quadrant optimal controlled switched reluctance machine drives with smooth transition between control operations," *IEEE Transactions on Power Electronics*, vol. 24, no. 1, pp. 301–306, 2009.

[159] R. T. Meyer, S. C. Johnson, R. A. DeCarlo, S. Pekarek, and S. D. Sudhoff, "Hybrid Electric Vehicle Fault Tolerant Control," *Journal of Dynamic Systems, Measurement, and Control*, vol. 140, no. 2, Feb. 2018.

[160] J. Cai and X. Zhao, "An on-board charger integrated power converter for ev switched reluctance motor drives," *IEEE Transactions on Industrial Electronics (early access)*, pp. 1–1, 2020.

[161] H. Oberlander, "Porsche Engineering Magazine - Digital Solutions," *Porsche Engineering*, no. 2/2019, 2019, library Catalog: www.porscheengineering.com.

[162] C. Gan, Q. Sun, J. Wu, W. Kong, C. Shi, and Y. Hu, "MMC-Based SRM Drives With Decentralized Battery Energy Storage System for Hybrid Electric Vehicles," *IEEE Transactions on Power Electronics*, vol. 34, no. 3, pp. 2608–2621, Mar. 2019.

[163] A. Bindra, "Wide-Bandgap-Based Power Devices: Reshaping the power electronics landscape," *IEEE Power Electronics Magazine*, vol. 2, no. 1, pp. 42–47, Mar. 2015.

[164] S. Vazquez, J. Rodriguez, M. Rivera, L. G. Franquelo, and M. Norambuena, "Model predictive control for power converters and drives: Advances and trends," *IEEE Transactions on Industrial Electronics*, vol. 64, no. 2, pp. 935–947, 2017.

[165] A. Salem and M. Narimani, "A Review on Multiphase Drives for Automotive Traction Applications," *IEEE Transactions on Transportation Electrification*, pp. 1–1, 2019.

[166] S. Vazquez, J. Rodriguez, M. Rivera, L. G. Franquelo, and M. Norambuena, "Model Predictive Control for Power Converters and Drives: Advances and

Trends," *IEEE Transactions on Industrial Electronics*, vol. 64, no. 2, pp. 935–947, Feb. 2017.

[167] G. Watthewaduge, E. Sayed, A. Emadi, and B. Bilgin, "Electromagnetic Modeling Techniques for Switched Reluctance Machines: State-of-the-Art Review," *IEEE Open Journal of the Industrial Electronics Society*, vol. 1, pp. 218–234, 2020.

[168] P. Vaclavek and P. Blaha, "PMSM model discretization for Model Predictive Control algorithms," in *Proceedings of the 2013 IEEE/SICE International Symposium on System Integration*, Dec. 2013, pp. 13–18.

[169] M. Kögel and R. Findeisen, "Discrete-time robust model predictive control for continuous-time nonlinear systems," in *2015 American Control Conference (ACC)*, Jul. 2015, pp. 924–930.

[170] Y. Zhou, H. Li, R. Liu, and J. Mao, "Continuous Voltage Vector Model-Free Predictive Current Control of Surface Mounted Permanent Magnet Synchronous Motor," *IEEE Transactions on Energy Conversion*, vol. 34, no. 2, pp. 899–908, Jun. 2019.

[171] F. Villarroel, J. R. Espinoza, C. A. Rojas, J. Rodriguez, M. Rivera, and D. Sbarbaro, "Multiobjective Switching State Selector for Finite-States Model Predictive Control Based on Fuzzy Decision Making in a Matrix Converter," *IEEE Transactions on Industrial Electronics*, vol. 60, no. 2, pp. 589–599, Feb. 2013.

[172] C. Xia, T. Liu, T. Shi, and Z. Song, "A Simplified Finite-Control-Set Model-Predictive Control for Power Converters," *IEEE Transactions on Industrial Informatics*, vol. 10, no. 2, pp. 991–1002, May 2014.

[173] P. Gonçalves, S. Cruz, and A. Mendes, "Finite Control Set Model Predictive Control of Six-Phase Asymmetrical Machines—An Overview," *Energies*, vol. 12, no. 24, p. 4693, Jan. 2019.

[174] L. Bigarelli, M. di Benedetto, A. Lidozzi, L. Solero, S. A. Odhano, and P. Zanchetta, "PWM-Based Optimal Model Predictive Control for Variable Speed Generating Units," *IEEE Transactions on Industry Applications*, vol. 56, no. 1, pp. 541–550, Jan. 2020.

[175] N. Nakao and K. Akatsu, "Vector control for switched reluctance motor drives using an improved current controller," in *2014 IEEE Energy Conversion Congress and Exposition (ECCE)*, Sep. 2014, pp. 1379–1386.

[176] W. Zhang, A. Xu, L. Han, and S. Wang, "Minimising torque ripple of SRM by applying DB-DTFC," *IET Electric Power Applications*, vol. 13, no. 11, pp. 1883–1890, Nov. 2019.

[177] P. Karamanakos, T. Geyer, T. Mouton, and R. Kennel, "Computationally efficient sphere decoding for long-horizon direct model predictive control," in *2016 IEEE Energy Conversion Congress and Exposition (ECCE)*, Sep. 2016, pp. 1–8.

[178] B. Li, X. Ling, Y. Huang, L. Gong, and C. Liu, "Predictive current control of a switched reluctance machine in the direct-drive manipulator of cloud robotics," *Cluster Computing*, vol. 20, no. 4, pp. 3037–3049, Dec. 2017.

[179] R. P. Aguilera and D. E. Quevedo, "Predictive Control of Power Converters: Designs With Guaranteed Performance," *IEEE Transactions on Industrial Informatics*, vol. 11, no. 1, pp. 53–63, Feb. 2015.

[180] F. Betin, G.-A. Capolino, D. Casadei, B. Kawkabani, R. I. Bojoi, L. Harnefors, E. Levi, L. Parsa, and B. Fahimi, "Trends in Electrical Machines Control: Samples for Classical, Sensorless, and Fault-Tolerant Techniques," *IEEE Industrial Electronics Magazine*, vol. 8, no. 2, pp. 43–55, Jun. 2014.

[181] J.-W. Ahn and G. F. Lukman, "Switched reluctance motor: Research trends and overview," *CES Transactions on Electrical Machines and Systems*, vol. 2, no. 4, pp. 339–347, Dec. 2018.

[182] K. K. Schwarz, *Design of Industrial Electric Motor Drives.* Oxford; Boston: Butterworth-Heinemann, 1991.

[183] E. W. Fairall, B. Bilgin, and A. Emadi, "State-of-the-art high-speed switched reluctance machines," in *2015 IEEE International Electric Machines Drives Conference (IEMDC)*, May 2015, pp. 1621–1627.

[184] J. W. Jiang, B. Bilgin, and A. Emadi, "Three-Phase 24/16 Switched Reluctance Machine for a Hybrid Electric Powertrain," *IEEE Transactions on Transportation Electrification*, vol. 3, no. 1, pp. 76–85, Mar. 2017.

[185] G. Gallegos-Lopez, F. Reiter, K. Rajashekara, and R. J. Krefta, "300 kW Switched Reluctance Generator for Hybrid Vehicle Applications," SAE International, Warrendale, PA, SAE Technical Paper 2002-01-1087, Mar. 2002.

[186] C. Gong and T. Habetler, "Electromagnetic design of an ultra-high speed switched reluctance machine over 1 million rpm," in *2017 IEEE Energy Conversion Congress and Exposition (ECCE)*, Oct. 2017, pp. 2368–2373.

[187] S. Kozuka, N. Tanabe, J. Asama, and A. Chiba, "Basic characteristics of 150,000r/min switched reluctance motor drive," in *2008 IEEE Power and Energy Society General Meeting - Conversion and Delivery of Electrical Energy in the 21st Century*, Jul. 2008, pp. 1–4.

[188] A. Radun and E. Richter, "A Detailed Power Inverter Design for a 250 kW Switched Reluctance Aircraft Engine Starter/Generator," SAE International, Warrendale, PA, SAE Technical Paper 931388, Apr. 1993.

[189] E. Richter, J. P. Lyons, C. Ferreira, A. V. Radun, and E. Ruckstadter, "Initial Testing of a 250 KW Starter/Generator for Aircraft Applications," SAE International, Warrendale, PA, SAE Technical Paper 941160, Apr. 1994.

[190] E. Richter and C. Ferreira, "Performance evaluation of a 250 kW switched reluctance starter generator," in *IAS '95. Conference Record of the 1995 IEEE Industry Applications Conference Thirtieth IAS Annual Meeting*, vol. 1, Oct. 1995, pp. 434–440 vol.1.

[191] C. Gan, Y. Chen, X. Cui, J. Sun, K. Ni, and R. Qu, "Investigation of rotor strength and rotor dynamics for high-speed high-power switched reluctance machines," *IET Electric Power Applications*, vol. 14, no. 9, pp. 1624–1630, 2020.

[192] L. Morel, H. Fayard, H. Vives Fos, A. Galindo, and G. Abba, "Study of ultra high speed switched reluctance motor drive," in *Conference Record of the*

2000 IEEE Industry Applications Conference. Thirty-Fifth IAS Annual Meeting and World Conference on Industrial Applications of Electrical Energy (Cat. No.00CH37129), vol. 1, Oct. 2000, pp. 87–92 vol.1.

[193] J. Kunz, S. Cheng, Y. Duan, J. R. Mayor, R. Harley, and T. Habetler, "Design of a 750,000 rpm switched reluctance motor for micro machining," in *2010 IEEE Energy Conversion Congress and Exposition*, Sep. 2010, pp. 3986–3992.

[194] M. Eull and M. Preindl, "An Optimization-Based Reduced Sensor Virtual Flux Observer for PM Synchronous Machines," *IEEE Transactions on Industrial Electronics*, pp. 1–1, 2020.

[195] S. M. Castano, B. Bilgin, E. Fairall, and A. Emadi, "Acoustic Noise Analysis of a High-Speed High-Power Switched Reluctance Machine: Frame Effects," *IEEE Transactions on Energy Conversion*, vol. 31, no. 1, pp. 69–77, Mar. 2016.

[196] C. Gan, J. Wu, Q. Sun, W. Kong, H. Li, and Y. Hu, "A Review on Machine Topologies and Control Techniques for Low-Noise Switched Reluctance Motors in Electric Vehicle Applications," *IEEE Access*, vol. 6, pp. 31 430–31 443, 2018.

[197] S. Li, S. Zhang, T. G. Habetler, and R. G. Harley, "Modeling, Design Optimization, and Applications of Switched Reluctance Machines—A Review," *IEEE Transactions on Industry Applications*, vol. 55, no. 3, pp. 2660–2681, May 2019.

[198] J. F. Gieras, C. Wang, J. C. Lai, C. Wang, and J. C. Lai, *Noise of Polyphase Electric Motors*.   CRC Press, Oct. 2018.

[199] Jin-Woo Ahn, Sung-Jun Park, and Dong-Hee Lee, "Hybrid excitation of SRM for reduction of vibration and acoustic noise," *IEEE Transactions on Industrial Electronics*, vol. 51, no. 2, pp. 374–380, Apr. 2004.

[200] A. Klein-Hessling, A. Hofmann, and R. W. D. Doncker, "Direct instantaneous torque and force control: A control approach for switched reluctance machines," *IET Electric Power Applications*, vol. 11, no. 5, pp. 935–943, 2017.

[201] A. D. Callegaro, J. Liang, J. W. Jiang, B. Bilgin, and A. Emadi, "Radial Force Density Analysis of Switched Reluctance Machines: The Source of Acoustic Noise," *IEEE Transactions on Transportation Electrification*, pp. 1–1, 2018.

[202] M. Kroneisl, V. Šmídl, Z. Peroutka, and M. Janda, "Predictive Control of IM Drive Acoustic Noise," *IEEE Transactions on Industrial Electronics*, vol. 67, no. 7, pp. 5666–5676, Jul. 2020.

[203] K. Aiso and K. Akatsu, "High speed SRM using vector control for electric vehicle," *CES Transactions on Electrical Machines and Systems*, vol. 4, no. 1, pp. 61–68, Mar. 2020.

[204] T. Husain, A. Elrayyah, Y. Sozer, and I. Husain, "Unified Control for Switched Reluctance Motors for Wide Speed Operation," *IEEE Transactions on Industrial Electronics*, vol. 66, no. 5, pp. 3401–3411, May 2019.

[205] Y. Zhang, B. Zhang, H. Yang, M. Norambuena, and J. Rodriguez, "Generalized Sequential Model Predictive Control of IM Drives With Field-Weakening Ability," *IEEE Transactions on Power Electronics*, vol. 34, no. 9, pp. 8944–8955, Sep. 2019.

[206] J. Brandon, "Dyson's New Vacuum Driven By the Fastest Motor Ever," https://www.popsci.com/gear-amp-gadgets/article/2009-06/dysons-new-vacuum-driven-fastest-motor-ever/, Jun. 2009, accessed: 2020-09-18.

[207] T. Murphy, "Valeo Launching Two Electric Superchargers," https://www.wardsauto.com/industry/valeo-launching-two-electric-superchargers, Jun. 2014, accessed 2020-09-18.

[208] C. Gong, S. Li, T. Habetler, J. Restrepo, and B. Soderholm, "Direct Position Control for Ultrahigh-Speed Switched-Reluctance Machines Based on Low-Cost Nonintrusive Reflective Sensors," *IEEE Transactions on Industry Applications*, vol. 55, no. 1, pp. 480–489, Jan. 2019.

[209] C. J. Bateman, B. C. Mecrow, A. C. Clothier, P. P. Acarnley, and N. D. Tuftnell, "Sensorless Operation of an Ultra-High-Speed Switched Reluctance Machine," *IEEE Transactions on Industry Applications*, vol. 46, no. 6, pp. 2329–2337, Nov. 2010.

[210] M. Ehsani and B. Fahimi, "Elimination of position sensors in switched reluctance motor drives: State of the art and future trends," *IEEE Transactions on Industrial Electronics*, vol. 49, no. 1, pp. 40–47, Feb. 2002.

[211] L. Rovere, A. Formentini, A. Gaeta, P. Zanchetta, and M. Marchesoni, "Sensorless Finite-Control Set Model Predictive Control for IPMSM Drives," *IEEE Transactions on Industrial Electronics*, vol. 63, no. 9, pp. 5921–5931, Sep. 2016.

[212] S. Nalakath, Y. Sun, M. Preindl, and A. Emadi, "Optimization-Based Position Sensorless Finite Control Set Model Predictive Control for IPMSMs," *IEEE Transactions on Power Electronics*, vol. 33, no. 10, pp. 8672–8682, Oct. 2018.

[213] S. Nalakath, M. Preindl, and A. Emadi, "Online multi-parameter estimation of interior permanent magnet motor drives with finite control set model predictive control," *IET Electric Power Applications*, vol. 11, no. 5, pp. 944–951, 2017.

[214] L. Sun, S. Nalakath, A. D. Callegaro, and A. Emadi, "Investigation of a Practical Convex-Optimization-Based Sensorless Scheme for IPMSM Drives," *IEEE Transactions on Power Electronics*, vol. 34, no. 12, pp. 12 437–12 452, Dec. 2019.

[215] D. F. Valencia, L. Sun, M. Preindl, and A. Emadi, "Convex Optimization-Based Sensorless Control for IPMSM Drives with Reduced Complexity," in *IECON 2018 - 44th Annual Conference of the IEEE Industrial Electronics Society*, Oct. 2018, pp. 439–444.

[216] C. Gan, Y. Chen, R. Qu, Z. Yu, W. Kong, and Y. Hu, "An overview of fault-diagnosis and fault-tolerance techniques for switched reluctance machine systems," *IEEE Access*, vol. 7, pp. 174 822–174 838, 2019.

[217] P. Dúbravka, P. Rafajdus, P. Makyš, and L. Szabó, "Control of switched reluctance motor by current profiling under normal and open phase operating condition," *IET Electric Power Applications*, vol. 11, no. 4, pp. 548–556, 2017.

[218] G. Liu, C. Song, and Q. Chen, "Fcs-mpc-based fault-tolerant control of five-phase ipmsm for mtpa operation," *IEEE Transactions on Power Electronics*, vol. 35, no. 3, pp. 2882–2894, 2019.

[219] T. Tao, W. Zhao, Y. Du, Y. Cheng, and J. Zhu, "Simplified fault-tolerant model predictive control for a five-phase permanent-magnet motor with reduced computation burden," *IEEE Transactions on Power Electronics*, vol. 35, no. 4, pp. 3850–3858, 2019.

[220] ., "IEEE Guide for the Presentation of Thermal Limit Curves for Squirrel Cage Induction Machines," *IEEE Std 620-1996*, pp. i–, 1996.

[221] A. Boglietti, I. R. Bojoi, S. Rubino, and M. Cossale, "Overload Capability of Multiphase Machines Under Normal and Open-Phase Fault Conditions: A Thermal Analysis Approach," *IEEE Transactions on Industry Applications*, vol. 56, no. 3, pp. 2560–2569, May 2020.

[222] V. T. Buyukdegirmenci and P. T. Krein, "Induction Machine Characterization for Short-Term or Momentary Stall Torque," *IEEE Transactions on Industry Applications*, vol. 51, no. 3, pp. 2237–2245, May 2015.

[223] F. Qi, A. Stippich, S. Koschik, and R. W. D. Doncker, "Model predictive overload control of induction motors," in *2015 IEEE International Electric Machines Drives Conference (IEMDC)*, May 2015, pp. 999–1005.

[224] T. Sun, R. Yang, H. Li, X. Zhang, and T. Xu, "Active Motor Rotor Temperature Management Based on One-Node Thermal Network Model Predictive Control," *IEEE Transactions on Power Electronics*, vol. 35, no. 10, pp. 11 213–11 221, Oct. 2020.

[225] P. Azer, B. Bilgin, and A. Emadi, "Mutually Coupled Switched Reluctance Motor: Fundamentals, Control, Modeling, State of the Art Review and Future Trends," *IEEE Access*, vol. 7, pp. 100 099–100 112, 2019.

[226] S. Mehta, I. Husain, and P. Pramod, "Predictive Current Control of Mutually Coupled Switched Reluctance Motors Using Net Flux Method," in *2019 IEEE Energy Conversion Congress and Exposition (ECCE)*, Sep. 2019, pp. 4918–4922.

[227] K. Hu, L. Guo, and J. Ye, "Model Predictive Current Control of Mutually Coupled Switched Reluctance Machines using a Three-Phase Voltage Source Converter," in *2020 IEEE Applied Power Electronics Conference and Exposition (APEC)*.   New Orleans, LA, USA: IEEE, Mar. 2020, pp. 704–710.

[228] C. Gan, J. Wu, Y. Hu, S. Yang, W. Cao, and J. M. Guerrero, "New Integrated Multilevel Converter for Switched Reluctance Motor Drives in Plug-in Hybrid Electric Vehicles With Flexible Energy Conversion," *IEEE Transactions on Power Electronics*, vol. 32, no. 5, pp. 3754–3766, May 2017.

[229] B. Bilgin, B. Howey, A. D. Callegaro, J. Liang, M. Kordic, J. Taylor, and A. Emadi, "Making the case for switched reluctance motors for propulsion applications," *IEEE Transactions on Vehicular Technology*, 2020.

[230] P. Harrop and K. Ghaffarzadeh, *Electric Motors for Electric Vehicles: Land, Water, Air 2020-2030.*   IDTechEx, Sep. 2019.

[231] M. Yilmaz and P. T. Krein, "Review of Battery Charger Topologies, Charging Power Levels, and Infrastructure for Plug-In Electric and Hybrid Vehicles,"

IEEE Transactions on Power Electronics, vol. 28, no. 5, pp. 2151–2169, May 2013.

[232] B. Singh, "Novel and Ruggedized Power Electronics for Off-Highway Vehicles," *IEEE Electrification Magazine*, vol. 2, no. 2, pp. 31–41, Jun. 2014.

[233] V. Madonna, P. Giangrande, and M. Galea, "Electrical Power Generation in Aircraft: Review, Challenges, and Opportunities," *IEEE Transactions on Transportation Electrification*, vol. 4, no. 3, pp. 646–659, Sep. 2018.

[234] A. D. Callegaro, J. Guo, M. Eull, B. Danen, J. Gibson, M. Preindl, B. Bilgin, and A. Emadi, "Bus Bar Design for High-Power Inverters," *IEEE Transactions on Power Electronics*, vol. 33, no. 3, pp. 2354–2367, Mar. 2018.

[235] M. Preindl, E. Schaltz, and P. Thogersen, "Switching Frequency Reduction Using Model Predictive Direct Current Control for High-Power Voltage Source Inverters," *IEEE Transactions on Industrial Electronics*, vol. 58, no. 7, pp. 2826–2835, Jul. 2011.

[236] X. D. Xue, K. W. E. Cheng, and S. L. Ho, "Optimization and Evaluation of Torque-Sharing Functions for Torque Ripple Minimization in Switched Reluctance Motor Drives," *IEEE Transactions on Power Electronics*, vol. 24, no. 9, pp. 2076–2090, Sep. 2009.

[237] G. Welch and G. Bishop, "An introduction to the kalman filter," University of North Carolina at Chapel Hill, Tech. Rep., 1994.

[238] C. Leffler, K. Hemphill, A. Sagg, R. Lee, C. Endsley, O. Almuharrami, S. Aluru, and V. Yaramasu, "Guidelines for dSPACE-based real-time implementation of

predictive current control for grid-connected converters," in *2017 IEEE Southern Power Electronics Conference (SPEC)*, Dec. 2017, pp. 1–8.

[239] H. Zeng, H. Chen, and J. Shi, "Direct instantaneous torque control with wide operating range for switched reluctance motors," *IET Electric Power Applications*, vol. 9, no. 9, pp. 578–585, 2015.